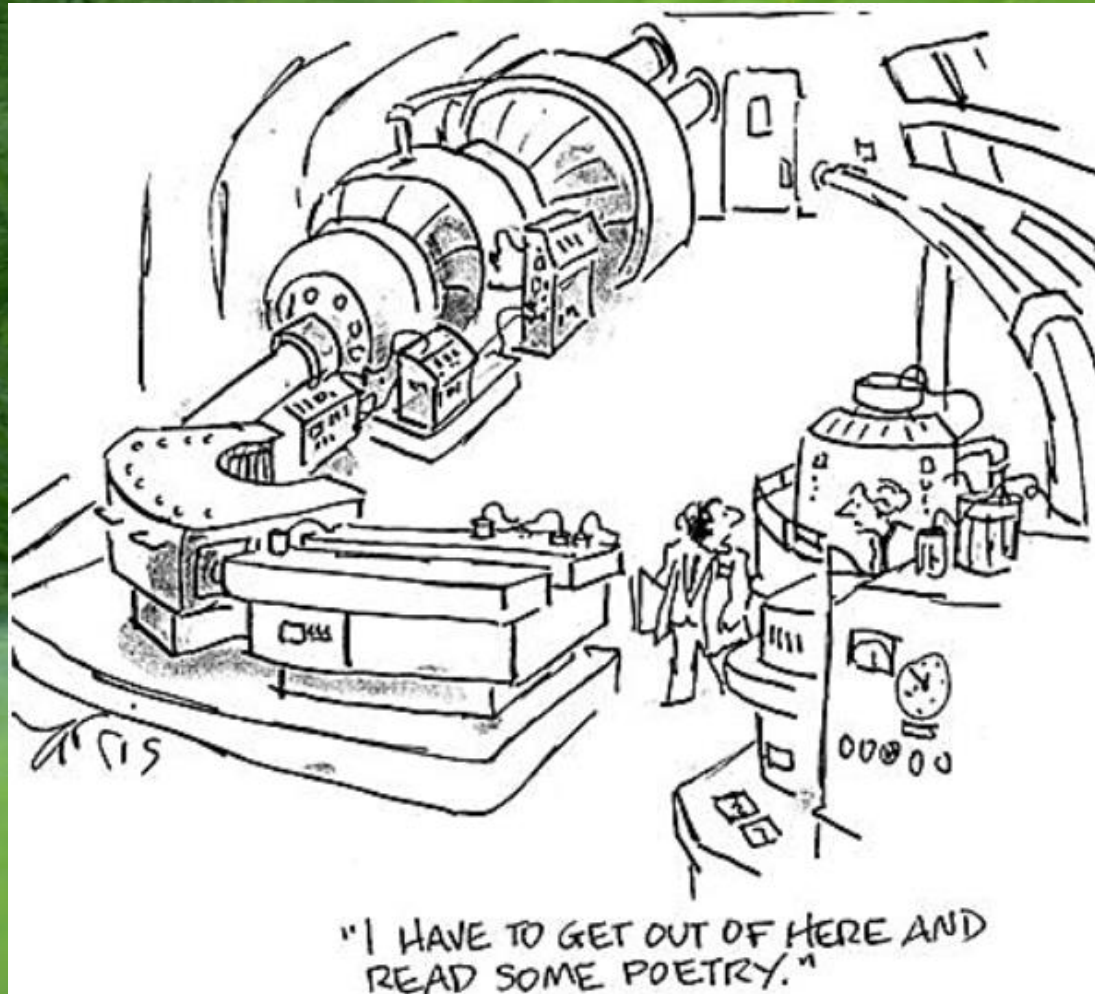


Quantum transport



Faculty of Physics UW

Jacek.Szczytko@fuw.edu.pl

The current and charge density



The current and charge density

Current density:
$$J(\vec{r}, t) = J(\vec{r}) = \frac{\hbar q}{2 i m} (\Psi^* \nabla \Psi - \Psi \nabla \Psi^*)$$

In the case of de Broigle wave:
$$\Psi(x, t) = [A_+ e^{ikx} + A_- e^{-ikx}] e^{-i\omega t}$$

$$J(\vec{r}) = \frac{\hbar q k}{m} (|A_+|^2 - |A_-|^2) \quad \text{each wave carry current}$$

In the case of the evanescent (decaying) wave:
$$\Psi(x, t) = [B_+ e^{\kappa x} + B_- e^{-\kappa x}] e^{-i\omega t}$$

$$J(\vec{r}) = \frac{\hbar q \kappa}{i m} (B_+ B_-^* - B_+^* B_-) = \frac{2 \hbar q \kappa}{m} \text{Im} (B_+ B_-^*)$$

Only the superpositioin of + i –
amplitudes gives real current!

The calssical wave:
$$\Psi(x, t) = \text{Re}\{[A_+ e^{ikx} + A_- e^{-ikx}] e^{-i\omega t}\}$$

The current and charge density

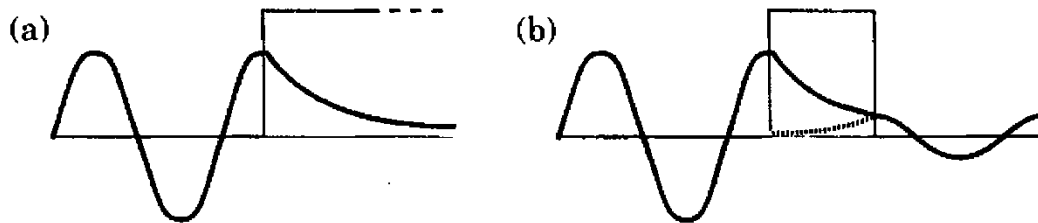
Current density:
$$J(\vec{r}, t) = J(\vec{r}) = \frac{\hbar q}{2 i m} (\Psi^* \nabla \Psi - \Psi \nabla \Psi^*)$$

In the case of de Broigle wave:
$$\Psi(x, t) = [A_+ e^{ikx} + A_- e^{-ikx}] e^{-i\omega t}$$

$$J(\vec{r}) = \frac{\hbar q k}{m} (|A_+|^2 - |A_-|^2) \quad \text{each wave carry current}$$

In the case of the evanescent (decaying) wave:
$$\Psi(x, t) = [B_+ e^{\kappa x} + B_- e^{-\kappa x}] e^{-i\omega t}$$

$$J(\vec{r}) = \frac{\hbar q \kappa}{i m} (B_+ B_-^* - B_+^* B_-) = \frac{2 \hbar q \kappa}{m} \text{Im} (B_+ B_-^*)$$

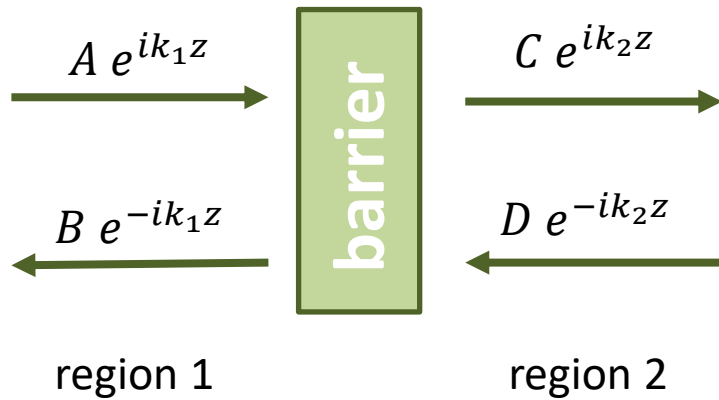


Only the superposition of + i - amplitudes gives real current!

FIGURE 1.5. Current carried by counter-propagating decaying waves. (a) An infinitely thick barrier contains a single decaying exponential that carries no current. (b) A finite barrier contains both growing and decaying exponentials and passes current. (The wave function is complex, so the figure is only a rough guide.)



Tunnelling



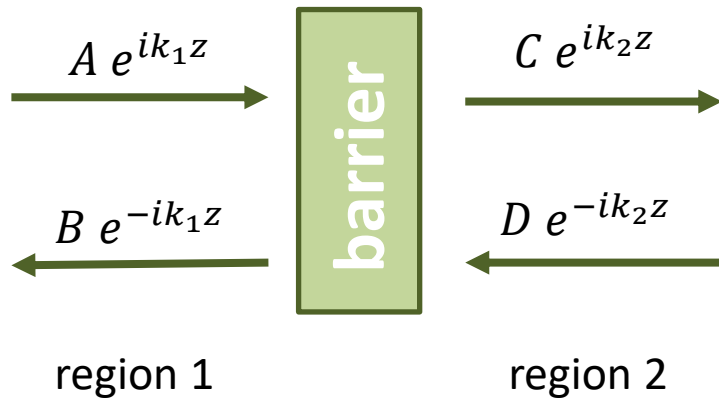
$$\begin{pmatrix} C \\ D \end{pmatrix} = T^{(21)} \begin{pmatrix} A \\ B \end{pmatrix} = \begin{pmatrix} T_{11} & T_{12} \\ T_{12}^* & T_{11}^* \end{pmatrix} \begin{pmatrix} A \\ B \end{pmatrix}$$

$$r = -\frac{T_{12}^*}{T_{11}^*} \quad t = -\frac{1}{T_{11}^*}$$

$$T^{(21)}(0) = \begin{pmatrix} 1/t^* & -r^*/t^* \\ -r/t & 1/t \end{pmatrix}$$

On exercises

Tunnelling



$$\begin{pmatrix} C \\ D \end{pmatrix} = T^{(21)} \begin{pmatrix} A \\ B \end{pmatrix} = \begin{pmatrix} T_{11} & T_{12} \\ T_{12}^* & T_{11}^* \end{pmatrix} \begin{pmatrix} A \\ B \end{pmatrix}$$

$$r = -\frac{T_{12}^*}{T_{11}^*} \quad t = -\frac{1}{T_{11}^*}$$

$$T^{(21)}(0) = \begin{pmatrix} 1/t^* & -r^*/t^* \\ -r/t & 1/t \end{pmatrix}$$

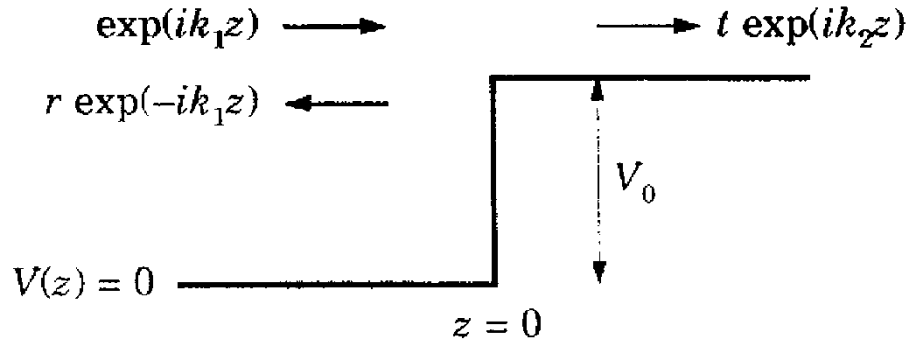
$$T^{(21)}(d) = \begin{pmatrix} e^{-ik_2 d} & 0 \\ 0 & e^{ik_2 d} \end{pmatrix} T^{(21)}(0) \begin{pmatrix} e^{ik_1 d} & 0 \\ 0 & e^{ik_1 d} \end{pmatrix} = A_2^{-1}(d) T(0) A_1(d)$$

The other direction: $\begin{pmatrix} B \\ A \end{pmatrix} = T^{(12)} \begin{pmatrix} D \\ C \end{pmatrix}$

$$T^{(12)}(0) = \begin{pmatrix} 1/t^* & r/t \\ r^*/t^* & 1/t \end{pmatrix}$$

Tunnelling

Examples:



$$T + R = 1$$

$$T = \frac{4k_1 k_2}{(k_1 + k_2)^2}$$

$$R = \left(\frac{k_1 - k_2}{k_1 + k_2} \right)^2$$

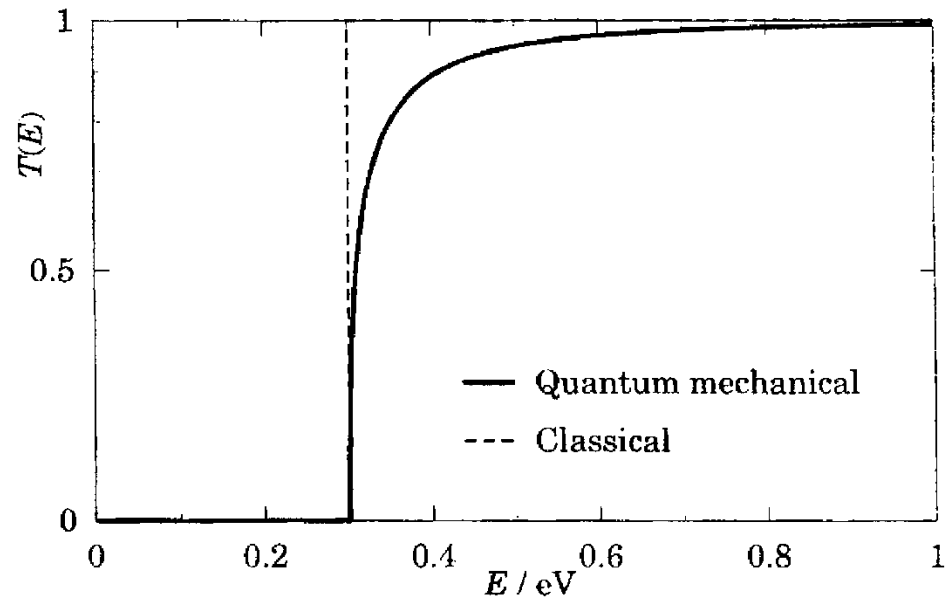


FIGURE 5.3. Transmission coefficient $T(E)$ as a function of the energy E of the incident electron for a step 0.3 eV high in GaAs. The broken line is the classical result.

Tunnelling

Przykłady:

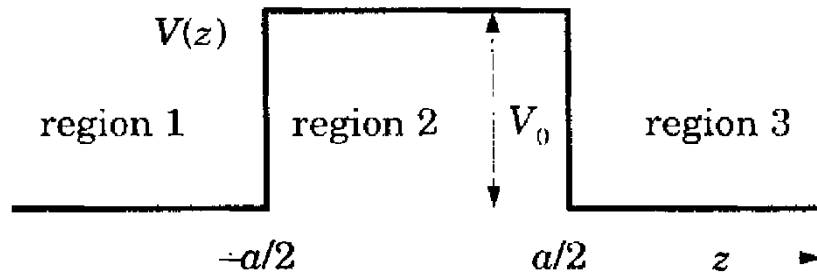


FIGURE 5.5. Potential barrier with $V(z) = V_0$ for $|z| < a/2$ and $V(z) = 0$ elsewhere.

$E > V_0$

$$T = \frac{4k_1^2 k_2^2}{4k_1^2 k_2^2 + (k_1^2 - k_2^2)^2 \sin^2 k_2 a} = \left[1 + \frac{V_0^2}{4E(E - V_0)} \sin^2 k_2 a \right]^{-1}$$

$E < V_0$

$$T = \frac{4k_1^2 \kappa_2^2}{4k_1^2 \kappa_2^2 + (k_1^2 + \kappa_2^2)^2 \sinh^2 \kappa_2 a} = \left[1 + \frac{V_0^2}{4E(V_0 - E)} \sinh^2 \kappa_2 a \right]^{-1}$$

Anti-well energy levels!

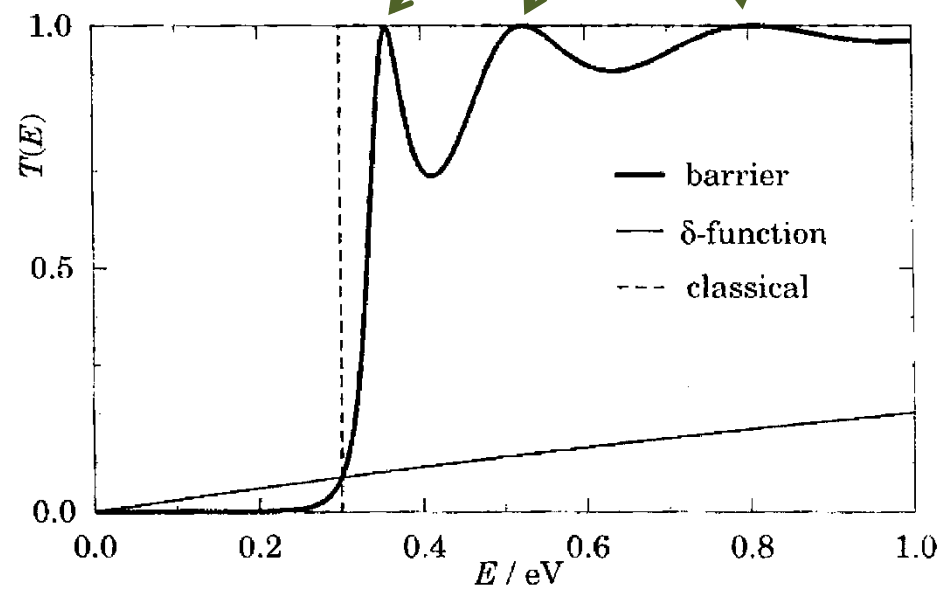


FIGURE 5.6. Transmission coefficient $T(E)$ as a function of energy E for a square potential barrier of height $V_0 = 0.3$ eV and thickness $a = 10$ nm in GaAs. The thin curve is for a δ -function barrier of the same strength $S = V_0 a$, and the broken curve is the classical result for a barrier of the same height.

Tunnelling

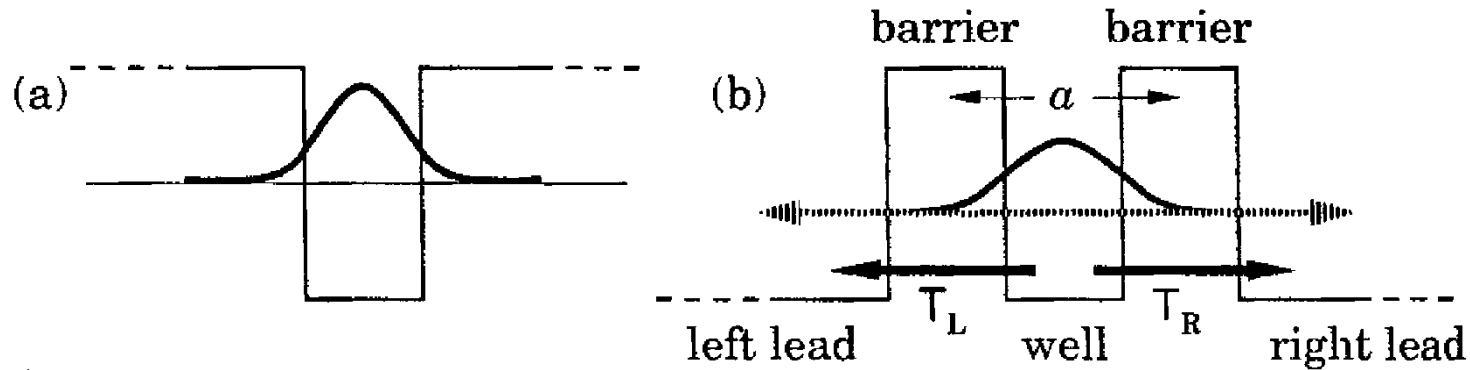


FIGURE 5.10. (a) A finite square potential well with a true bound state. (b) The same well but with barriers of finite thickness, where the bound state becomes resonant or quasi-bound.

$$t = \frac{t_L t_R}{1 - r_L r_R \exp 2ika}$$

$$\phi = 2ka + \rho_L + \rho_R$$

$$T = |t|^2 = \frac{T_L T_R}{(1 - \sqrt{R_L R_R})^2 + 4\sqrt{R_L R_R} \sin^2 \frac{1}{2} \phi}$$

$$T_{pk} = \frac{T_L T_R}{(1 - \sqrt{R_L R_R})^2} \approx \frac{4T_L T_R}{(T_L + T_R)^2}$$

Tunnelling

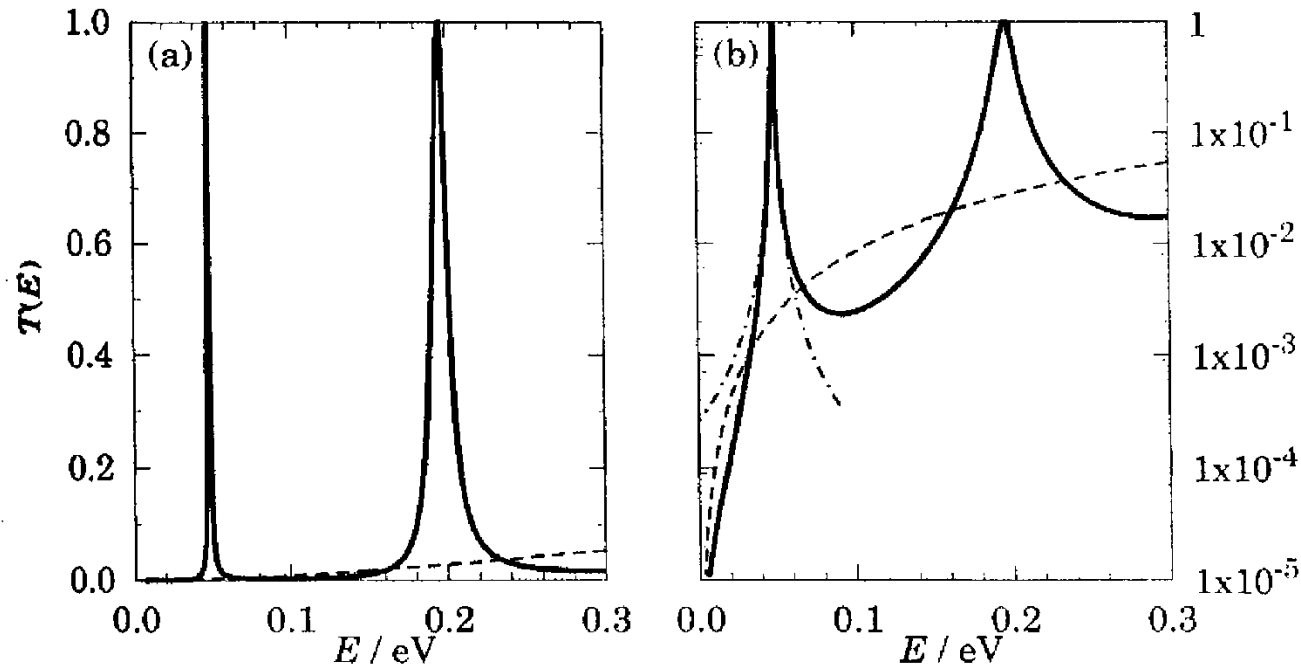


FIGURE 5.11. Transmission coefficient of a resonant-tunnelling structure on (a) linear and (b) logarithmic scales. The barriers are δ -functions of strength $0.3 \text{ eV} \times 5 \text{ nm}$ separated by 10 nm . The solid curve is $T(E)$ for the whole structure, the dashed curve shows the square of $T(E)$ for a single barrier and would apply to the double-barrier structure if there were no resonance, and the chain curve is the Lorentzian approximation to the lowest resonance.

$$T = |t|^2 = \frac{T_L T_R}{(1 - \sqrt{R_L R_R})^2 + 4\sqrt{R_L R_R} \sin^2 \frac{1}{2} \phi}$$

$$T_{pk} = \frac{T_L T_R}{(1 - \sqrt{R_L R_R})^2} \approx \frac{4T_L T_R}{(T_L + T_R)^2}$$

Tunnelling

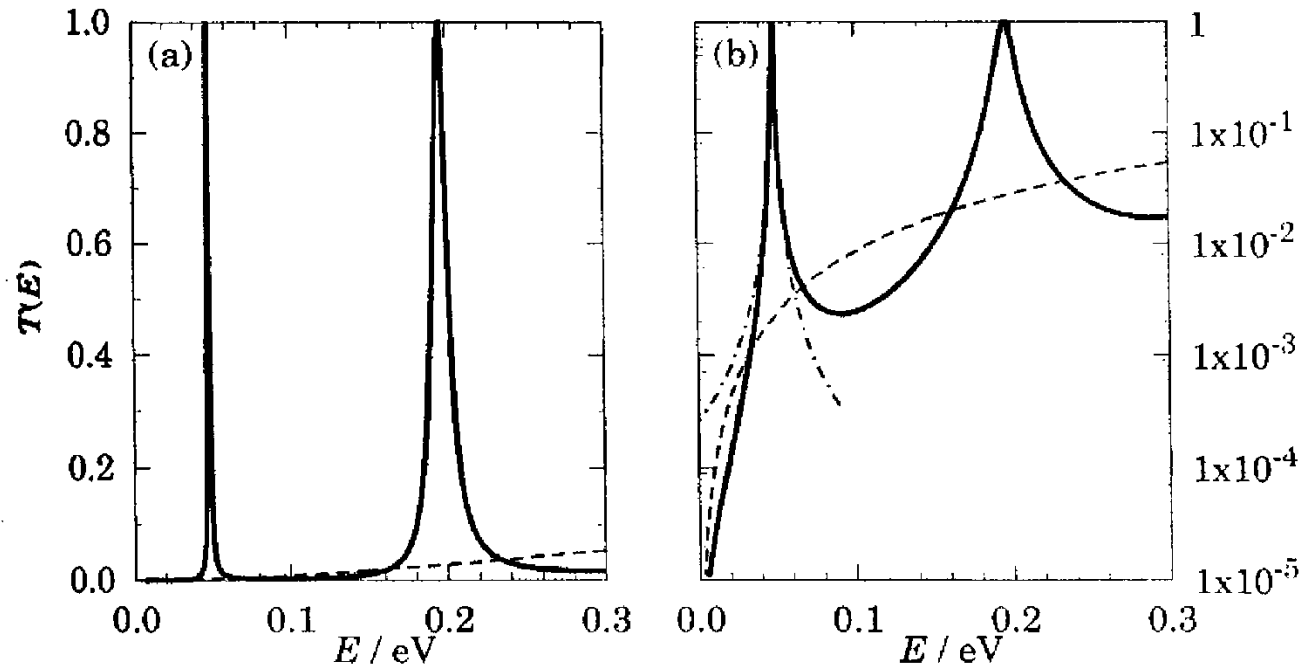


FIGURE 5.11. Transmission coefficient of a resonant-tunnelling structure on (a) linear and (b) logarithmic scales. The barriers are δ -functions of strength $0.3 \text{ eV} \times 5 \text{ nm}$ separated by 10 nm . The solid curve is $T(E)$ for the whole structure, the dashed curve shows the square of $T(E)$ for a single barrier and would apply to the double-barrier structure if there were no resonance, and the chain curve is the Lorentzian approximation to the lowest resonance.

$$T \approx \frac{T_{pk}}{1 + \left(\frac{\delta\phi}{\frac{1}{2}\phi_0}\right)^2} \quad \text{profil Lorentza}$$

$$\phi_0 = T_L + T_R$$

$$T_{pk} = \frac{T_L T_R}{(1 - \sqrt{R_L R_R})^2} \approx \frac{4T_L T_R}{(T_L + T_R)^2}$$

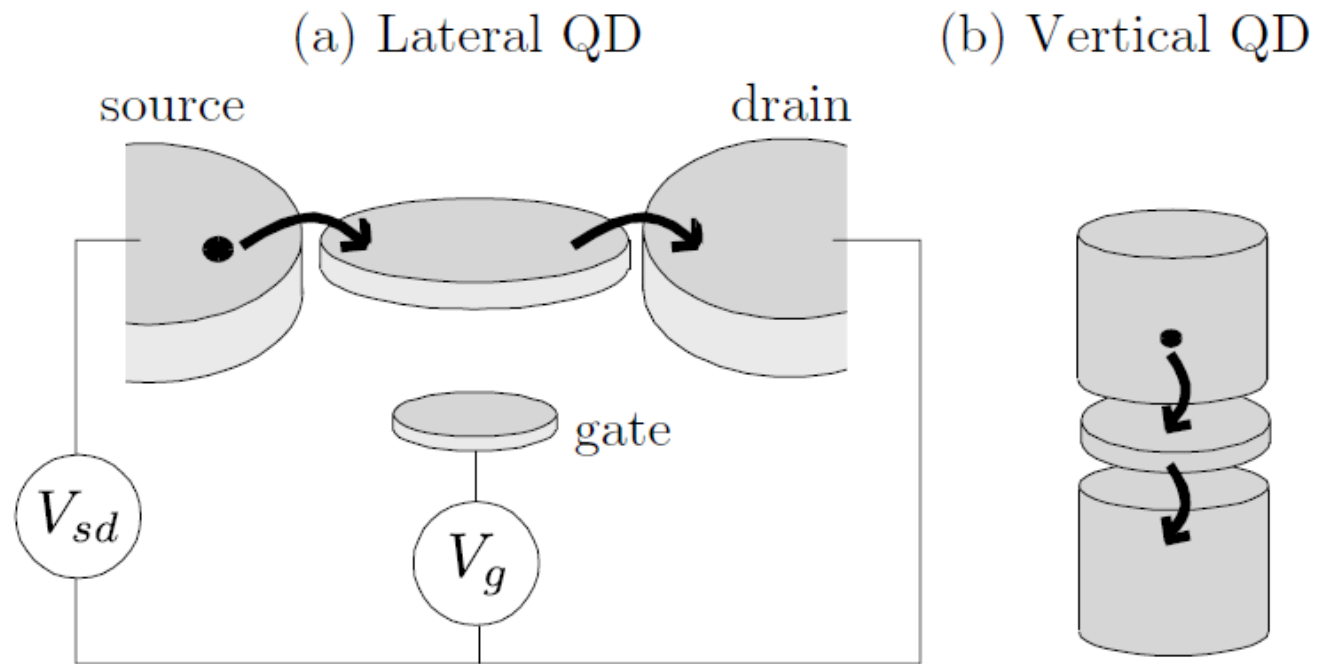
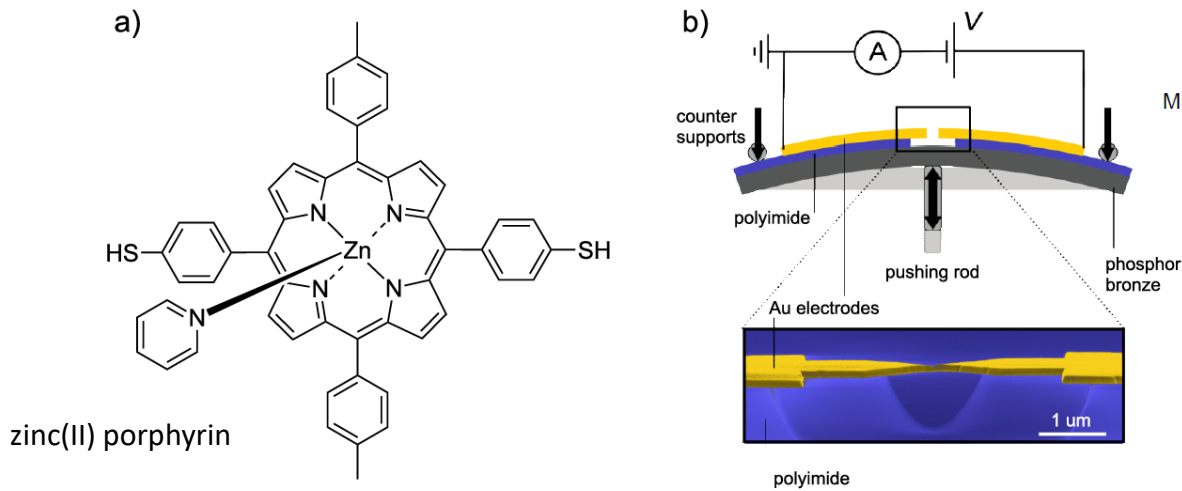


Figure 1.5: Electron flow in planar (a) and vertical (b) QD setup.

Tunnelling



Charge transport in a zinc-porphyrin single-molecule junction

Mickaël L. Perrin¹, Christian A. Martin¹, Ferry Prins¹, Ahson J. Shaikh², Rienk Eelkema², Jan H. van Esch², Jan M. van Ruitenbeek³, Herre S. J. van der Zant¹ and Diana Dulić¹

Beilstein J. Nanotechnol. **2011**, *2*, 714–719.

Figure 1: Structural formula of ZnTPPdT-Pyr (b) Top: Setup of the mechanically controllable break-junction (MCBJ). Bottom: Scanning electron micrograph of a MCBJ device (colored for clarity). The scale bar shows that the suspended bridge is about 1 μm in length.

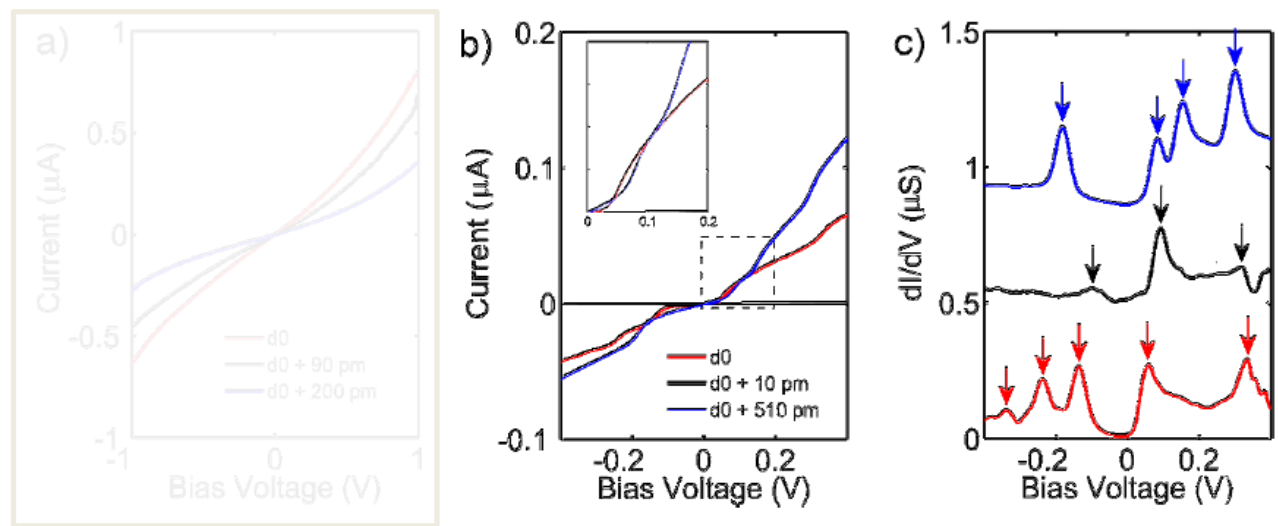
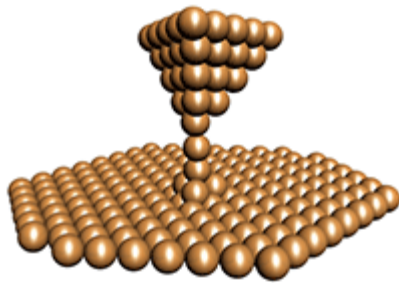
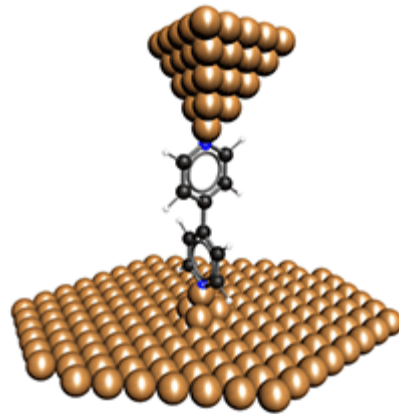


Figure 3: Low-temperature $I(V)$ characteristics of junctions exposed to (a) DCM and (b) ZnTPPdT-Pyr. The DCM sample clearly shows vacuum-tunneling behavior. The porphyrin sample exhibits Coulomb blockade and steps. (c) dI/dV of a junction exposed to a ZnTPPdT-Pyr solution; curves are offset vertically for clarity. Resonances correspond to electronic or vibrational energy levels of the molecular junction. Note, for the black line the dI/dV has been scaled by a factor of 100.

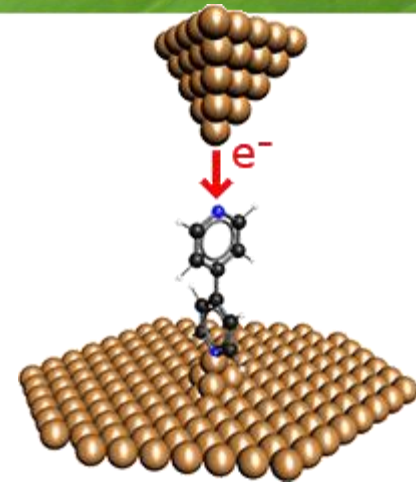
Tunnelling



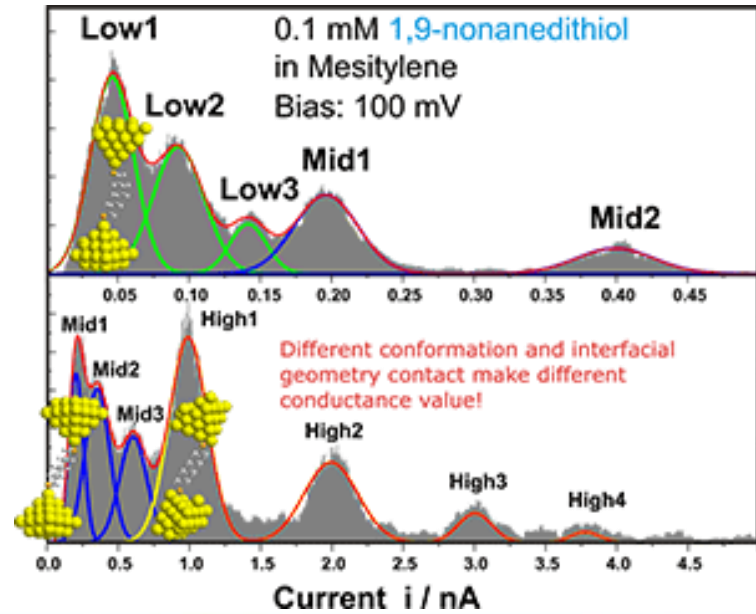
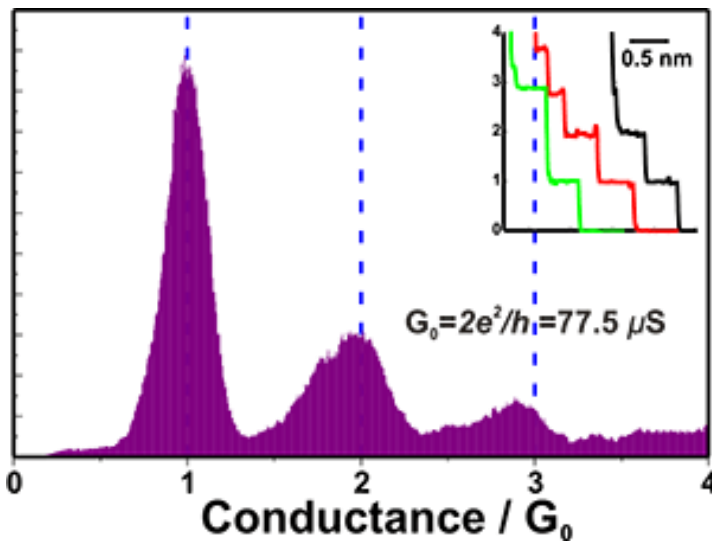
Metal nanocontact



Single molecule junction



Resonant tunneling



<http://wandlowski.dcb.unibe.ch/research/nanostructures/me.html>

Tunnelling

APPLIED PHYSICS LETTERS

VOLUME 77, NUMBER 26

25 DECEMBER 2000

Measurements of discrete electronic states in a gold nanoparticle using tunnel junctions formed from self-assembled monolayers

Jason R. Petta,^{a)} D. G. Salinas, and D. C. Ralph
Laboratory of Atomic and Solid State Physics, Cornell Univer.

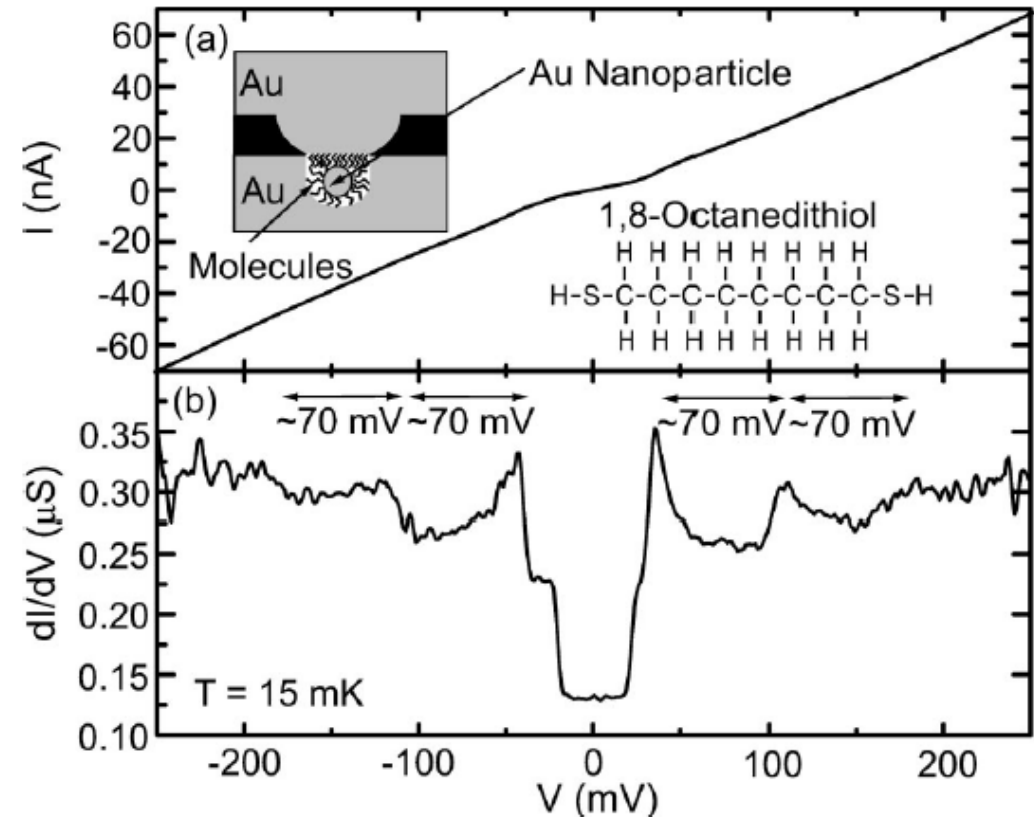


FIG. 2. (a) I - V curve for a device containing an Au nanoparticle with 1,8-octanedithiol barriers. (b) dI/dV - V determined by numerical differentiation. The regularly spaced peaks in dI/dV indicate tunneling through a single particle. Inset: Device schematic.

Tunnelling

TOPICAL REVIEW

Effects of electron–vibration coupling in transport through single molecules

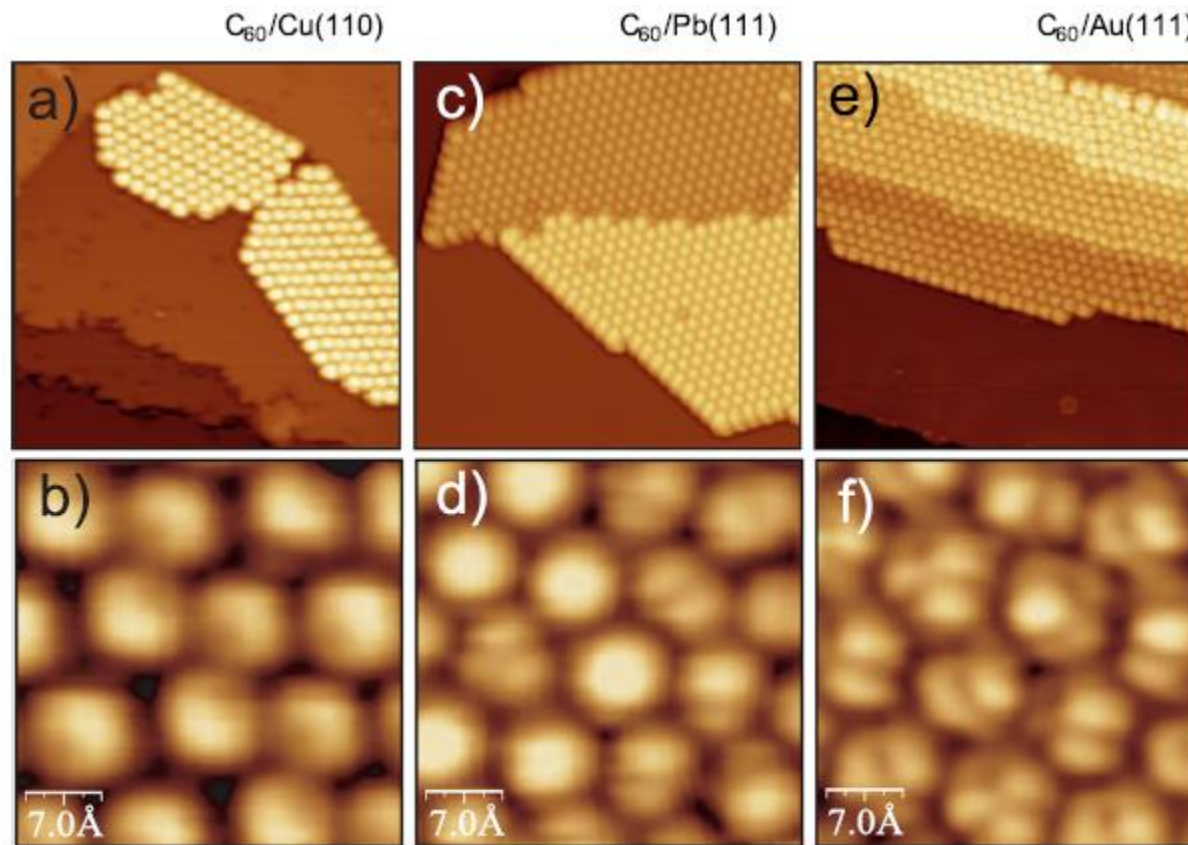
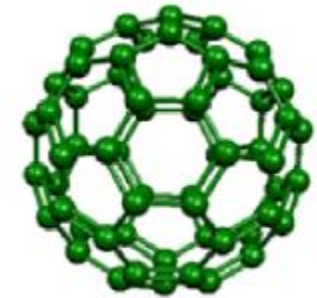


Figure 2. Large scale STM images and zoomed regions enhancing the intramolecular resolution of C_{60} monolayer islands grown on ((a), (b)) Cu(110), ((c), (d)) Pb(111) and ((e), (f)) Au(111). In all cases, the STM images were obtained with positive sample bias, hence corresponding to the unoccupied density of states. In this way, the lobed structure observed in some molecules can be identified with the spatial shape of unoccupied orbitals. Reproduced with permission from [108]. Copyright 2011 Pan Stanford Publishing.

Effects of electron–vibration coupling in transport through single molecules

Katharina J Franke and Jose Ignacio Pascual

Fachbereich Physik, Freie Universität Berlin, Arnimallee 14, 14195 Berlin, Germany

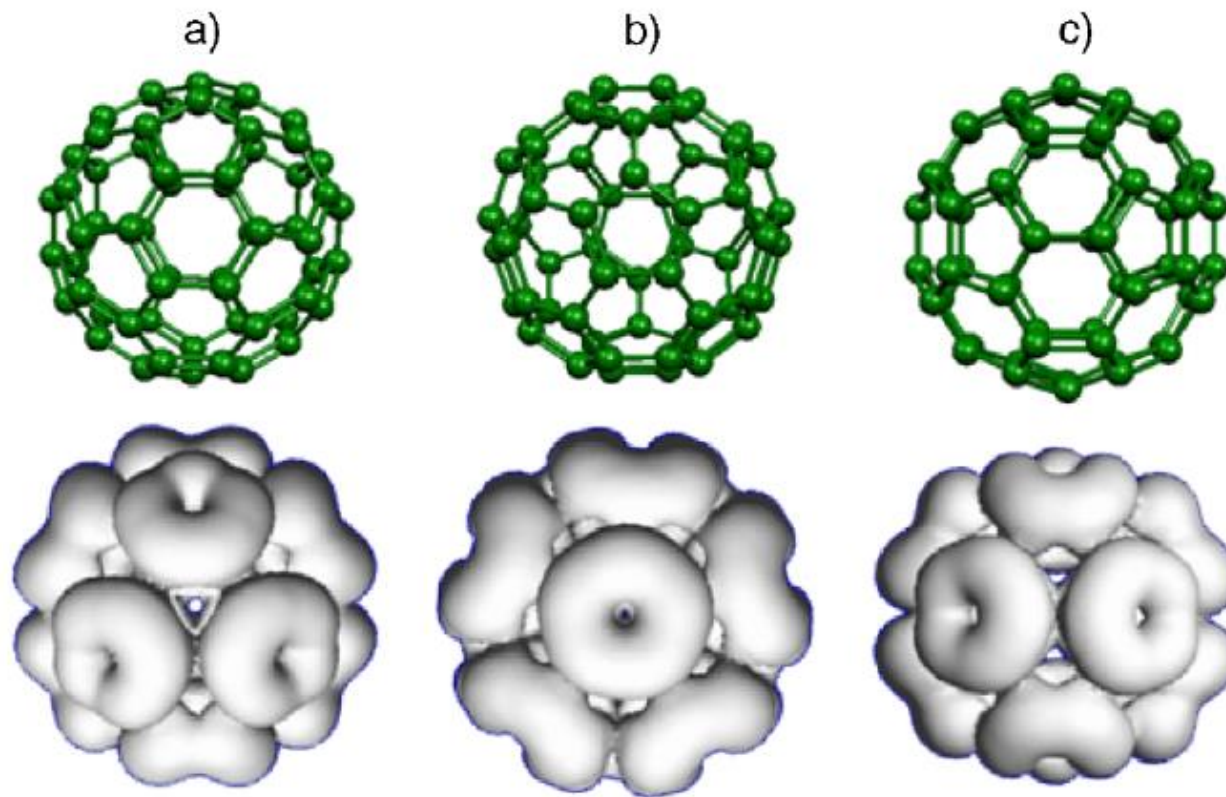


Figure 1. Molecular structure of a C₆₀ molecule. When the molecule is adsorbed on a surface, there are three outstanding high-symmetry orientations. The molecule may expose (a) a hexagon on top, (b) a pentagon on top, or (c) a C–C double bond on top. The LUMO isosurface is mainly located on the carbon pentagons, giving rise to the typical symmetries seen in STM images for the three orientations (compare figure 2).

TOPICAL REVIEW

Effects of electron–vibration coupling in transport through single molecules

Katharina J Franke and Jose Ignacio Pascual

Fachbereich Physik, Freie Universität Berlin, Arnimallee 14, 14195 Berlin, Germany

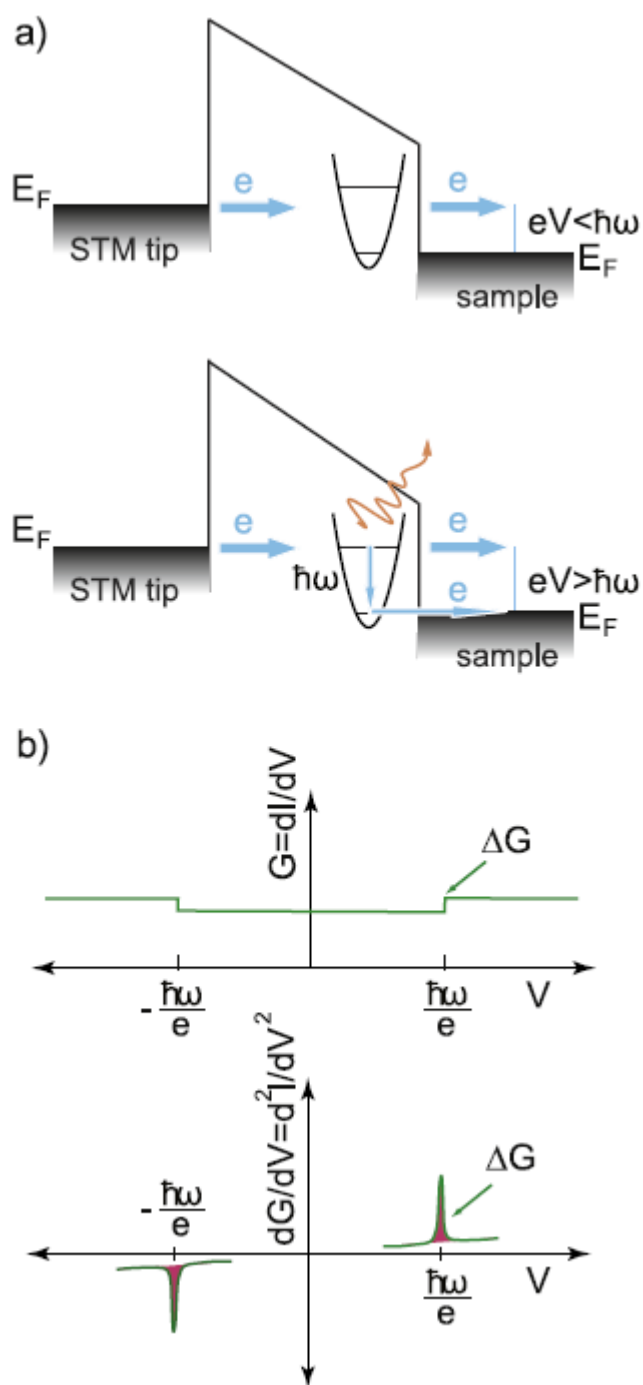


Figure 4. (a) Model potential tunneling barrier with a molecule placed in the barrier. The molecular vibrations are represented as a simple harmonic oscillator. When the energy of the tunneling electrons is below any molecular excitation they can only tunnel elastically. When the electron energy exceeds the energy threshold for molecular excitation an additional tunneling path is opened, where the electrons tunnel inelastically off the molecule. (b) The effect of the inelastic channels is ideally a small step-wise increase in the differential tunneling conductance ($dI/dV-V$). This induces a peak in the d^2I/dV^2-V spectrum.

Tunnelling

TOPICAL REVIEW

Effects of electron–vibration coupling in transport through single molecules

Katharina J Franke and Jose Ignacio Pascual

Fachbereich Physik, Freie Universität Berlin, Arnimallee 14, 14195 Berlin, Germany

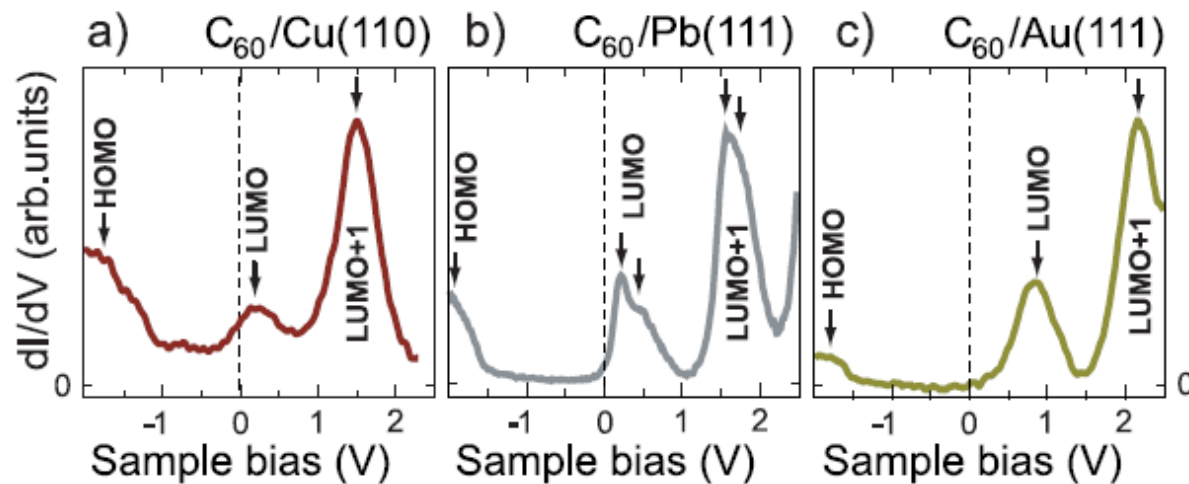


Figure 3. Differential conductance spectra of C_{60} on the different surfaces shown in figure 2. Arrows mark the fitted positions of HOMO, LUMO and LUMO + 1. The spectra were measured by positioning the STM tip on top of a single molecule and ramping the bias voltage V while keeping the tip–molecule distance constant (feedback loop open). Arrows identify the molecular states. dI/dV data were obtained by using a lock-in amplifier with an rms modulation amplitude V_{ac} . (Cu: $R_{\text{junct}} = 1.1 \text{ G}\Omega$, $V_{ac} = 20 \text{ mV}$; Pb: $R_{\text{junct}} = 0.7 \text{ G}\Omega$, $V_{ac} = 5 \text{ mV}$; Au: $R_{\text{junct}} = 0.3 \text{ G}\Omega$, $V_{ac} = 30 \text{ mV}$.) Reproduced with permission from [108]. Copyright 2011 Pan Stanford Publishing.

Tunnelling

Science

AAAS

Conductance of a Molecular Junction

M. A. Reed *et al.*

Science 278, 252 (1997);

DOI: 10.1126/science.278.5336.252

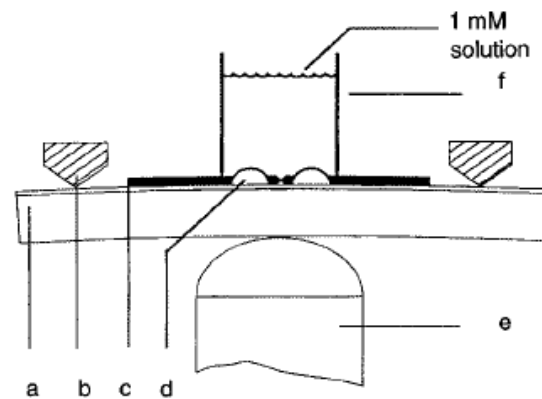
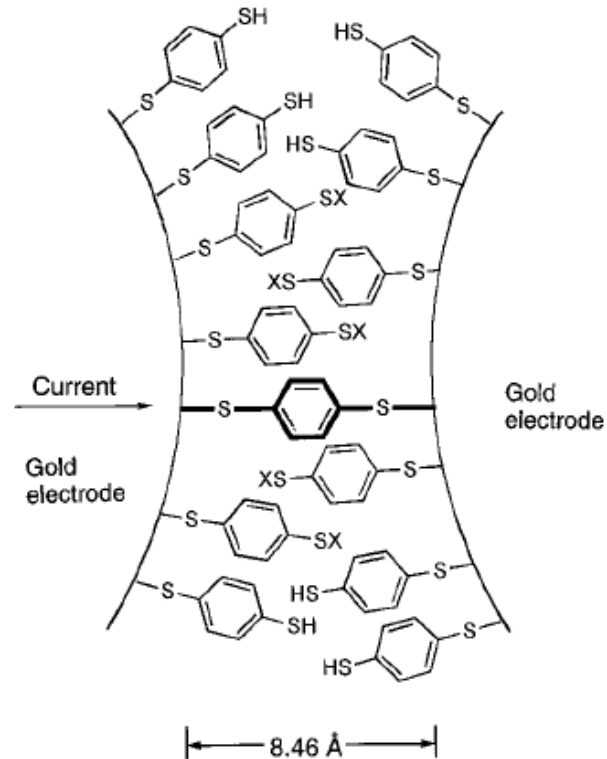
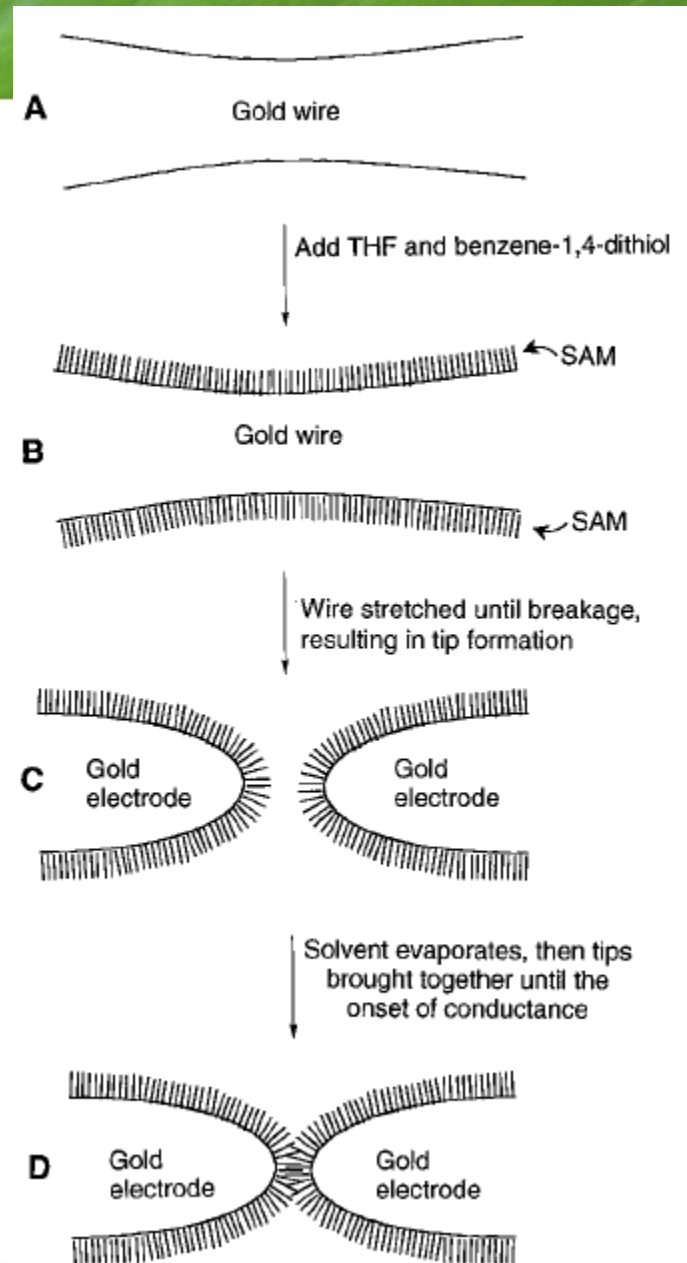


Fig. 1. A schematic of the MCB junction with (a) the bending beam, (b) the counter supports, (c) the notched gold wire, (d) the glue contacts, (e) the piezo element, and (f) the glass tube containing the solution.



Tunnelling

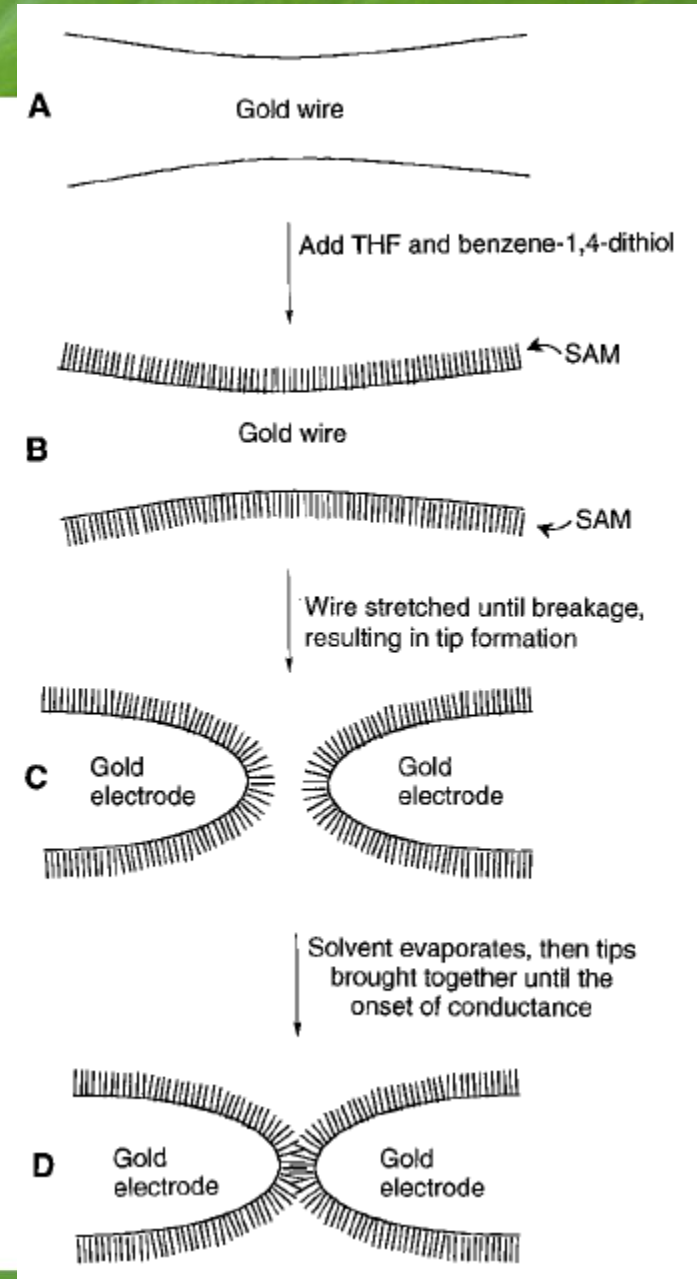
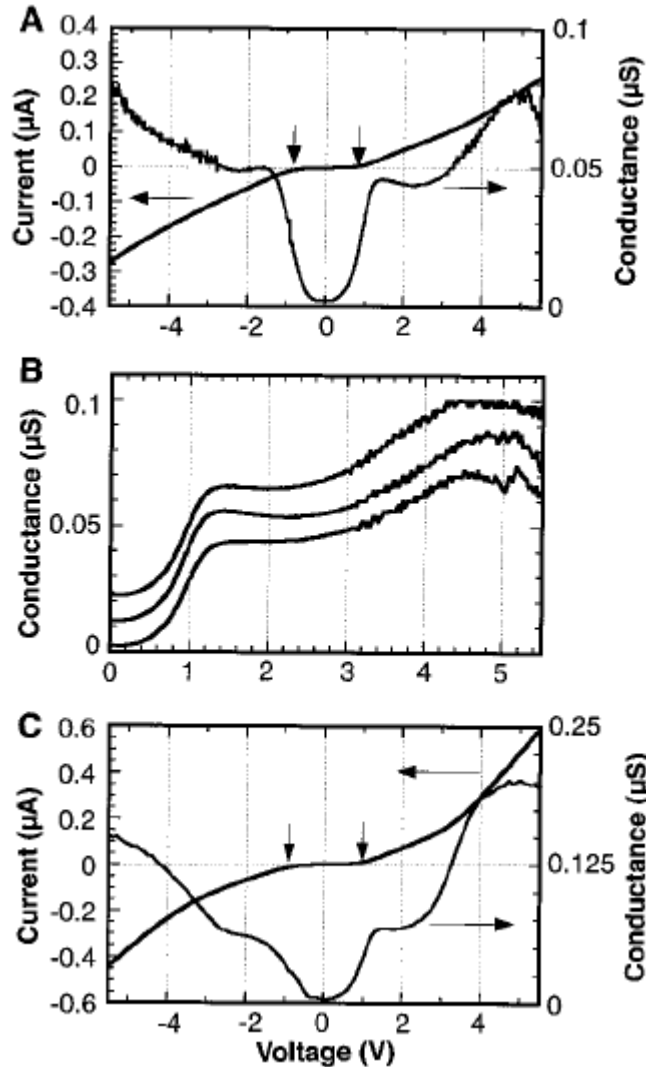
Science

AAAS

Conductance of a Molecular Junction

M. A. Reed *et al.*

Science 278, 252 (1997);



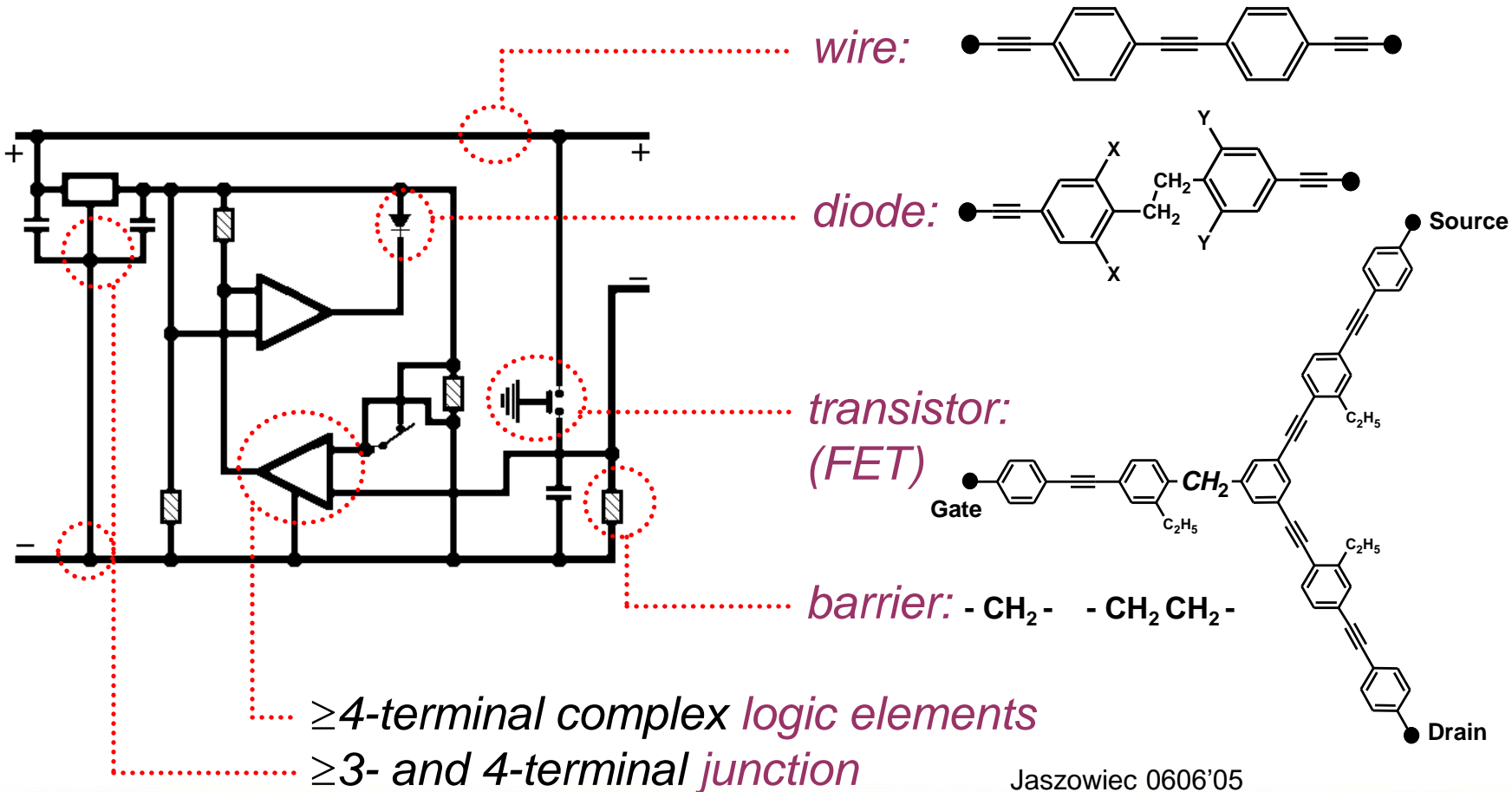
State-of-the-Art: Electronic Circuits

Kees Hummelen - University of Groningen

From macroscopic
copper ($\sim 1 \mu\text{m}$)

to

nanoscale electronics
organic molecules ($\sim 0.3\text{-}3 \text{ nm}$)



Jaszowiec 0606'05

Nanotransistors

Self-assembled monolayer organic field-effect transistors

Jan Hendrik Schön, Hong Meng & Zhenan Bao

Bell Laboratories, Lucent Technologies, Mountain Avenue, Murray Hill, New Jersey 07974, USA

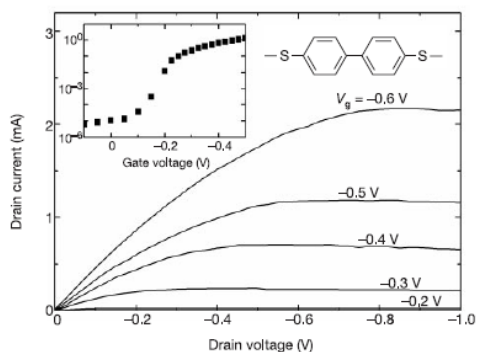


Figure 2 Transistor characteristics of a 4,4'-biphenyldithiol (molecule **2**) SAMFET at room temperature. The inset shows the transfer characteristics, that is, drain current at $V_d = -1$ V as a function of V_g .

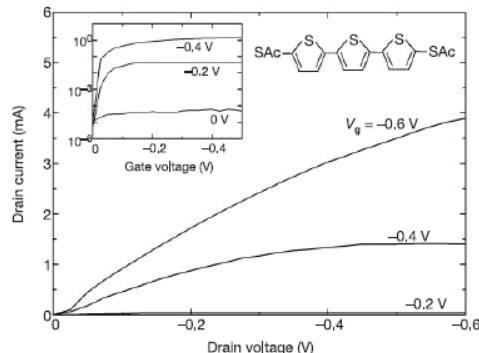


Figure 3 Transistor characteristics of molecule **6** SAMFET at room temperature. The inset shows the characteristics on a logarithmic scale. For $V_g = 0$ V, more or less linear and symmetric I - V characteristics are observed.

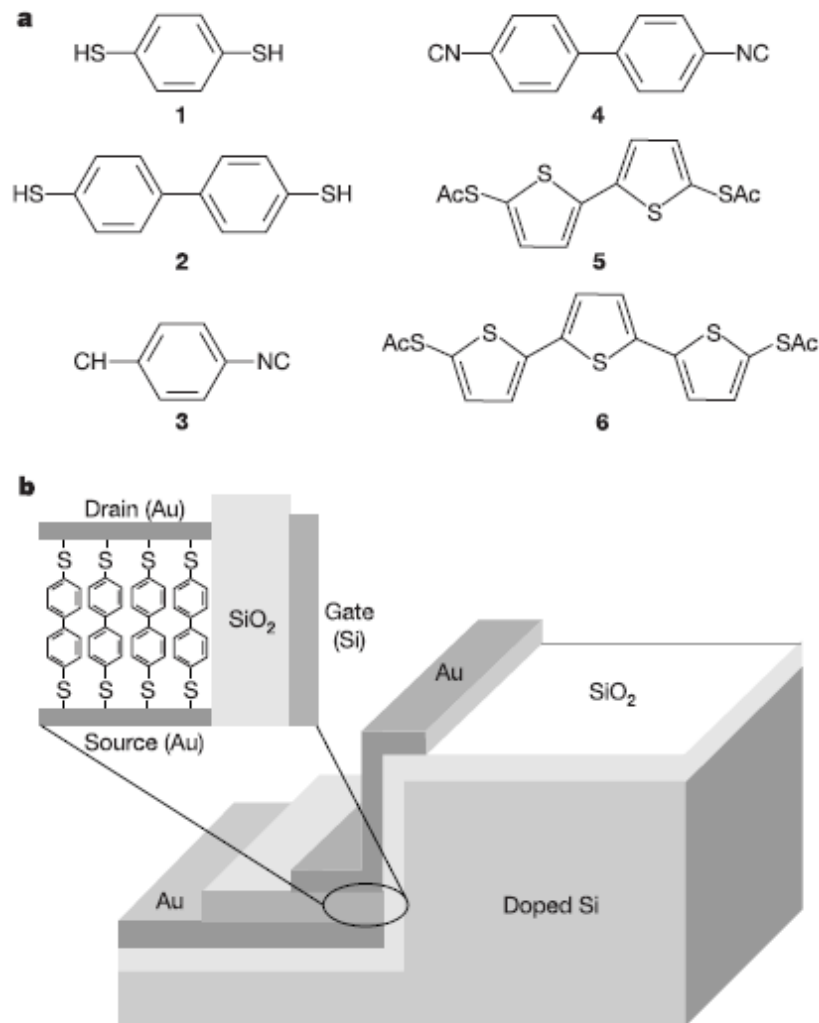


Figure 1 Structure of the investigated molecules and transistors. **a**, Molecular structure of the investigated materials; **b**, SAMFET structure: a highly doped Si-substrate is used as the gate electrode, a thermally grown SiO_2 layer acts as gate insulator, the gold source electrode is deposited by thermal evaporation, the active semiconducting material is a self-assembled monolayer (SAM) of one of the six molecules (**1**–**6**), and the drain contact is defined by shallow-angle shadow evaporation of gold. The active region of the device is magnified.

Nanotransistors

REPORT OF THE INVESTIGATION COMMITTEE ON THE POSSIBILITY OF SCIENTIFIC MISCONDUCT IN THE WORK OF HENDRIK SCHÖN AND COAUTHORS

http://www.lucent.com/news_events/pdf/researchreview.pdf

September 2002

Self-assembled monolayer organic field-effect transistors

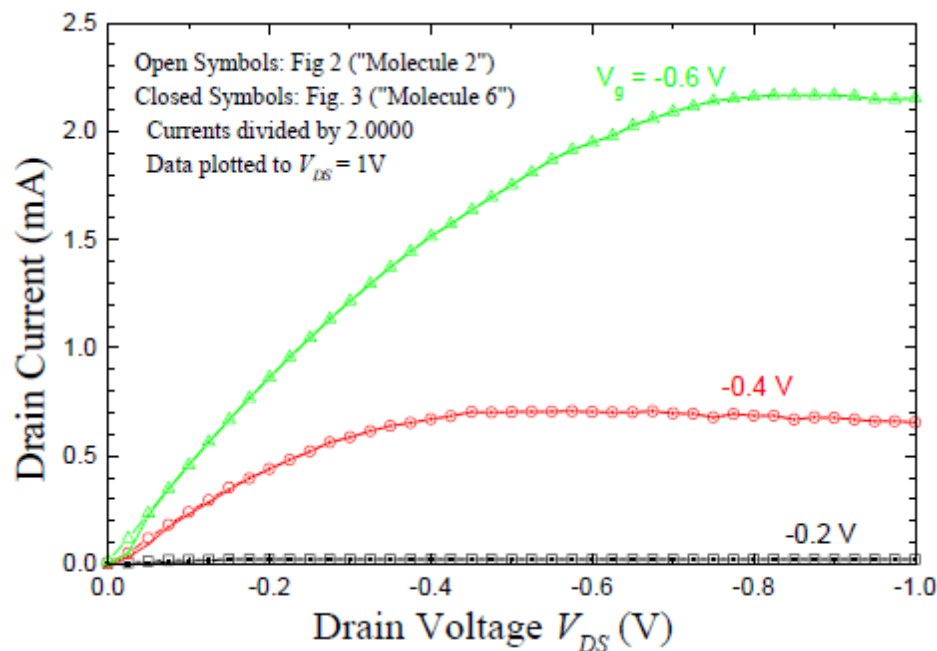
Jan Hendrik Schön, Hong Meng & Zhenan Bao

Nature 413, 713–716 (2001); correction *Nature* 414, 470 (2001).

This manuscript was, in part, the subject of an independent investigation¹ conducted at the behest of Bell Laboratories, Lucent Technologies. The independent committee reviewed concerns related to the validity of data associated with the device measurements described in the paper. As a result of the committee's findings, we are issuing a retraction of the paper. We note nevertheless that this paper may also contain some legitimate ideas and contributions. □

1. Beasley, M. R., Datta, S., Kogelnik, H., Kroemer, H. & Monroe, D. Report of the Investigation Committee on the Possibility of Scientific Misconduct in the Work of Hendrik Schön and Coauthors. (<http://publish.aps.org/reports/>) (doi:10.1103/aps.reports.lucent) (Lucent Technologies/American Physical Society, September 2002).

Figure 3. Original plotting data from Figure 1 and Figure 2 (extracted from an electronic draft), replotted to illustrate that the data present in both are exactly the same, after dividing the latter by 2. All but a few of the solid symbols are within the open symbols, and agree with each other to five significant figures, although they represent distinct data sets.



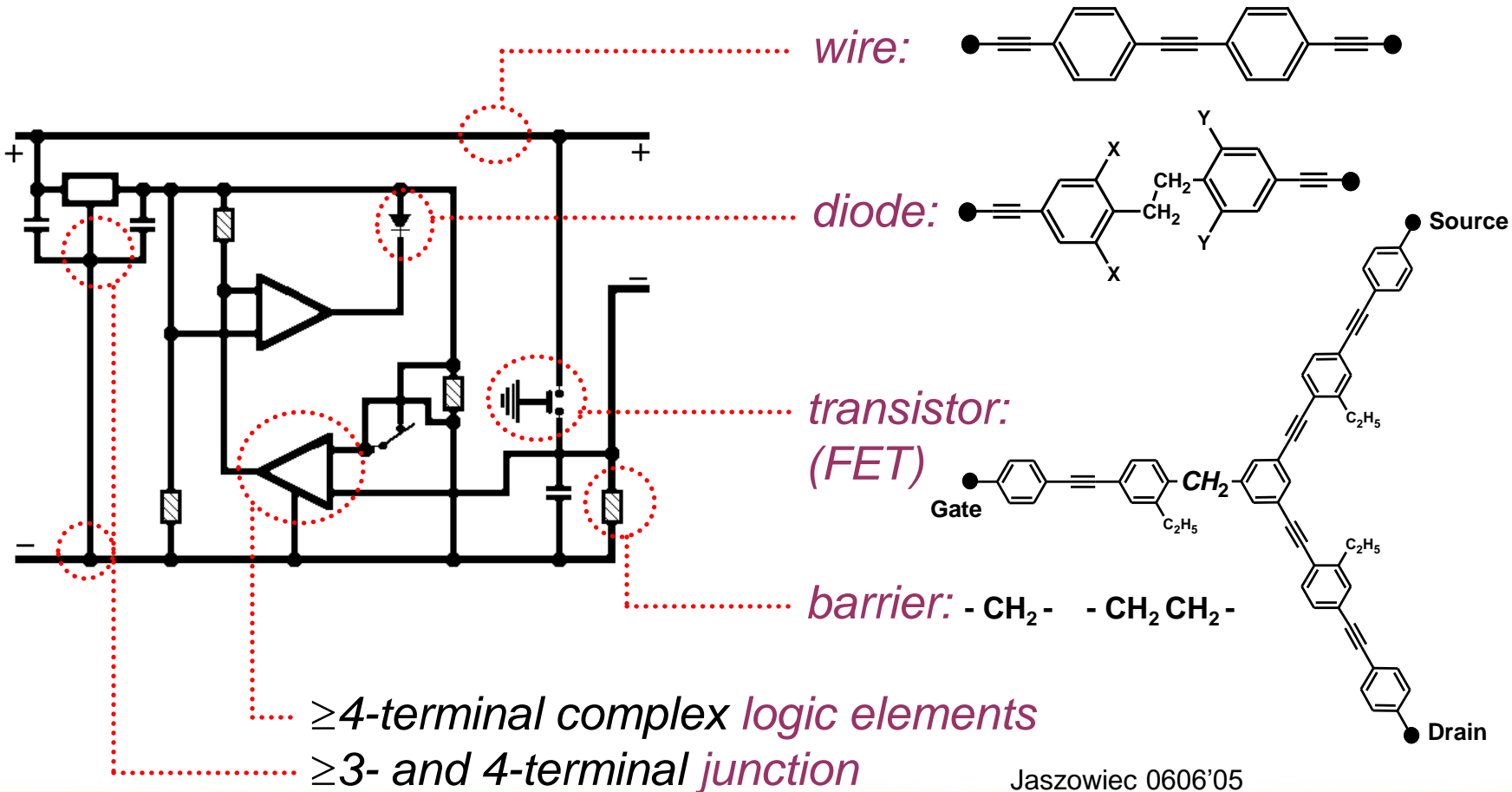
State-of-the-Art: Electronic Circuits

Kees Hummelen - University of Groningen

From macroscopic
copper ($\sim 1 \mu\text{m}$)

to

nanoscale electronics
organic molecules ($\sim 0.3\text{-}3 \text{ nm}$)



Jaszowiec 0606'05

State-of-the-Art: Electronic Circuits

Kees Hummelen - University of Groningen

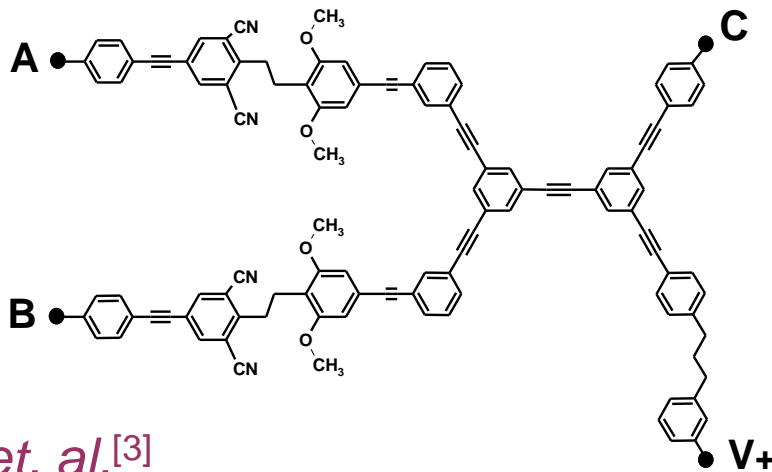
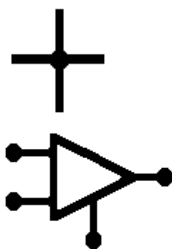
3-terminal junctions: 'T-junction' wires^[1]



M.A. Ratner et. al.^[2]

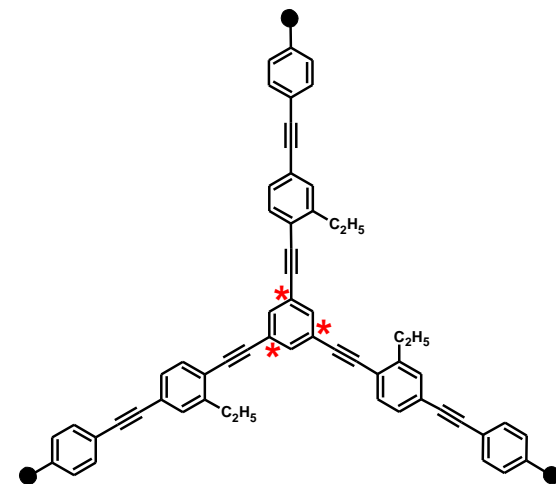
"...failure to measure transport when built on meta-positions..."

≥4-terminal: junctions ... no examples
logic elements, AND-gate:



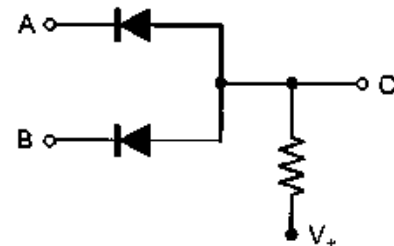
C. Joachim et. al.^[3]

"...molecules remain based on 3-branch molecules..."



AND circuit diagram

Ain	Bin	Cout
1	1	1
0	1	0
1	0	0
0	0	0



[3] *Chem. Phys. Lett.*, 2003, 367, 662.

Hwang Woo-Suk

SCIENCE VOL 308 17 JUNE 2005

Patient-Specific Embryonic Stem Cells Derived from Human SCNT Blastocysts

Woo Suk Hwang,^{1,2*} Sung Il Roh,³ Byeong Chun Lee,¹
Sung Keun Kang,¹ Dae Kee Kwon,¹ Sue Kim,¹ Sun Jong Kim,³
Sun Woo Park,¹ Hee Sun Kwon,¹ Chang Kyu Lee,² Jung Bok Lee,³
Jin Mee Kim,³ Curie Ahn,⁴ Sun Ha Paek,⁴ Sang Sik Chang,⁵
Jung Jin Koo,⁵ Hyun Soo Yoon,⁶ Jung Hye Hwang,⁶
Youn Young Hwang,⁶ Ye Soo Park,⁶ Sun Kyung Oh,⁴ Hee Sun Kim,⁴
Jong Hyuk Park,⁷ Shin Yong Moon,⁴ Gerald Schatten^{7*}

Patient-specific, immune-matched human embryonic stem cells (hESCs) are anticipated to be of great biomedical importance for studies of disease and development and to advance clinical deliberations regarding stem cell transplantation. Eleven hESC lines were established by somatic cell nuclear transfer (SCNT) of skin cells from patients with disease or injury into donated oocytes. These lines, nuclear transfer (NT)-hESCs, grown on human feeders from the same NT donor or from genetically unrelated individuals, were established at high rates, regardless of NT donor sex or age. NT-hESCs were pluripotent, chromosomally normal, and matched the NT patient's DNA. The major histocompatibility complex identity of each NT-hESC when compared to the patient's own showed immunological compatibility, which is important for eventual transplantation. With the generation of these NT-hESCs, evaluations of genetic and epigenetic stability can be made. Additional work remains to be done regarding the development of reliable directed differentiation and the elimination of remaining animal components. Before clinical use of these cells can occur, preclinical evidence is required to prove that transplantation of differentiated NT-hESCs can be safe, effective, and tolerated.

Hwang Woo-Suk



Hwang Woo-Suk

RETRACTION

Post date 12 January 2006

The final report from the Investigation Committee of Seoul National University (SNU) (1) has concluded that the authors of two papers published in *Science* (2, 3) have engaged in research misconduct and that the papers contain fabricated data. With regard to Hwang *et al.*, 2004 (2), the Investigation Committee reported that the data showing that DNA from human embryonic stem cell line NT-1 is identical to that of the donor are invalid because they are the result of fabrication, as is the evidence that NT-1 is a bona fide stem cell line. Further, the committee found that the claim in Hwang *et al.*, 2005 (3) that 11 patient-specific embryonic stem cells line were derived from cloned blastocysts is based on fabricated data. According to the report of the Investigation Committee, the laboratory "does not possess patient-specific stem cell lines or any scientific basis for claiming to have created one." Because the final report of the SNU investigation indicated that a significant amount of the data presented in both papers is fabricated, the editors of *Science* feel that an immediate and unconditional retraction of both papers is needed. We therefore retract these two papers and advise the scientific community that the results reported in them are deemed to be invalid.

As we post this retraction, seven of the 15 authors of Hwang *et al.*, 2004 (2) have agreed to retract their paper. All of the authors of Hwang *et al.*, 2005 (3) have agreed to retract their paper.

Science regrets the time that the peer reviewers and others spent evaluating these papers as well as the time and resources that the scientific community may have spent trying to replicate these results.

Donald Kennedy
Editor-in-Chief



Hwang Woo-Suk

Hwang Woo-Suk

SCIENCE VOL 303 12 MARCH 2004

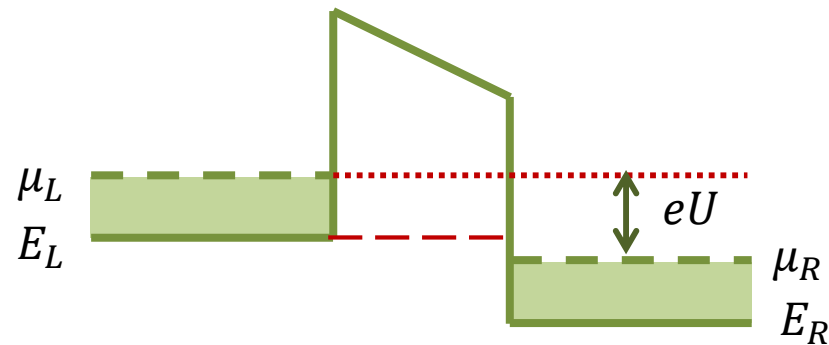
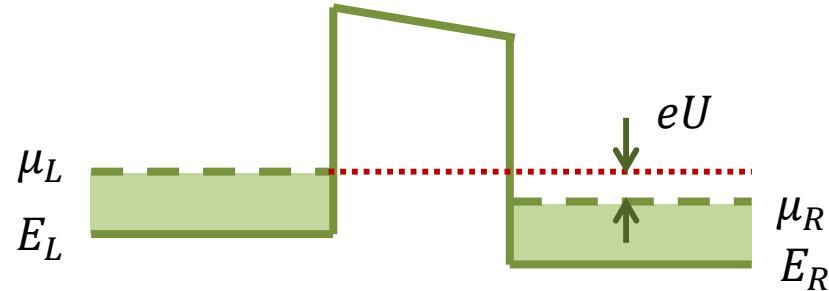
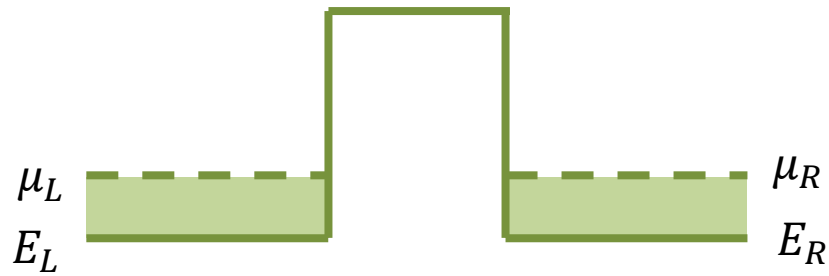
Evidence of a Pluripotent Human Embryonic Stem Cell Line Derived from a Cloned Blastocyst

Woo Suk Hwang,^{1,2*} Young June Ryu,¹ Jong Hyuk Park,³ Eul Soon Park,¹ Eu Gene Lee,¹ Ja Min Koo,⁴ Hyun Yong Jeon,¹ Byeong Chun Jung,¹ and Jung Hyun Hwang,⁵

Somatic cell nuclei from adult transgenic mice were cloned into mice to generate pluripotent embryonic stem (ES) cells. The ES cells were derived from a blastocyst. The ES cells expressed pluripotency markers and were able to differentiate into all three germ layers in severe combined immunodeficiency (SCID) mice. More than 70 passages of ES cells were maintained, and genetically identical ES cells were derived. These results exclude the possibility that the cells had a parthenogenetic origin, imprinting analyses support a SCNT origin of the derived human ES cells.



Quantized conductance



$$I = I_L + I_R$$

$$I_L = \frac{2e}{h} \int_{E_L}^{\infty} f(E, \mu_L) T(E) dE$$

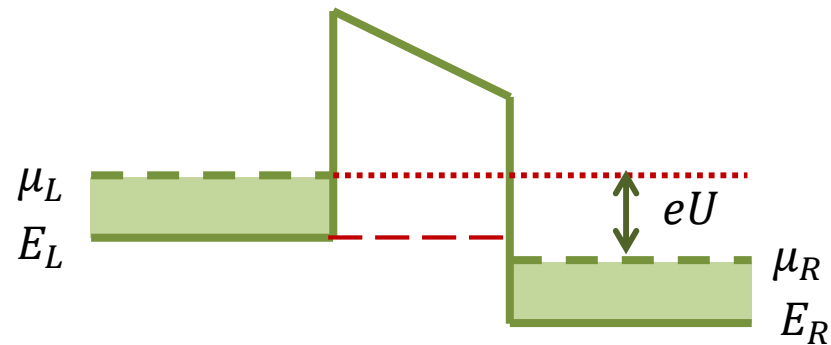
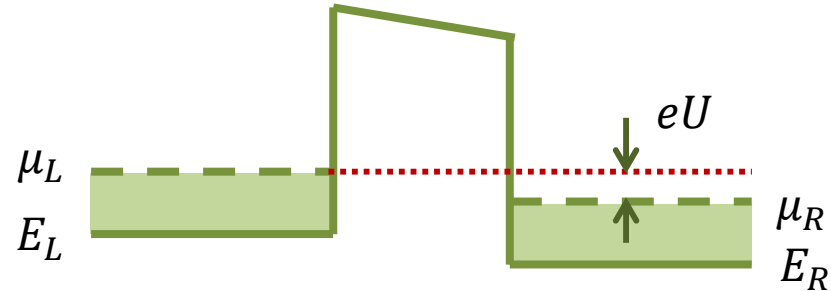
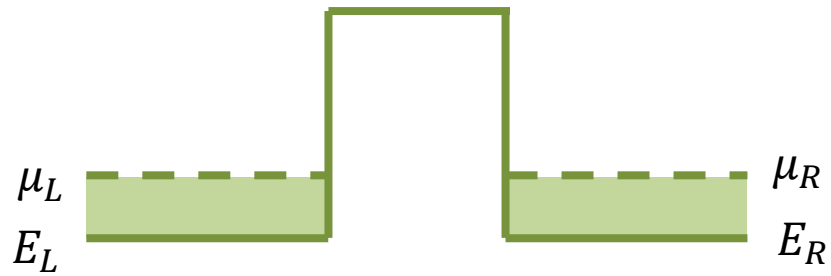
$$I_R = -\frac{2e}{h} \int_{E_R}^{\infty} f(E, \mu_R) T(E) dE$$

$$I = \frac{2e}{h} \int_{E_L}^{\infty} [f(E, \mu_L) - f(E, \mu_R)] T(E) dE$$

On exercises

$$I = \frac{2e}{h} \int_{E_L}^{\infty} f(E, \mu_L) T(E) dE$$

Quantized conductance

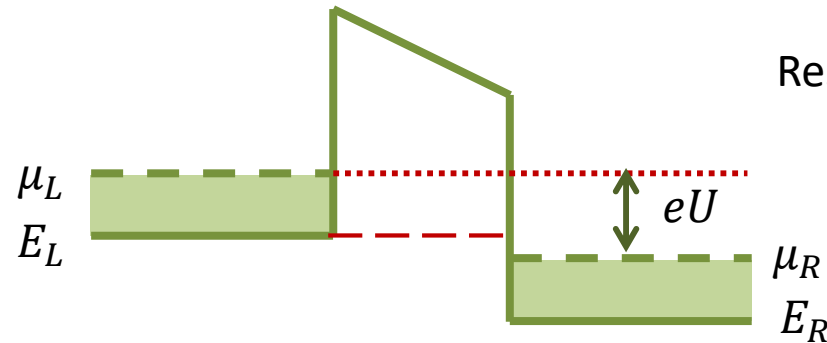
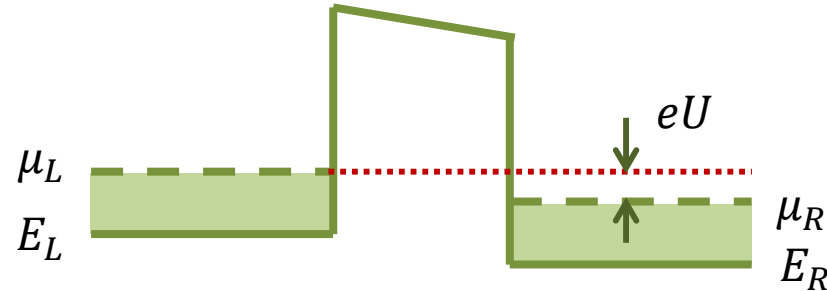
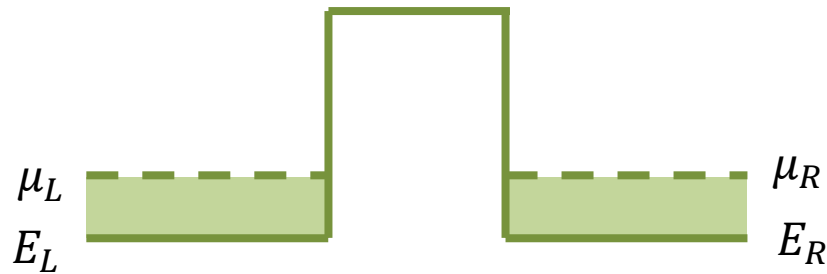


For temperatures $T \rightarrow 0$:

$$I = \frac{2e}{h} \int_{\mu_R}^{\mu_L} [f(E, \mu_L) - f(E, \mu_R)] T(E) dE$$

$$I = \frac{2e}{h} \int_{E_L}^{\mu_L} f(E, \mu_L) T(E) dE$$

Quantized conductance



For metals $\mu_L = \mu + \frac{1}{2}eU$ i $\mu_R = \mu - \frac{1}{2}eU$:

$$f(E, \mu_L) - f(E, \mu_R) \approx eU \frac{\partial f(E, \mu)}{\partial \mu} = -eU \frac{\partial f(E, \mu)}{\partial E}$$

$$I = \frac{2e^2 U}{h} \int_{E_L}^{\infty} \frac{\partial f(E, \mu)}{\partial E} T(E) dE$$

$$G = \frac{dI}{dU} = \frac{2e^2}{h} \int_{E_L}^{\infty} \frac{\partial f(E, \mu)}{\partial E} T(E) dE \approx \frac{2e^2}{h} T(\mu)$$

Resistance is finite even for the ideal conductor!

$$\frac{e^2}{h} = 38,7 \mu\text{S}$$

$$\frac{h}{e^2} = 25,8 \text{ k}\Omega$$

Quantized conductance (S – Simens)

Quantized conductance

$$G = \frac{dI}{dU} = \frac{2e^2}{h} \int_{E_L}^{\infty} \frac{\partial f(E, \mu)}{\partial E} T(E) dE \approx \frac{2e^2}{h} T(\mu) = 2G'_0 T(\mu) = G_0 T(\mu)$$

$$\frac{e^2}{h} = 38,7 \mu S$$

Different definitions of G_0 - more often with 2:

$$\frac{2e^2}{h} = 77,4 \mu S$$

Landauer formula (*wzór Landauera*) – when dealing with multiple channels of the conductance

$$G = G_0 \sum_n T_n(\mu) \approx NG'_0$$

Mind the definition of G_0 !

N is the sum of various conductivity channels
eg. two different spins give $N = 2$

For $T = const$ we obtain Ohm law.

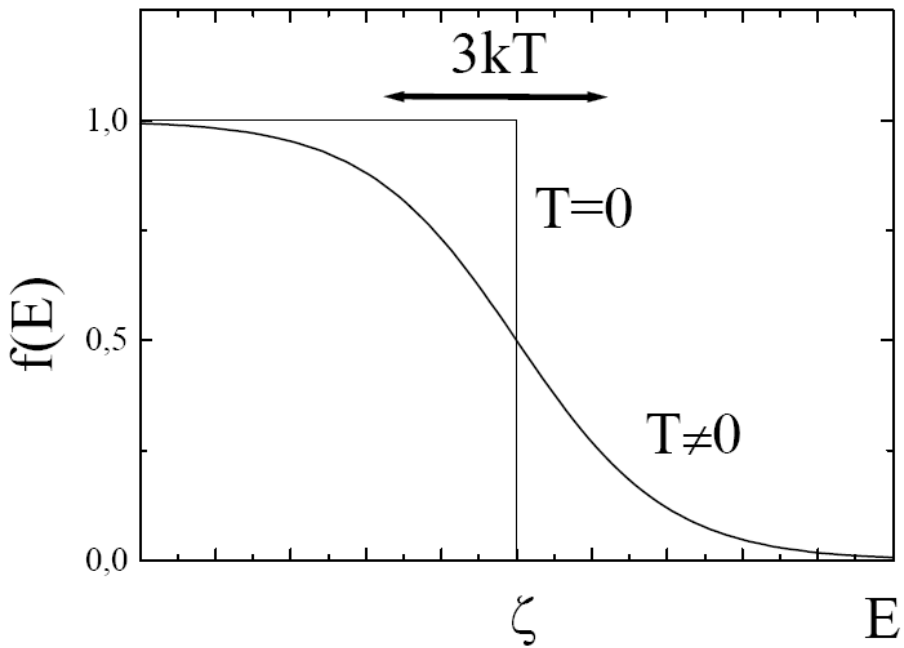
Classical metal

DIGRESSION

The system in the thermodynamic equilibrium at $T \neq 0$ (under $V = \text{const}$ i $N = \text{const}$) corresponds to the minimum of the Helmholtz free energy $F = U - TS$, and not the minimum of U – states with higher energies are also occupied.

For fermions in thermodynamical equilibrium - Fermi-Dirac distribution (μ – chemical potential, "Fermi level"):

$$f(E, T) = \frac{1}{e^{\frac{E-\mu}{k_B T}} + 1}$$



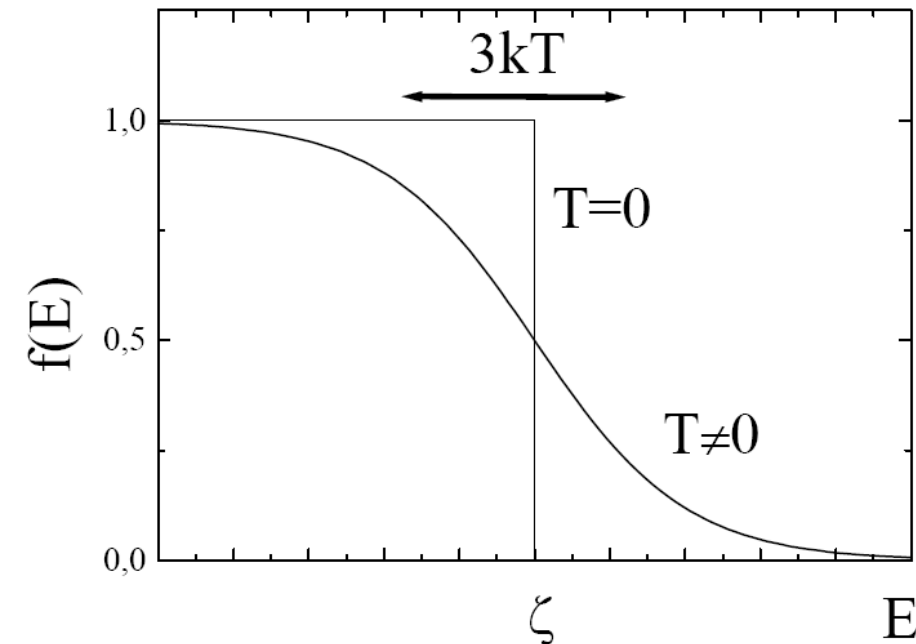
- $0 < f(E) < 1$
- $f(\mu) = 0,5$
- for $T = 0$ – step-like distribution
- for $T \neq 0$ – the smear of $3 kT$
- $1 - f(E)$ – the the probability that the state is unoccupied

Classical metal

Derivative of Fermi-Dirac distribution

$$f(E, T) = \frac{1}{e^{\frac{E-\mu}{k_B T}} + 1} \equiv \frac{1}{e^x + 1}$$
$$-\frac{\partial f(x)}{\partial x} = \frac{e^x}{(e^x + 1)^2} = \frac{e^{-x}}{(e^{-x} + 1)^2}$$

It is an even function, for which:



$$\int_{-\infty}^{\infty} \left(-\frac{\partial f(x)}{\partial x} \right) dx = 1$$

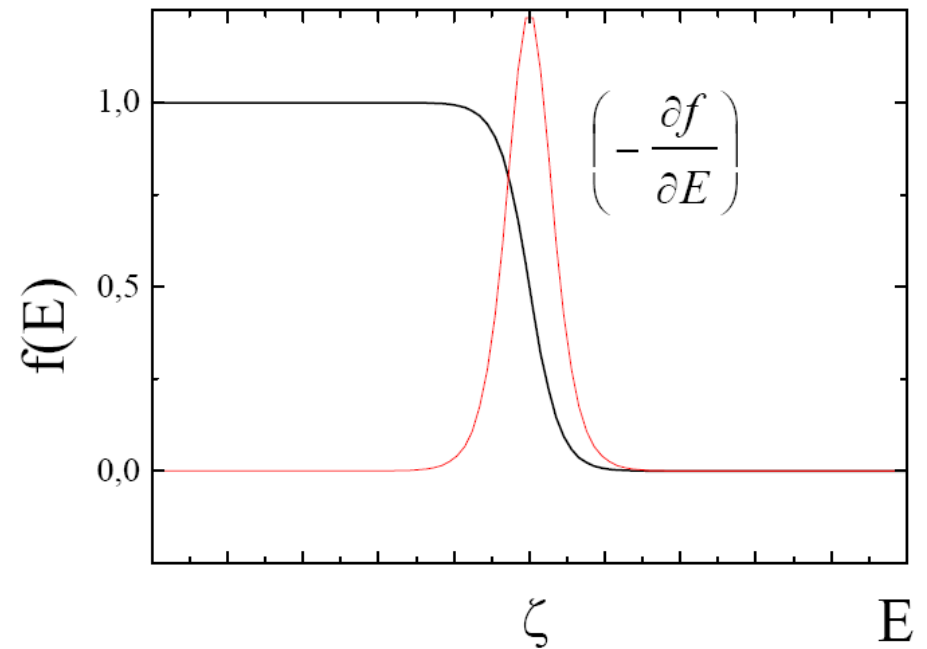
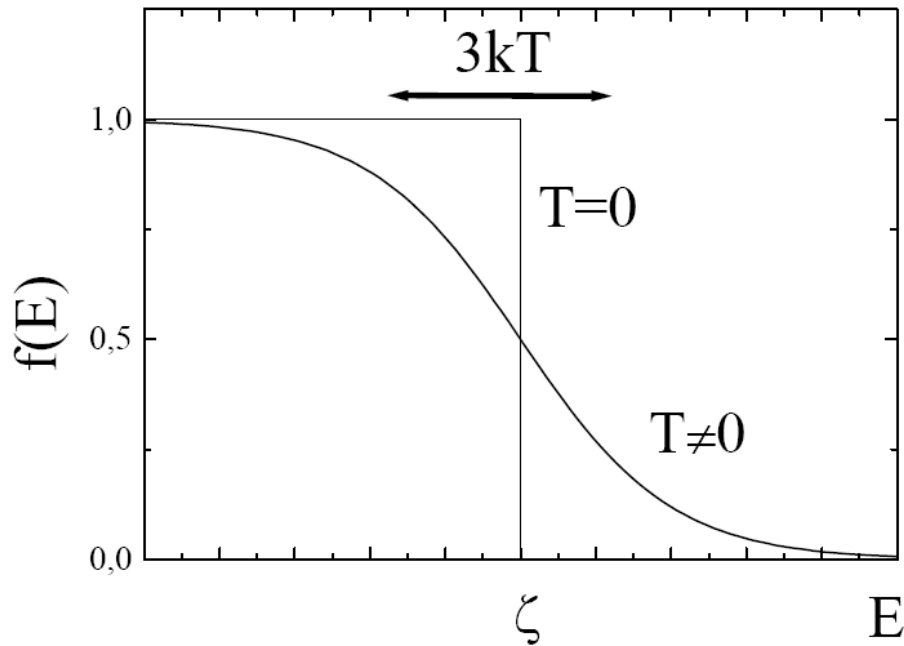
Czyli dla $T \rightarrow 0$

$$-\frac{\partial f(E, T)}{\partial E} = \delta(\mu)$$

Classical metal

Thus, for $T \rightarrow 0$

$$-\frac{\partial f(E, T)}{\partial E} = \delta(\mu)$$



Classical metal

The statistical average (of the energy-dependent quantity):

Let $A(E)$ is an energy-dependent physical quantity of the electron

$$A(T) = \int_{SB} A(E(\vec{k})) \cdot f(E(\vec{k}), T) \cdot \rho(\vec{k}) dV_k = \int_{band} A(E) \cdot f(E, T) \cdot \rho(E) dE$$

A(T) is a thermodynamically averaged total contribution to the quantity A of all the electrons in the band;

For example, the concentration of electrons in the band ($A = 1$):

$$A(T) \equiv n(T) = \int_{SB} 1 \cdot f(E(\vec{k}), T) \cdot \rho(\vec{k}) dV_k = \int_{band} 1 \cdot f(E, T) \cdot \rho(E) dE$$

Classical metal

The statistical average (of the energy-dependent quantity):

Let $A(E)$ is an energy-dependent physical quantity of the electron

$$A(T) = \int_{SB} A(E(\vec{k})) \cdot f(E(\vec{k}), T) \cdot \rho(\vec{k}) dV_k = \int_{band} A(E) \cdot f(E, T) \cdot \rho(E) dE$$

$A(T)$ is a thermodynamically averaged total contribution to the quantity A of all the electrons in the band;

For metals $\mu \equiv E_F \approx 5$ eV, thus $\frac{E_F}{k_B T} \gg 1$ at $T = 300$ K ($k_B T = 25$ meV). Therefore

$$G(E) = \int_0^E A(E') \cdot \rho(E') dE'$$

we obtain

$$A(T) = \int_{band} A(E) \cdot f(E, T) \cdot \rho(E) dE = \int_{band} \frac{\partial G}{\partial E} \cdot f(E, T) dE$$

Classical metal

The statistical average (of the energy-dependent quantity):

$$\begin{aligned}
 A(T) &= \int_{\text{band}} A(E) \cdot f(E, T) \cdot \rho(E) dE = \int_{\text{band}} \frac{\partial G}{\partial E} \cdot f(E, T) dE = \int_0^{E_{\max}} \frac{\partial G}{\partial E} \cdot f(E, T) dE \approx \\
 &\approx [G(E) \cdot f(E, T)] \Big|_0^{E_{\max}} - \int_0^{E_{\max}} G(E) \cdot \left(\frac{\partial f}{\partial E} \right) dE \approx \int_0^{\infty} G(E) \cdot \left(-\frac{\partial f}{\partial E} \right) dE
 \end{aligned}$$

Vanishes in 0, because $\rho(0) = 0$

For metals: vanishes in E_{\max} , because $f(E) = 0$

Introducing $x = \frac{E - E_F}{k_B T}$ thus $E = E_F + x k_B T$

$$A(T) = \int_0^{\infty} G(E) \cdot \left(-\frac{\partial f}{\partial E} \right) dE = \int_{-\frac{E_F}{k_B T}}^{\infty} G(E_F + x k_B T) \cdot \left(-\frac{\partial f}{\partial x} \right) dx \approx \int_{-\infty}^{\infty} \dots dx$$

Classical metal

The statistical average (of the energy-dependent quantity):

Introducing $x = \frac{E-E_F}{k_B T}$ thus $E = E_F + x k_B T$

$$A(T) \approx \int_{-\infty}^{\infty} G(E_F + x k_B T) \cdot \left(-\frac{\partial f}{\partial x} \right) dx$$

Due to the strong degeneration only the values near $x = 0$ give important contribution to the integral \Rightarrow expanding G :

$$G(E_F + x k_B T) = G(E_F) + \left(\frac{\partial G}{\partial E} \right)_{E_F} x k_B T + \frac{1}{2} \left(\frac{\partial^2 G}{\partial E^2} \right)_{E_F} x^2 (k_B T)^2 + \dots$$

Using the integration by parts and the formula:

$$\int_0^{\infty} \frac{x}{e^x + 1} dx = \frac{\pi^2}{12}$$

We obtain:

$$A(T) \approx \int_0^{E_F} A(E) \cdot \rho(E) dE + \frac{\pi^2}{6} (k_B T)^2 \left(\frac{\partial [A(E) \cdot \rho(E)]}{\partial E} \right)_{E_F}$$

Classical metal

end of DIGRESSION

The statistical average (of the energy-dependent quantity):

The example:

The dependence $E_F(T)$ (substituting $A(E) = 1$ and assuming $n(T) = const$)

$$A(T) \approx \int_0^{E_F} A(E) \cdot \rho(E) dE + \frac{\pi^2}{6} (k_B T)^2 \left(\frac{\partial [A(E) \cdot \rho(E)]}{\partial E} \right)_{E_F}$$
$$E_F = E_{F0} - \frac{\pi^2}{6} (k_B T)^2 \left(\frac{\partial [\ln \rho(E)]}{\partial E} \right)_{E_F}$$

The example :

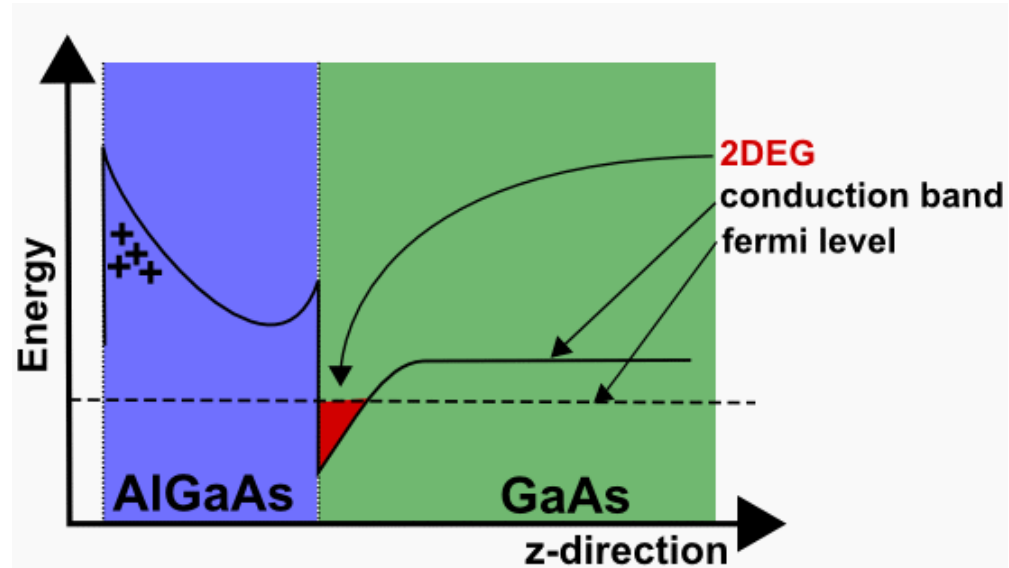
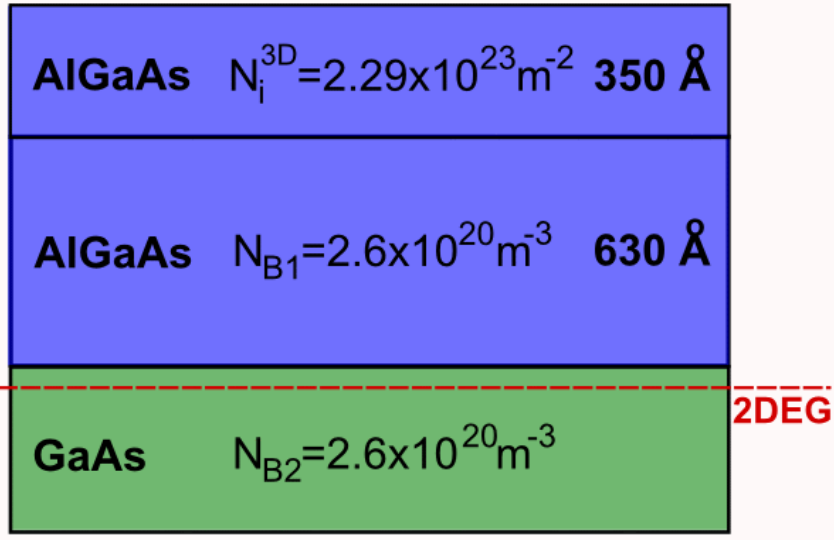
Internal energy of the electron gas (substituting $A(E) = E$)

$$U(T) = U_0 - \frac{\pi^2}{6} (k_B T)^2 \rho(E_F)$$

In metals, the density of states at the Fermi surface decides!

Triangular well

WKB approximation (Wentzel – Krammers – Brillouin) – for slowly varying potential

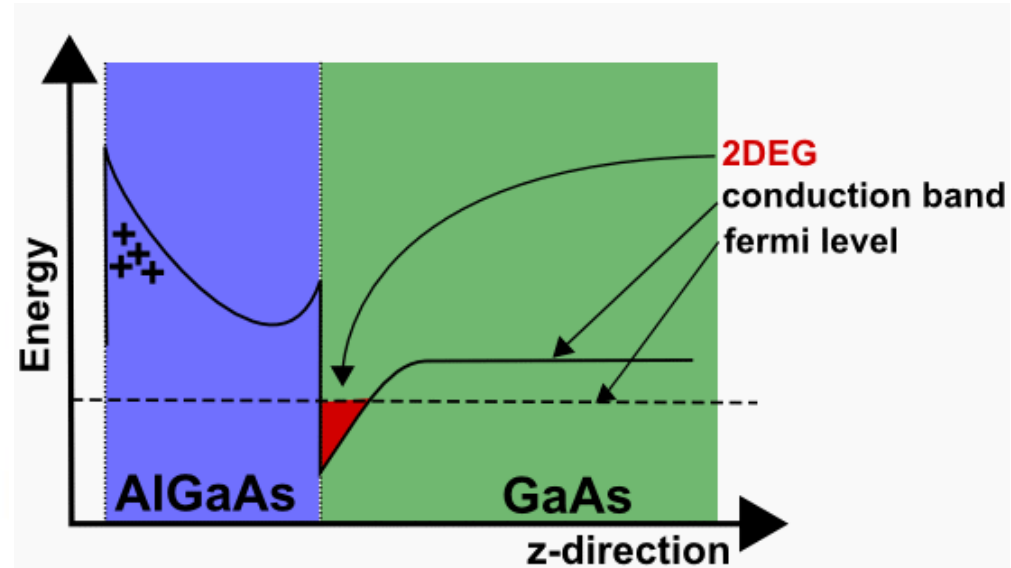
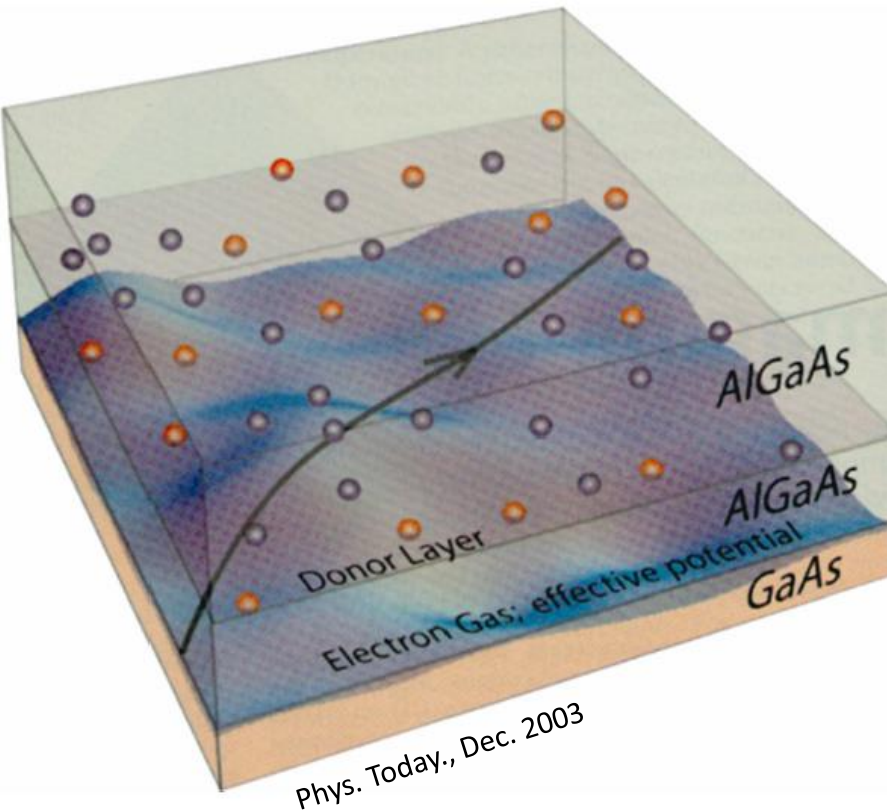


http://www.phys.unsw.edu.au/QED/research/2D_scattering.htm

$$E_n = \left[\frac{3}{2} \pi \left(n - \frac{1}{4} \right) \right]^{2/3} \left[\frac{(eF\hbar)^2}{2m} \right]^{1/3}$$

Triangular well

WKB approximation (Wentzel – Krammers – Brillouin) – for slowly varying potential



http://www.phys.unsw.edu.au/QED/research/2D_scattering.htm

$$E_n = \left[\frac{3}{2} \pi \left(n - \frac{1}{4} \right) \right]^{2/3} \left[\frac{(eF\hbar)^2}{2m} \right]^{1/3}$$

Quantized conductance

$$G = \frac{dI}{dU} = \frac{2e^2}{h} \int_{E_L}^{\infty} \frac{\partial f(E, \mu)}{\partial E} T(E) dE \approx \frac{2e^2}{h} T(\mu) = G_0 T(\mu)$$

$$\frac{e^2}{h} = 38,7 \mu S$$

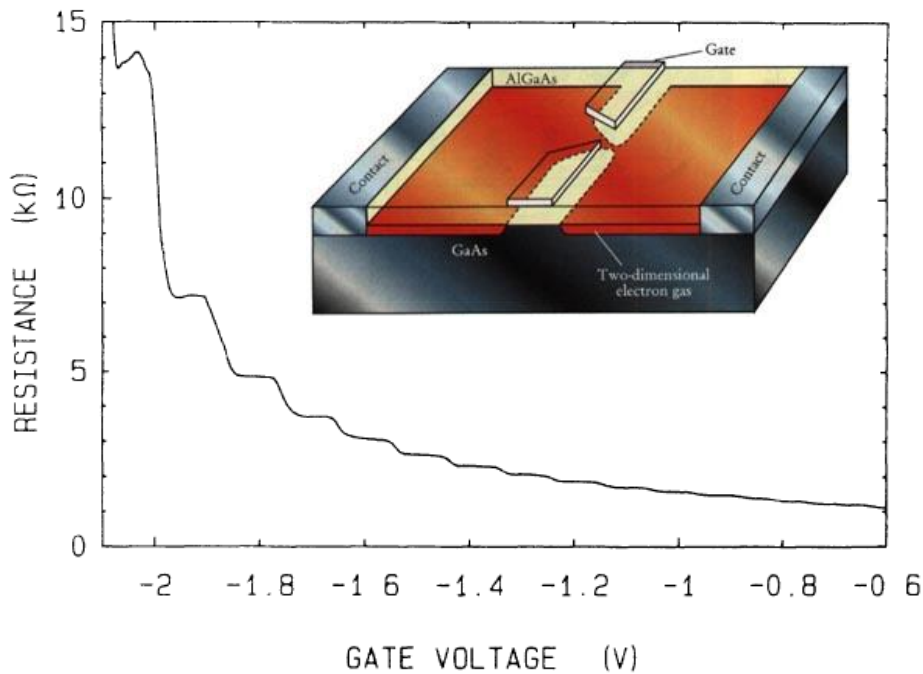


FIG. 1. Point-contact resistance as a function of gate voltage at 0.6 K. Inset: Point-contact layout.

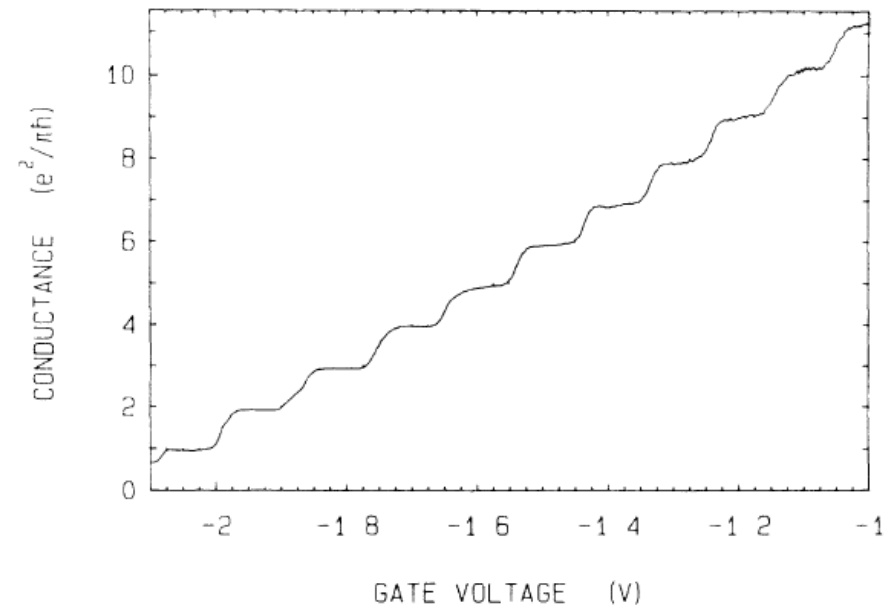
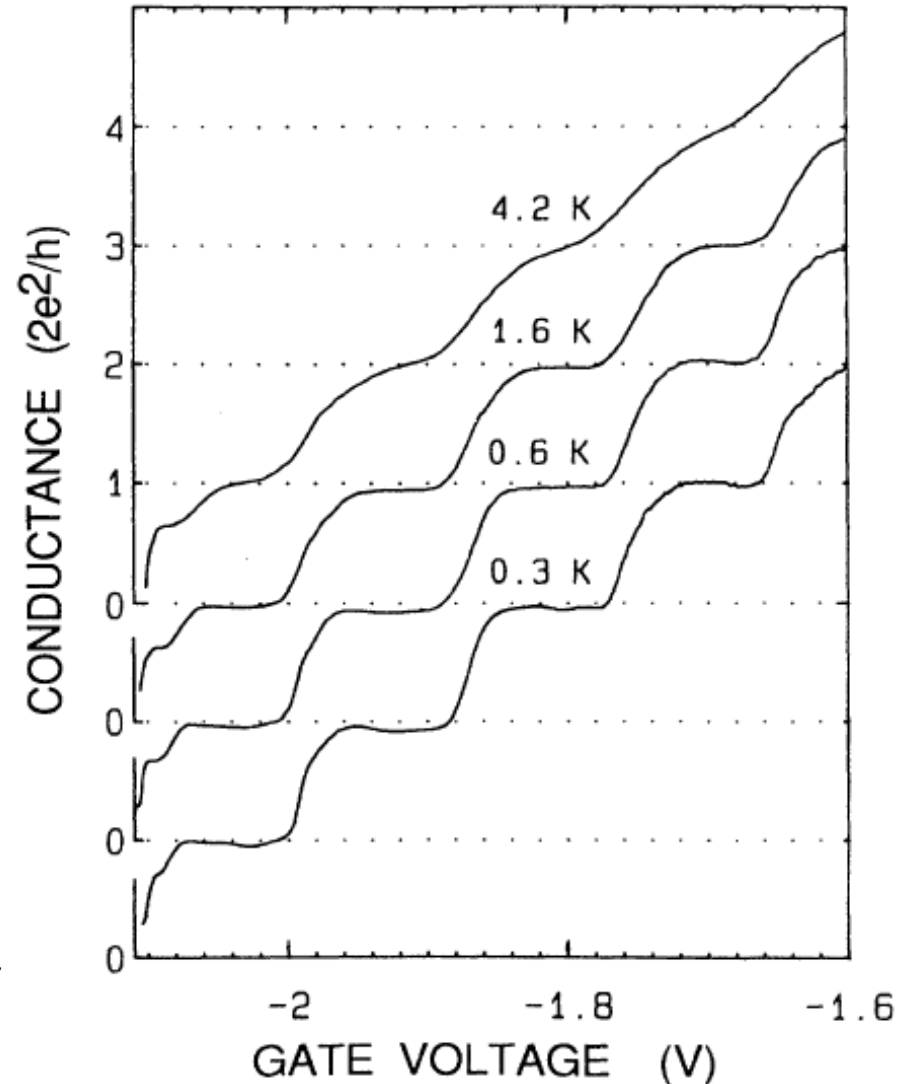


FIG. 2. Point-contact conductance as a function of gate voltage, obtained from the data of Fig. 1 after subtraction of the lead resistance. The conductance shows plateaus at multiples of $e^2/\pi\hbar$.

B. J. van Wees et al. *Quantized conductance of point contacts in a two-dimensional electron gas*
 Phys. Rev. Lett. **60**, 848–850 (1988)

Quantized conductance

$$G = \frac{2e^2}{h} T(\mu) = G_0 T(\mu)$$

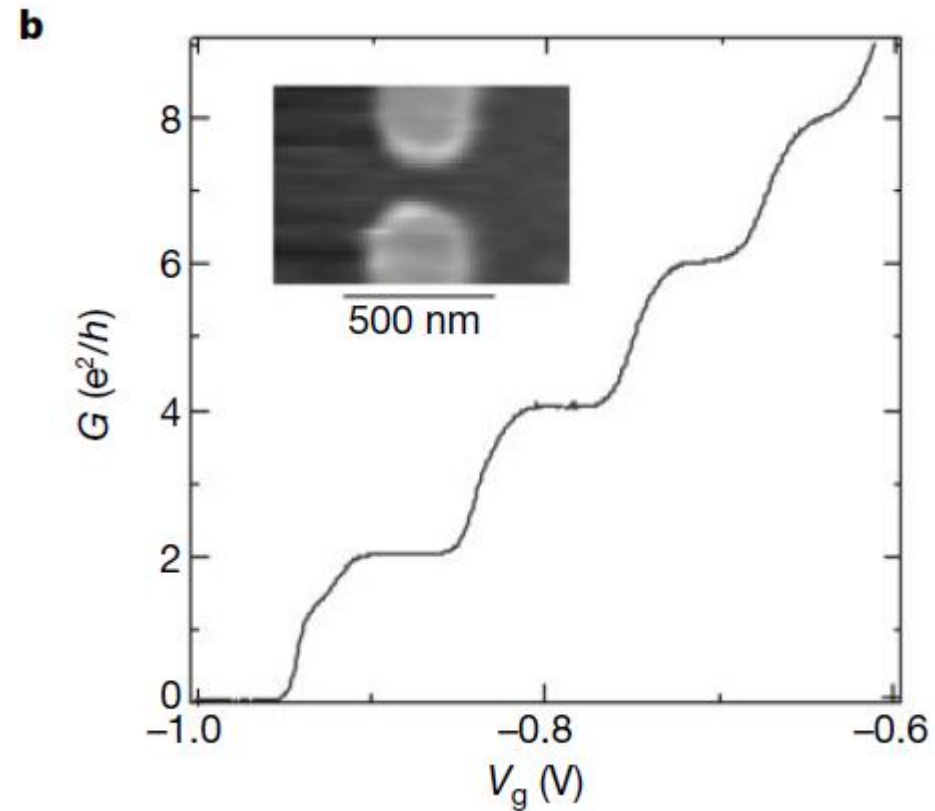
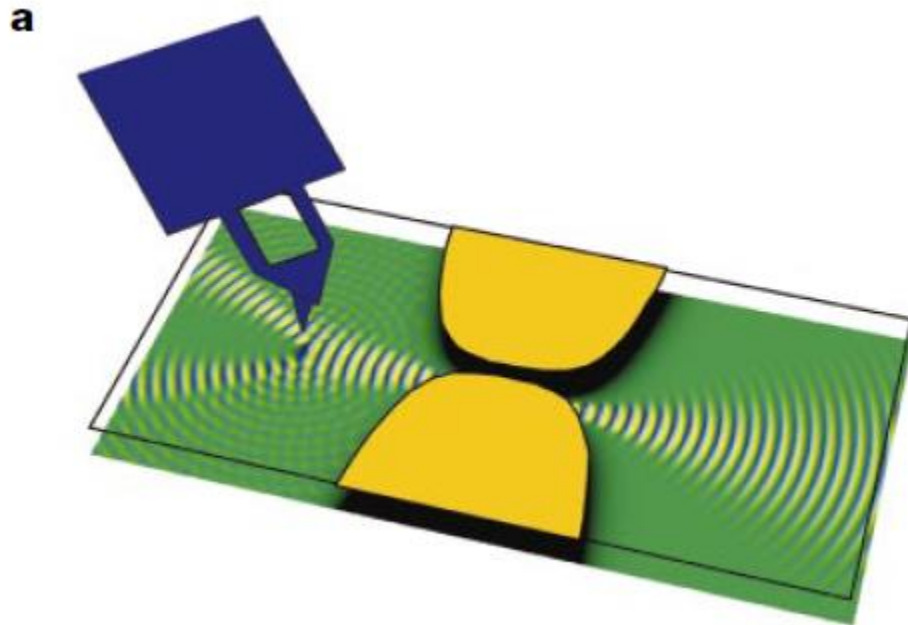


B. J. van Wees et al. *Quantum ballistic and adiabatic electron transport studied with quantum point contacts* Phys. Rev. B 43, 12431–12453 (1991)

FIG. 6. Breakdown of the conductance quantization due to temperature averaging. The curves have been offset for clarity.

Quantized conductance

$$G = \frac{2e^2}{h} T(\mu) = G_0 T(\mu)$$



M. A. Topinka et al. *Coherent branched flow in a two-dimensional electron gas* Nature 410, 183 (2001)

Quantized conductance

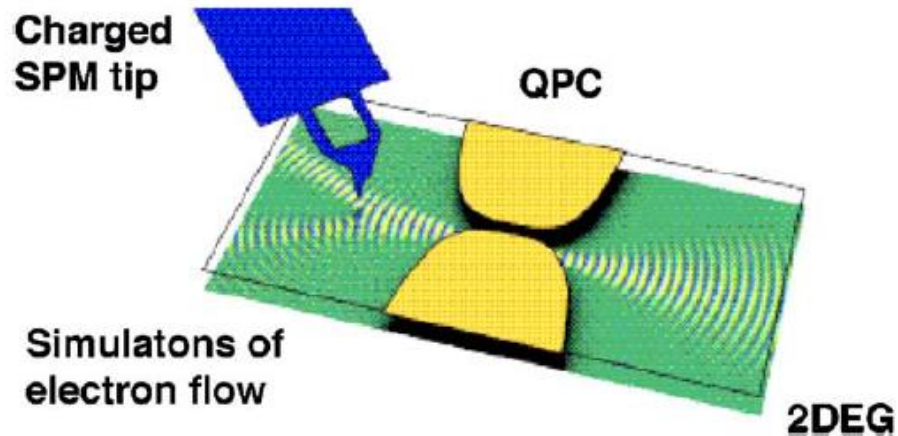
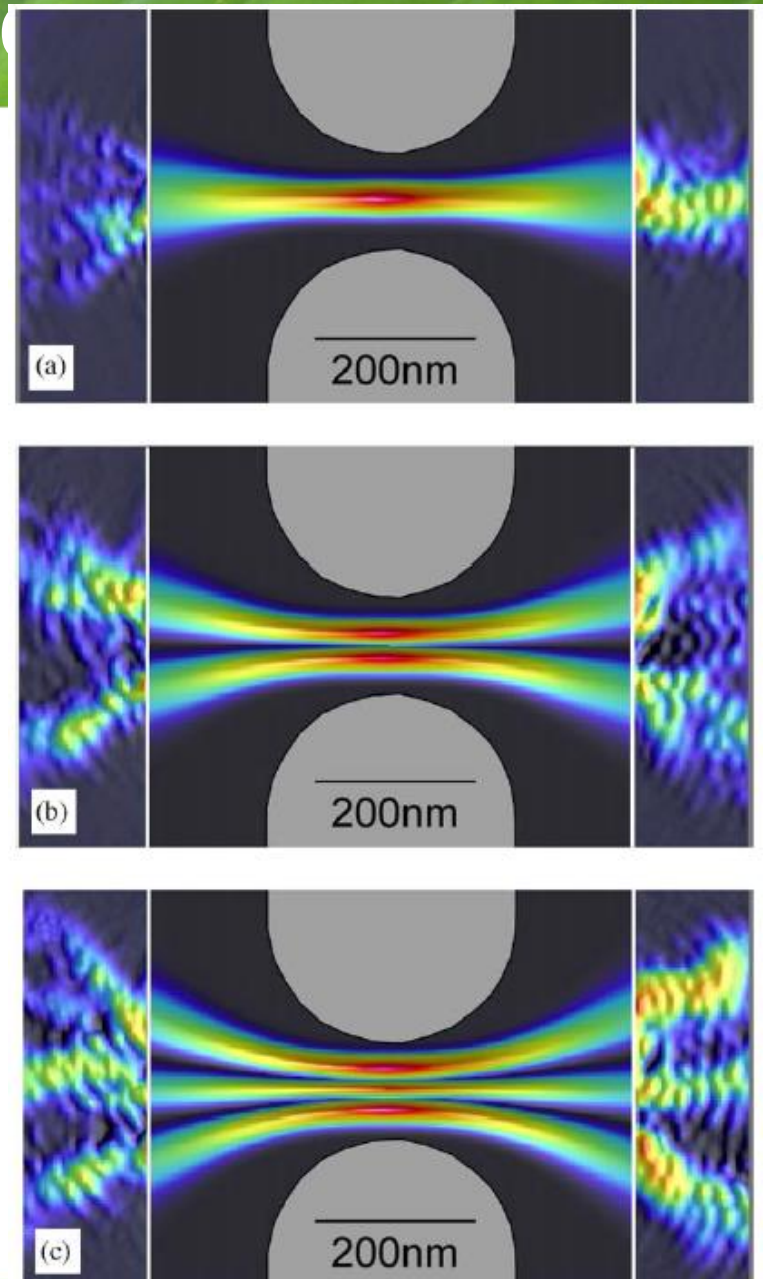


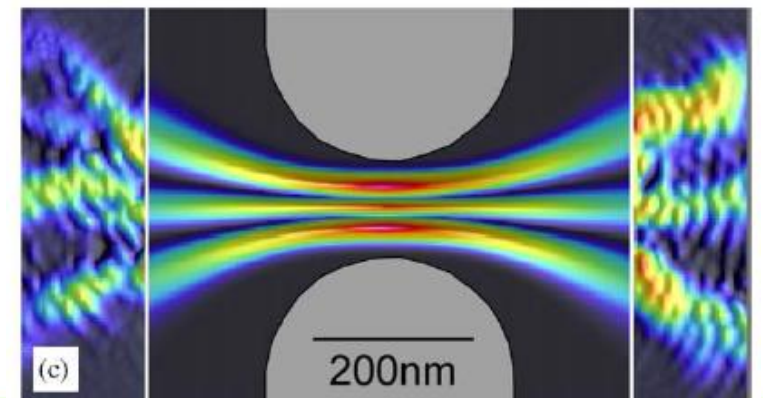
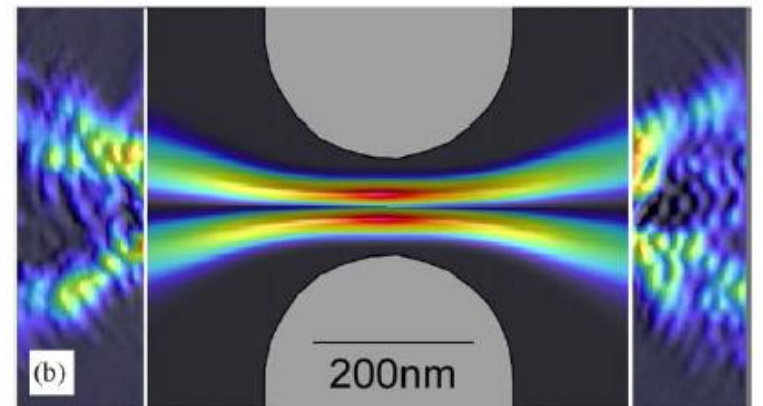
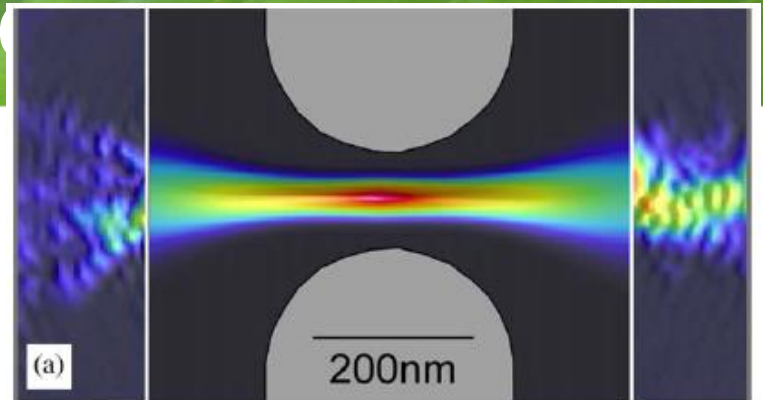
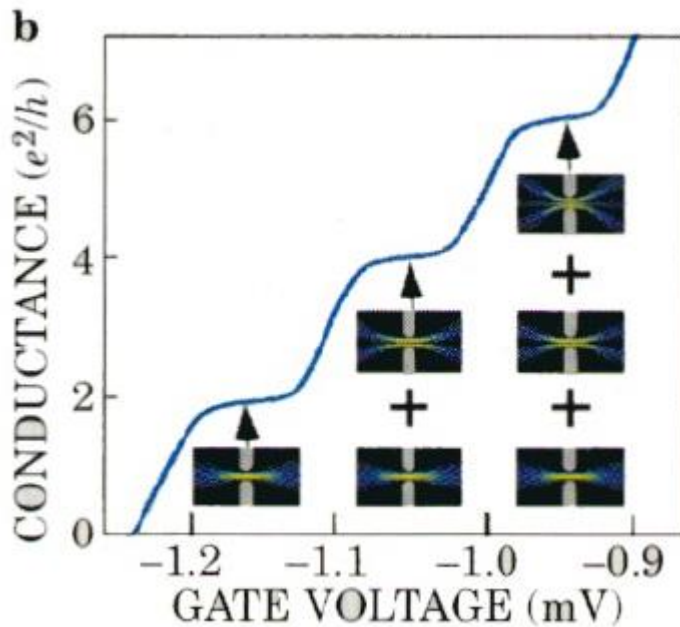
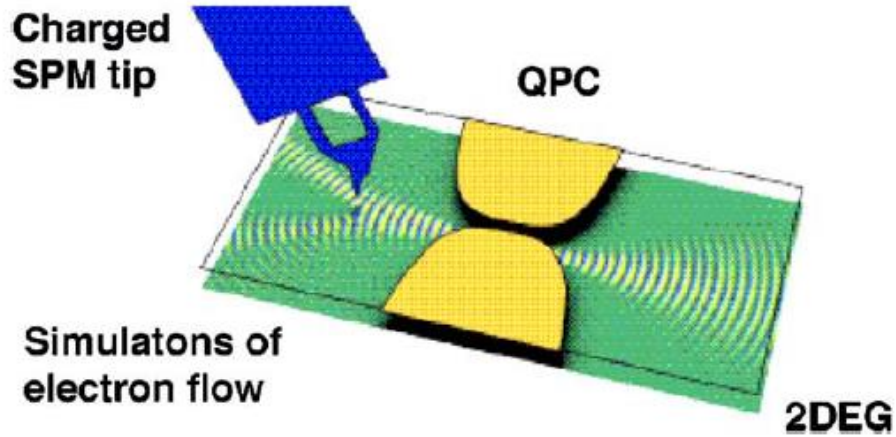
Fig. 1. Schematic diagram showing a negatively charged SPM tip positioned above a quantum point contact (QPC) formed in a two-dimensional electron gas (2DEG) by electrostatic gates. Simulations of electron flow in the diagram show how electron waves are scattered by the depleted disc beneath the tip Topinka et al. [16].

Fig. 2. Experimental images (outside) and theoretical simulations (inside) of the flow of electron waves through a quantum point contact for the first three modes (a)–(c). Fringes spaced by half the Fermi wavelength demonstrate coherence in the flow Topinka et al. [6].

R.M. Westervelt, M. A. Topinka et al.
Physica E 24 (2004) 63–69

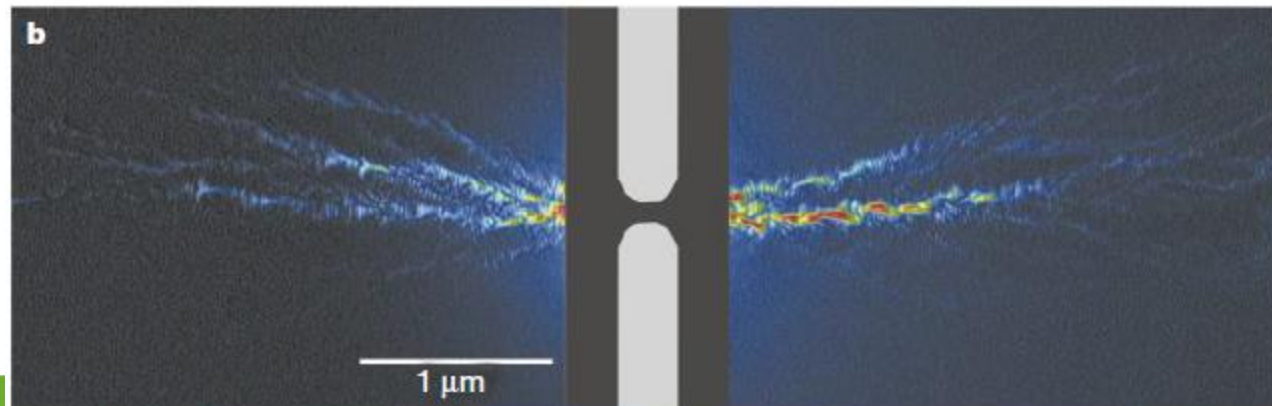
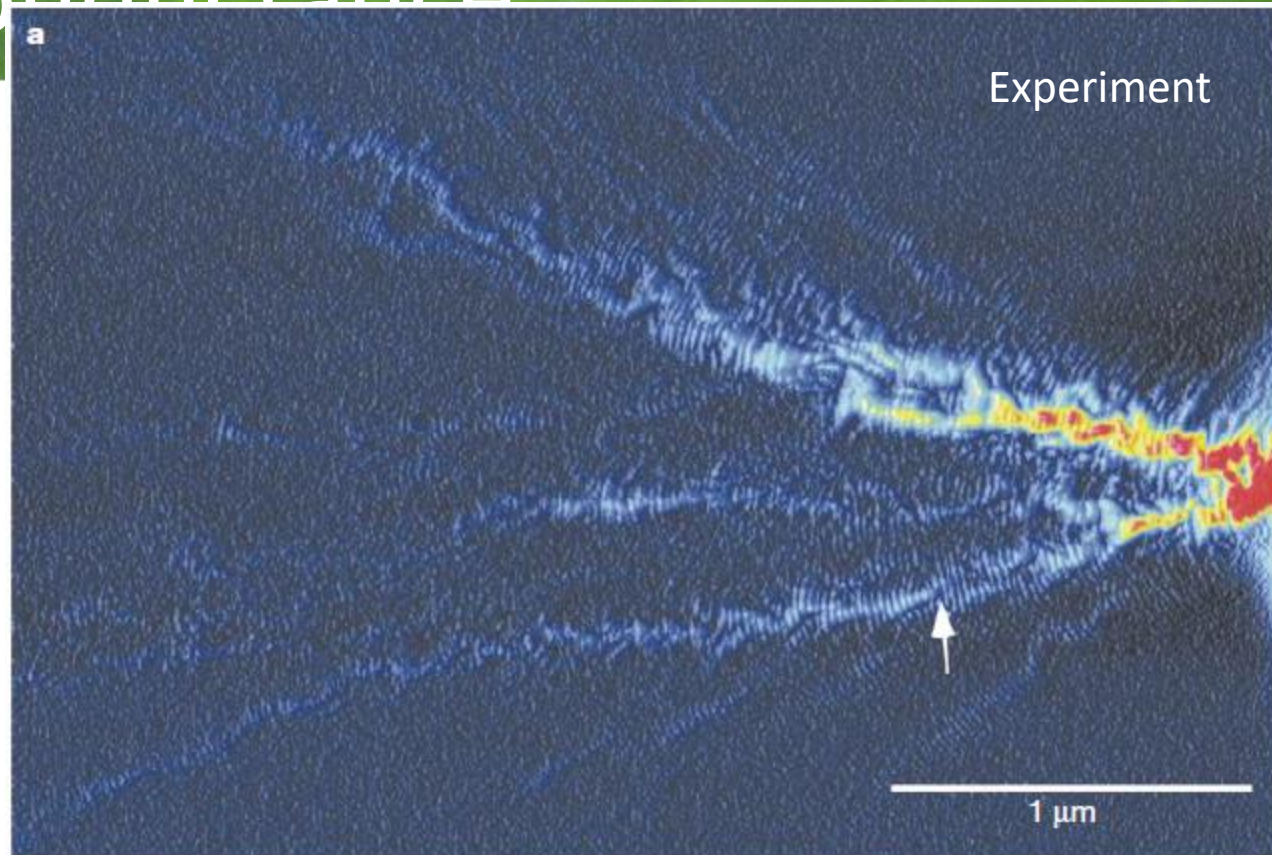


Quantized conductance



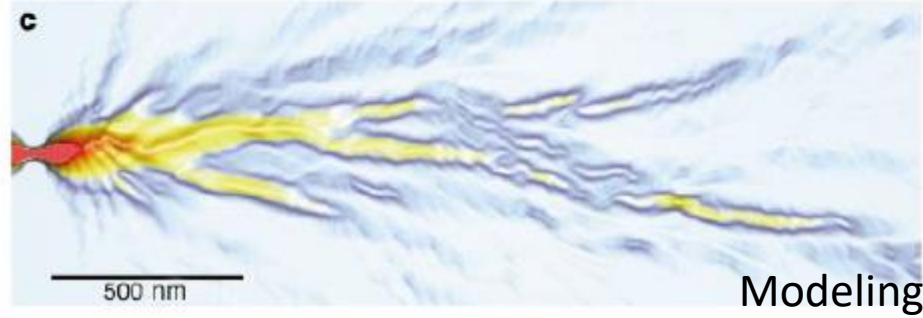
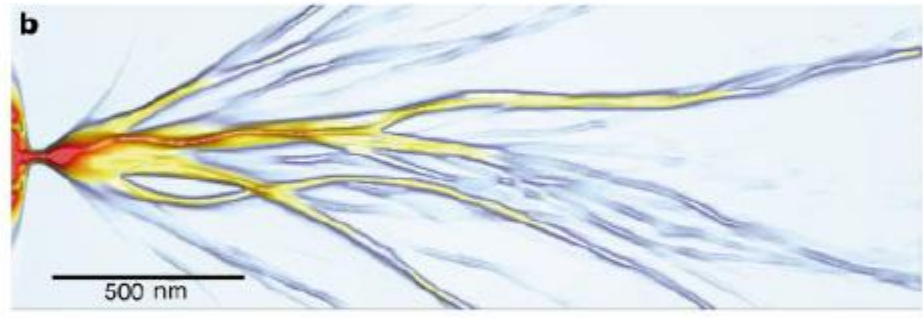
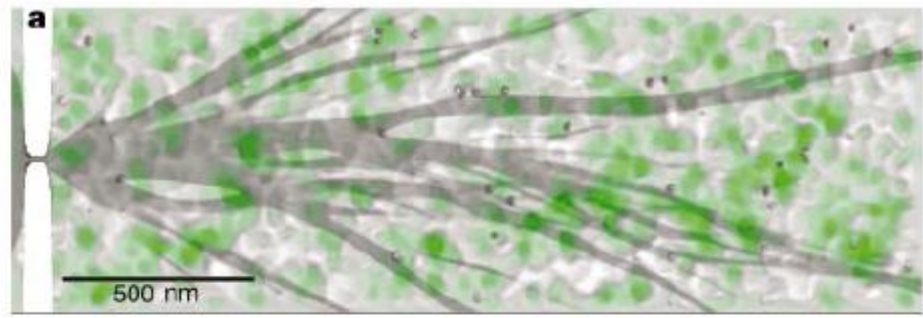
Quantized conductance

$$G = \frac{2e^2}{h} T(\mu) = G_0 T(\mu)$$

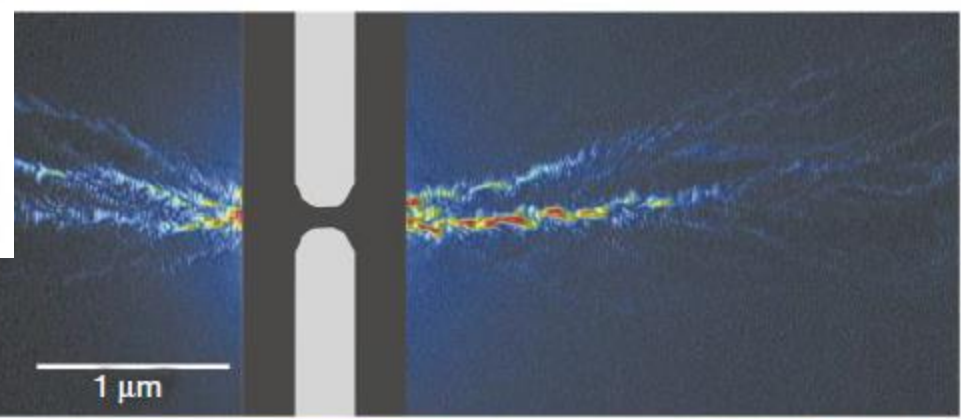
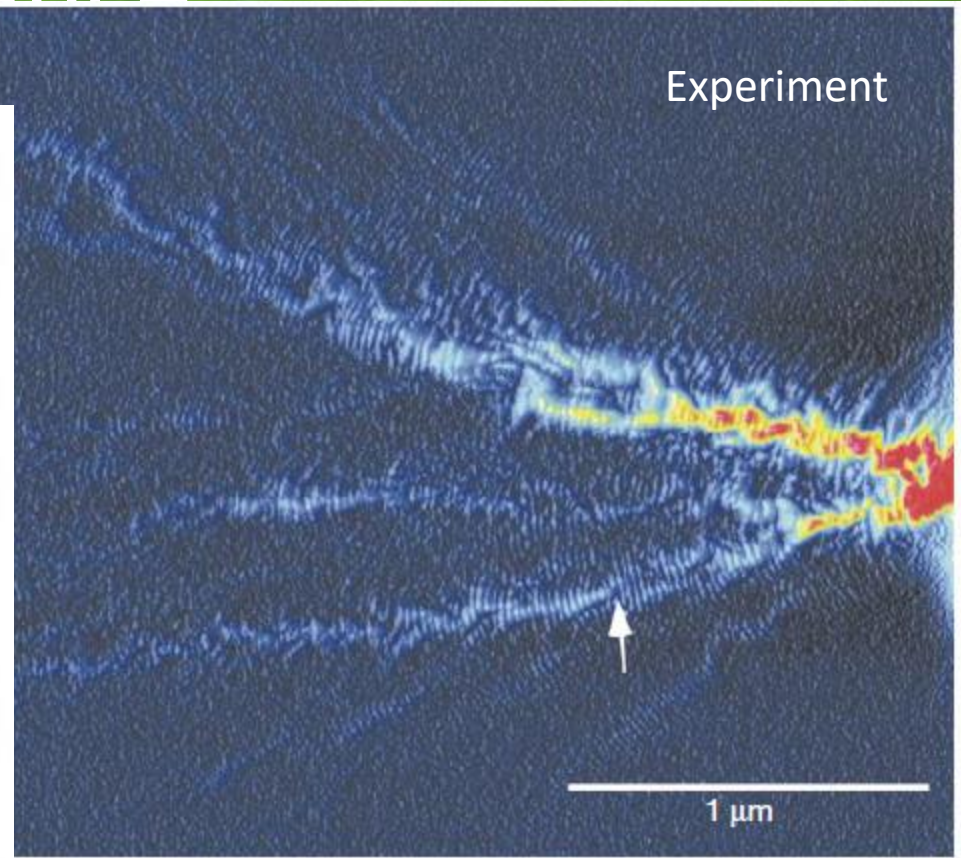


M. A. Topinka et al.
Nature 410, 183 (2001)

Quantized conductance



Modeling



M. A. Topinka et al.
Nature **410**, 183 (2001)

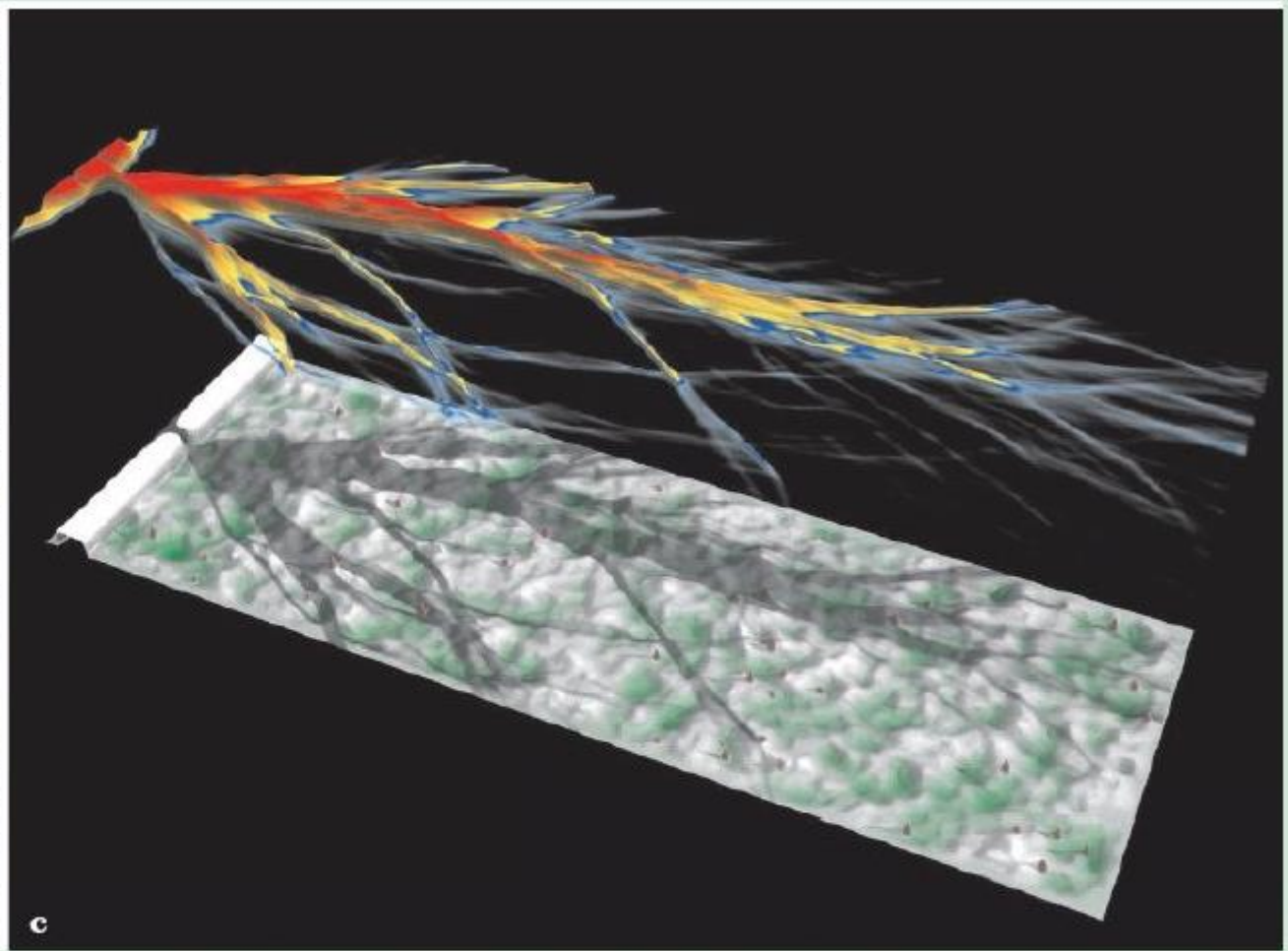
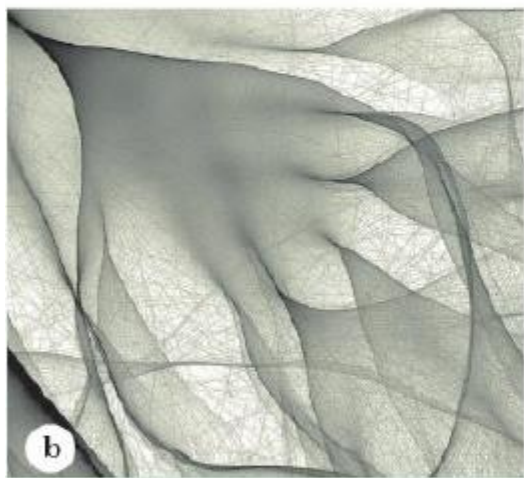
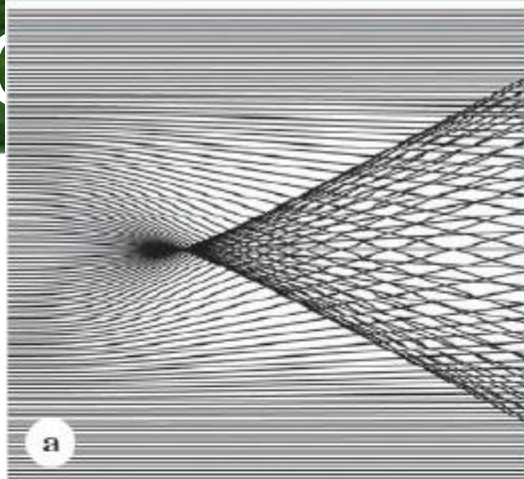


Figure 6. Simulations of electron flow. (a) Parallel electron trajectories, going from left to right, form a V-shaped cusp due to focusing by a potential-energy dip caused by a charged donor atom (not seen) above a two-dimensional electron gas. (b) A realistic 2DEG simulation that includes many ionized donors forms several generations of cusps. The electrons travel here from upper left to lower right. (c) Ray-tracing simulations of electron flux emerging from a small opening into a region of random potential reflect the features seen in experimental images of 2DEG quantum point contact samples. The potential is shown green in the valleys and white on the peaks. The electron flux is coded by height and color, with blue corresponding to regions of low flux; still lower flux is transparent. The “shadow” of the flux on the potential plot shows where the flux lies relative to the hills and valleys; no guiding valleys are seen. A slight change of the position of the opening changes the location and direction of the branches. (S. E. J. Shaw, PhD thesis, Harvard University, 2002.)

Quantized conductance

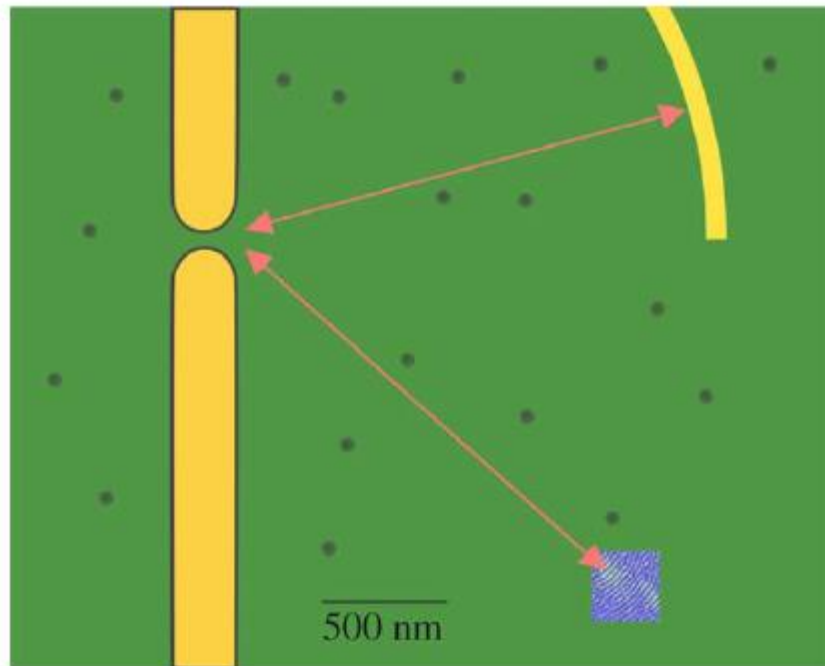


Fig. 3. Schematic diagram showing how a V-shaped electron interferometer was constructed using a QPC and a reflecting gate (gates in gold color). The SPM tip was scanned over the small blue area at approximately the same distance from the QPC as the reflector gate. Electrons passing from the QPC travel along both legs of the interferometer at once (paths shown in red, with arrows), and interfere when they return to their starting point.

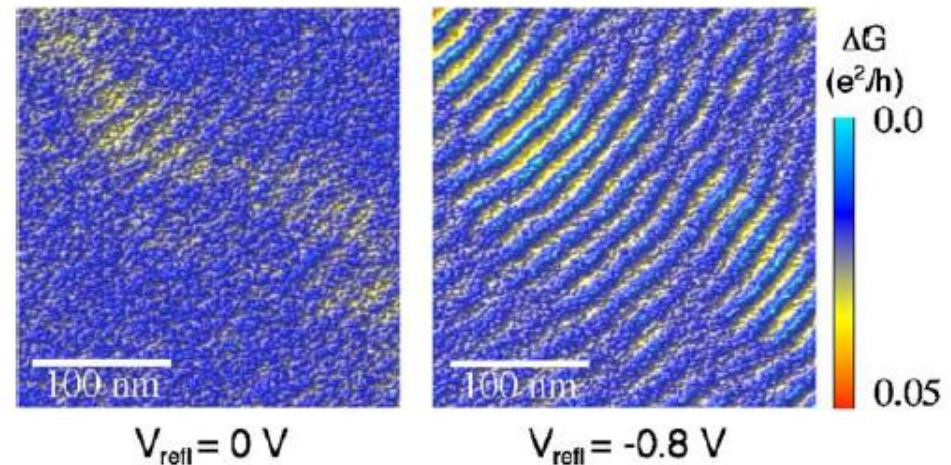


Fig. 4. Experimental images that show that fringes are created in the interferometer of Fig. 3, when the reflector mirror is turned on by depleting the electron gas below. Only weak fringes are observed in the left panel when the reflector mirror is off ($V_{\text{refl}} = 0 \text{ V}$), while strong fringes are observed in the right panel when the reflector mirror is on ($V_{\text{refl}} = -0.8 \text{ V}$).

R.M. Westervelt, M. A. Topinka et al.
Physica E 24 (2004) 63–69

Quantized conductance

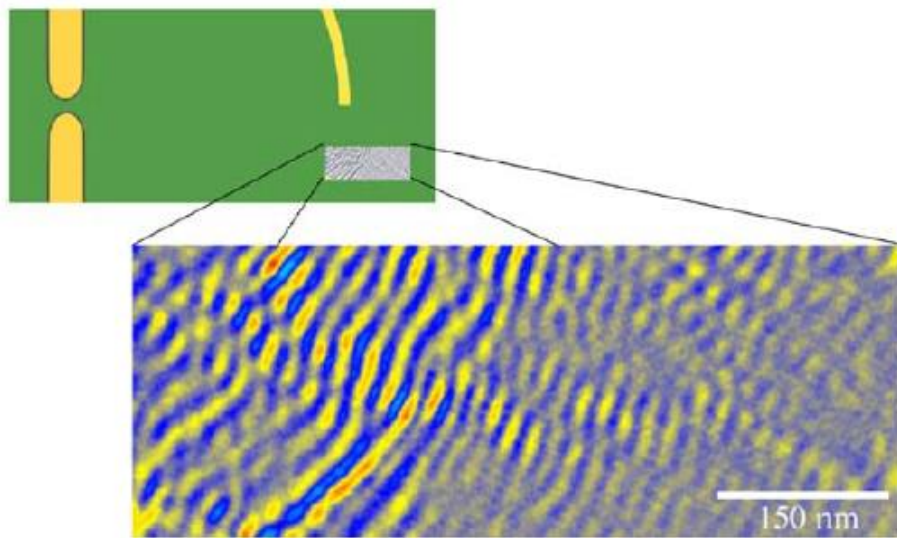


Fig. 6. Image of fringes in an electron interferometer that show how the fringe intensity varies with distance from the QPC—the fringes are strongest at the same distance from the QPC as the reflector mirror. An ensemble average over the thermal distribution of electron energies tends to wash out fringes at other distances.

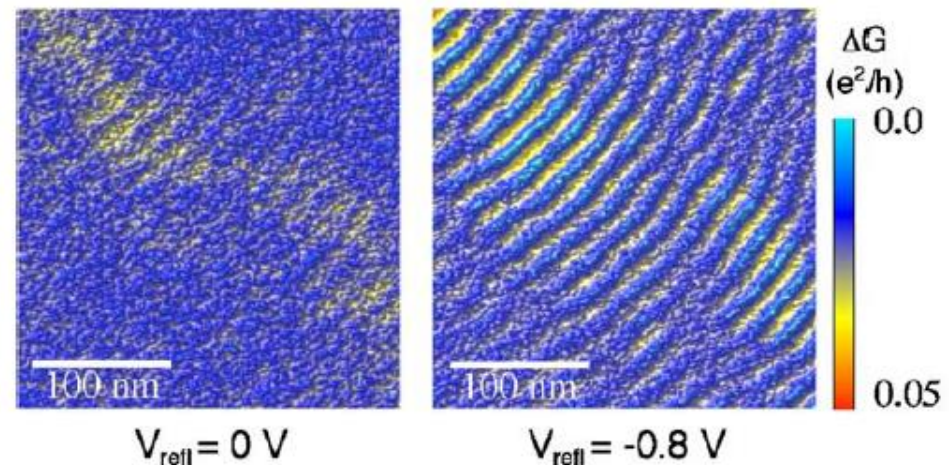
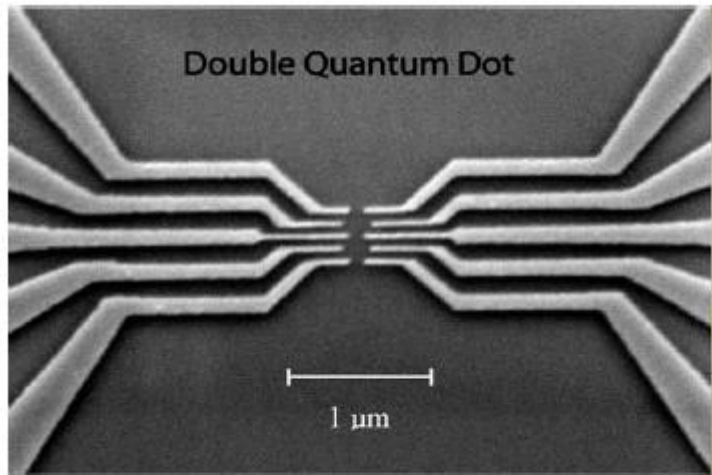


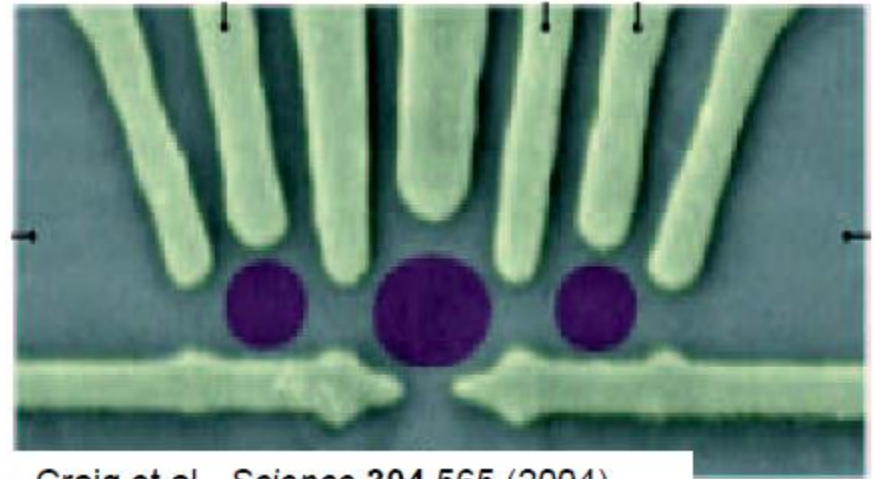
Fig. 4. Experimental images that show that fringes are created in the interferometer of Fig. 3, when the reflector mirror is turned on by depleting the electron gas below. Only weak fringes are observed in the left panel when the reflector mirror is off ($V_{\text{refl}} = 0 \text{ V}$), while strong fringes are observed in the right panel when the reflector mirror is on ($V_{\text{refl}} = -0.8 \text{ V}$).

R.M. Westervelt, M. A. Topinka et al.
Physica E 24 (2004) 63–69

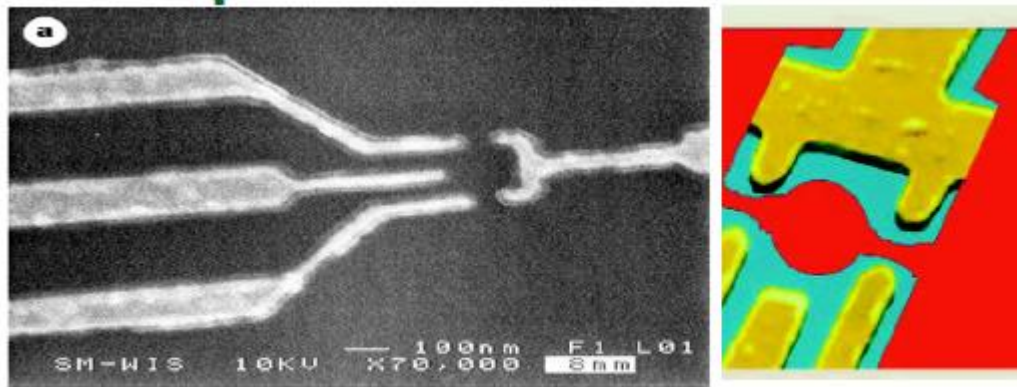
Tunnelling



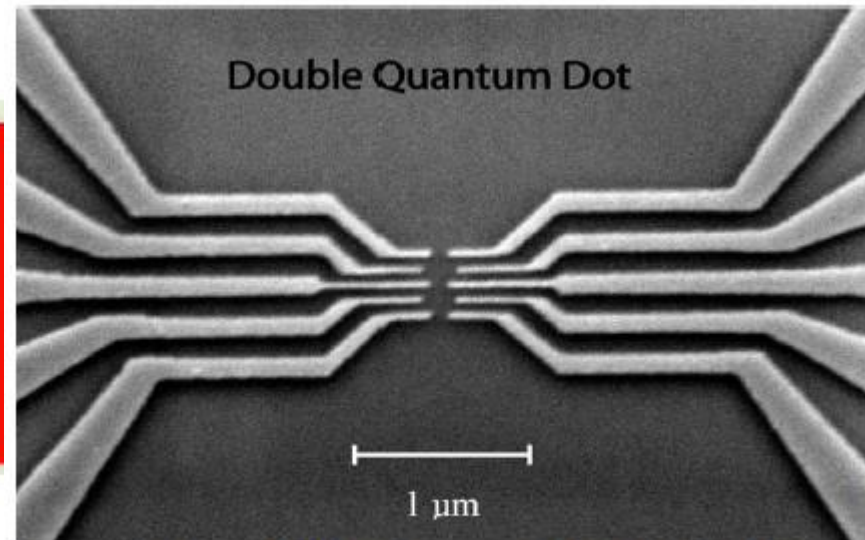
Jeong, Chang, Melloch *Science* 293 2222 (2001)



Craig et al., *Science* 304 565 (2004)



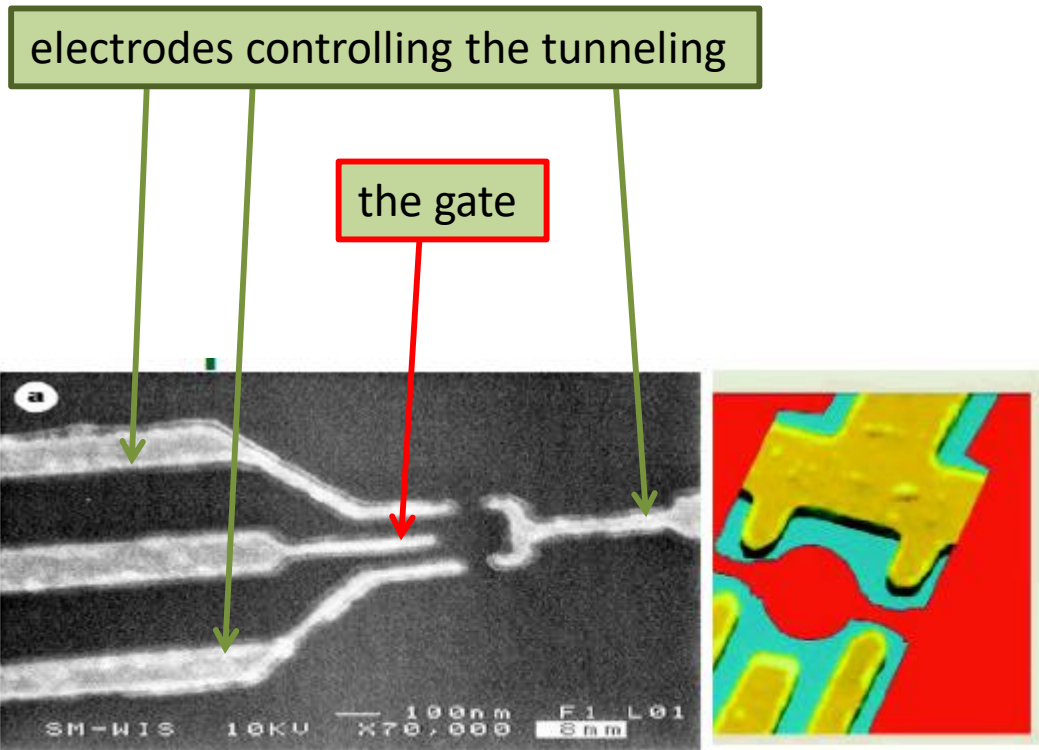
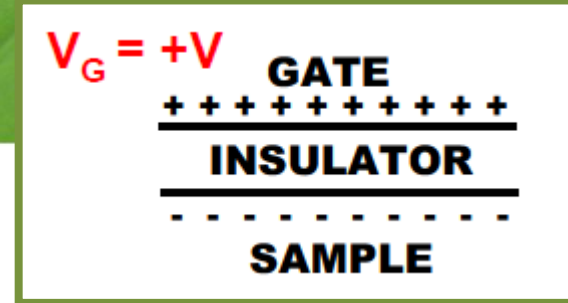
Goldhaber-Gordon et al. *Nature* 391 156 (1998)



Jeong, Chang, Melloch *Science* 293 2222 (2001)

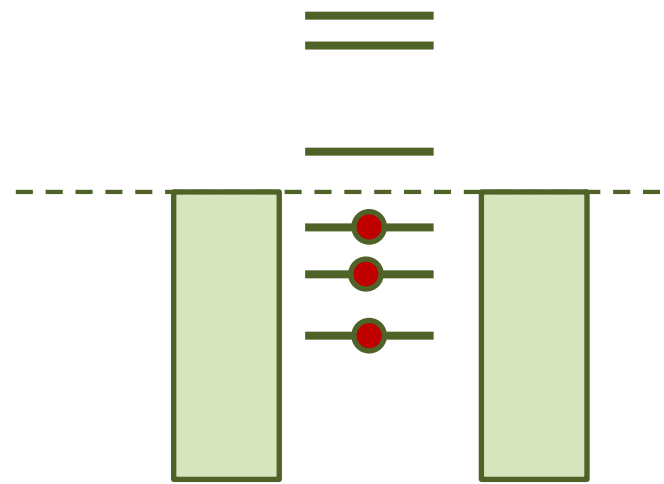
Tunnelling

Dot behaves like a small capacitor of energy $E_c \sim \frac{1}{2} \frac{e^2}{C}$



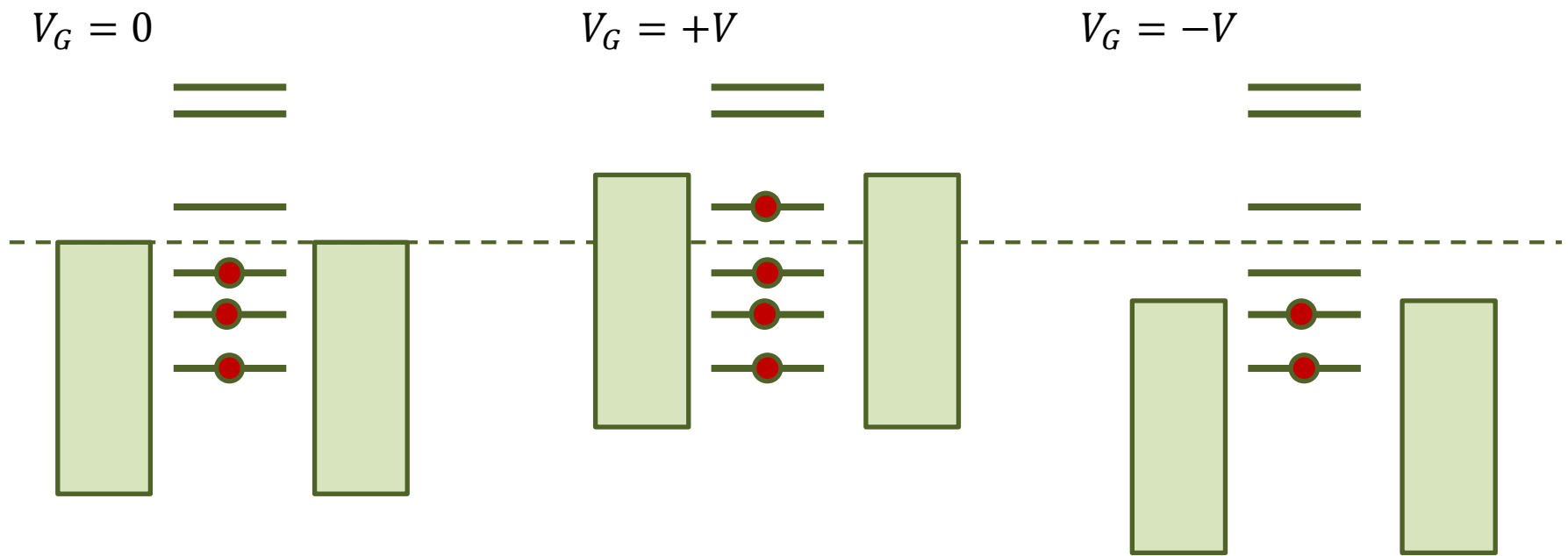
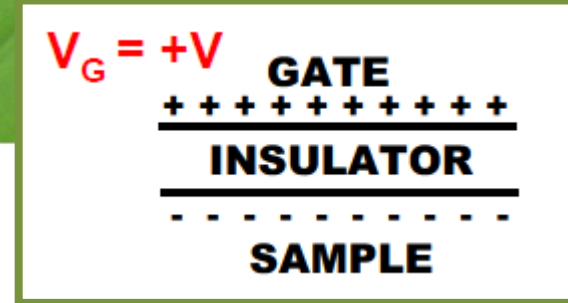
Goldhaber-Gordon *et al.* *Nature* 391 156 (1998)

$V_G = 0$

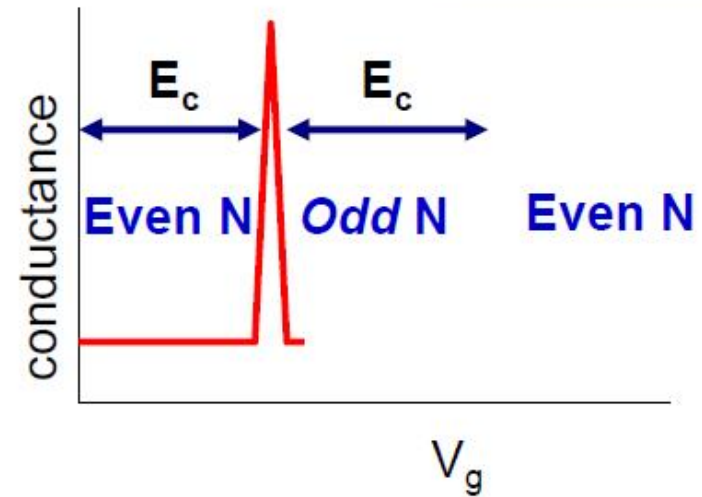
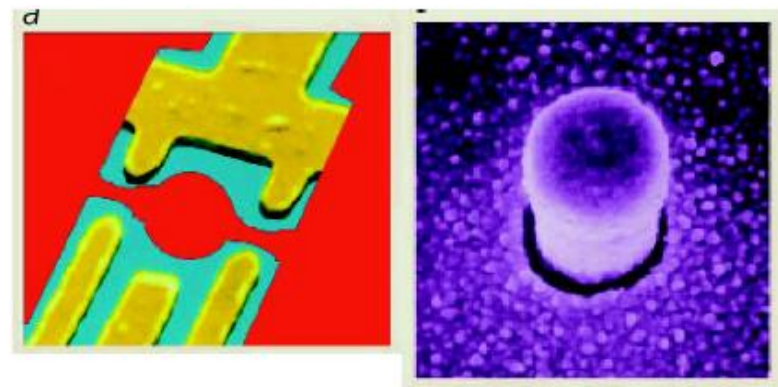
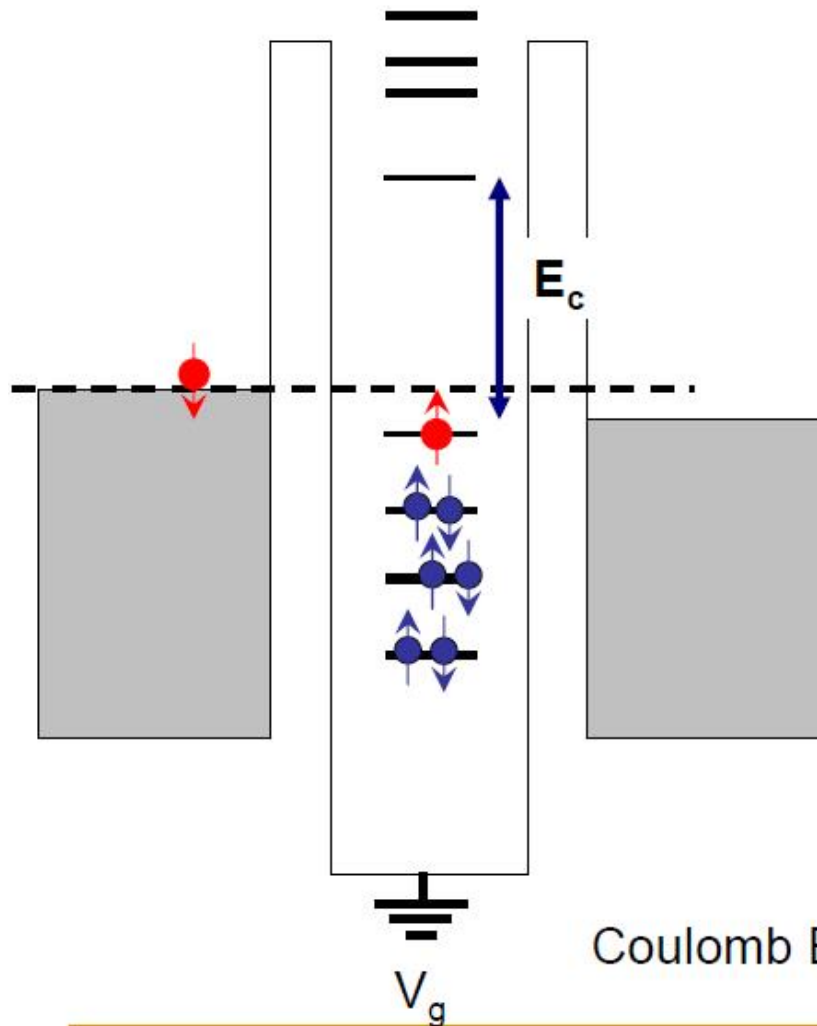


Coulomb blockade

Dot behaves like a small capacitor of energy $E_c \sim \frac{1}{2} \frac{e^2}{C}$



Coulomb blockade



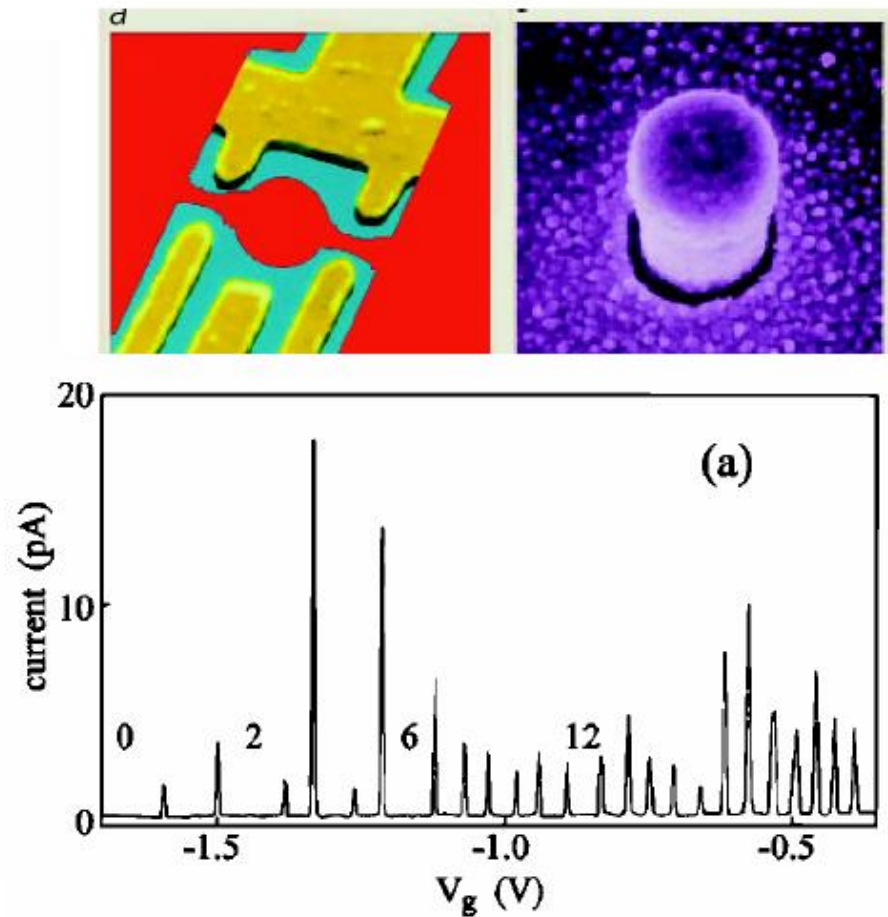
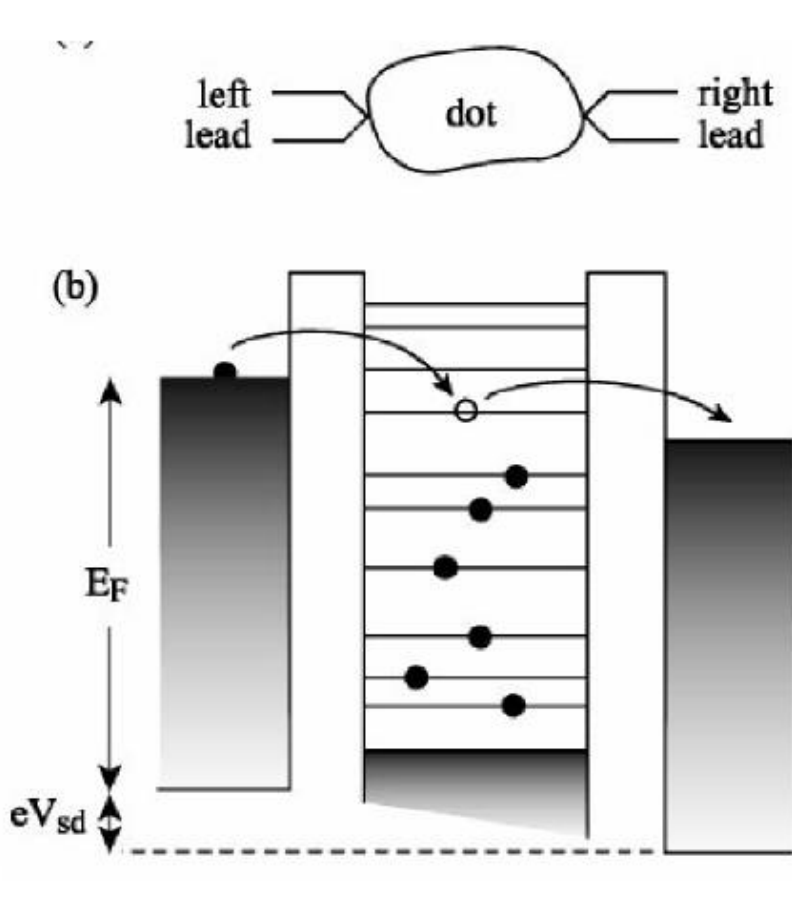
Coulomb Blockade in Quantum Dots

Y. Alhassid *Rev. Mod. Phys.* 72 895 (2000).

http://sces.phys.utk.edu/~dagotto/condensed/Lectures_2008/UTK_Lecture1_March08.pdf

Luis Dias – UT/ORNL

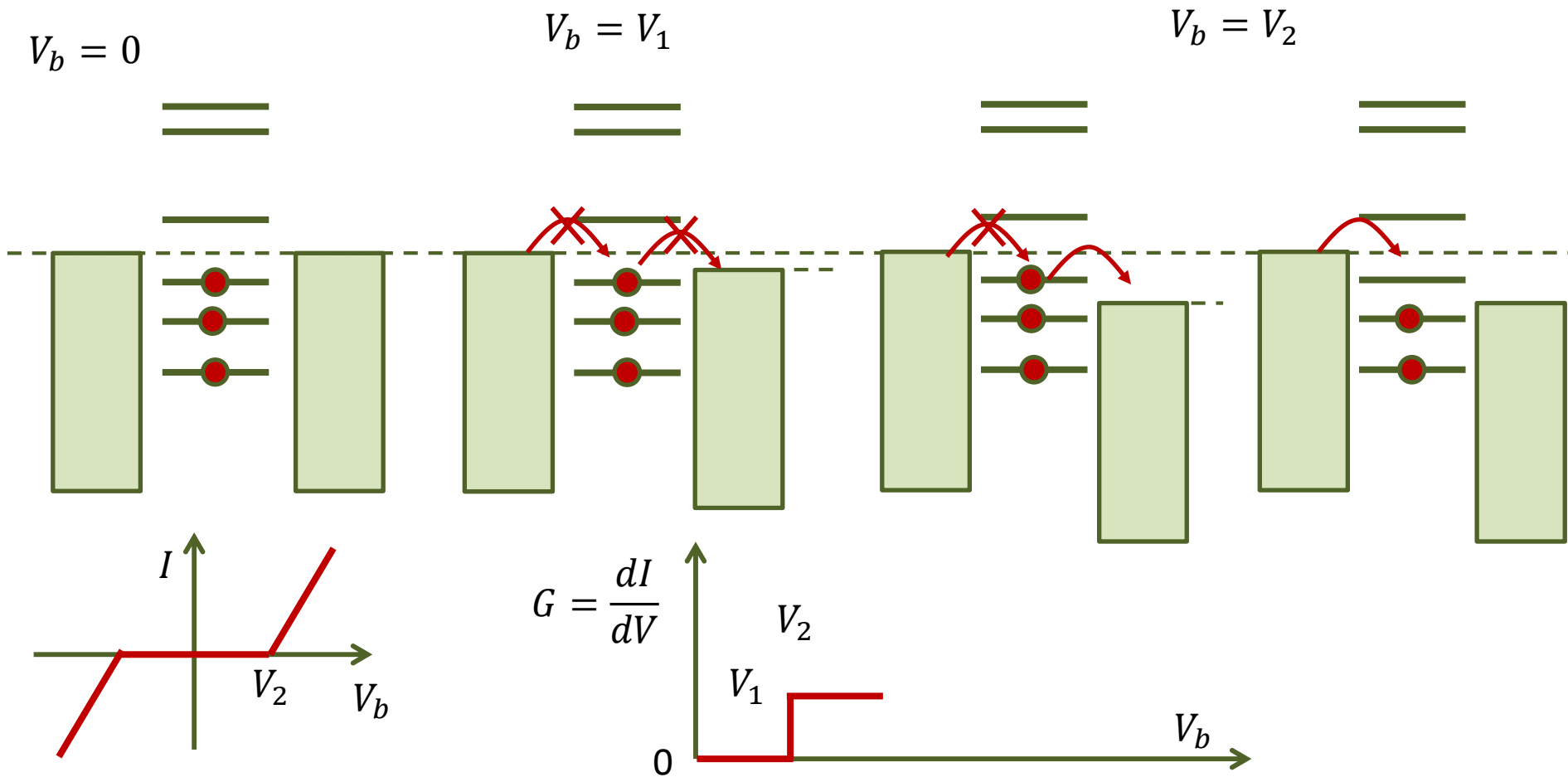
Coulomb blockade



Coulomb Blockade in Quantum Dots: “dot spectroscopy”

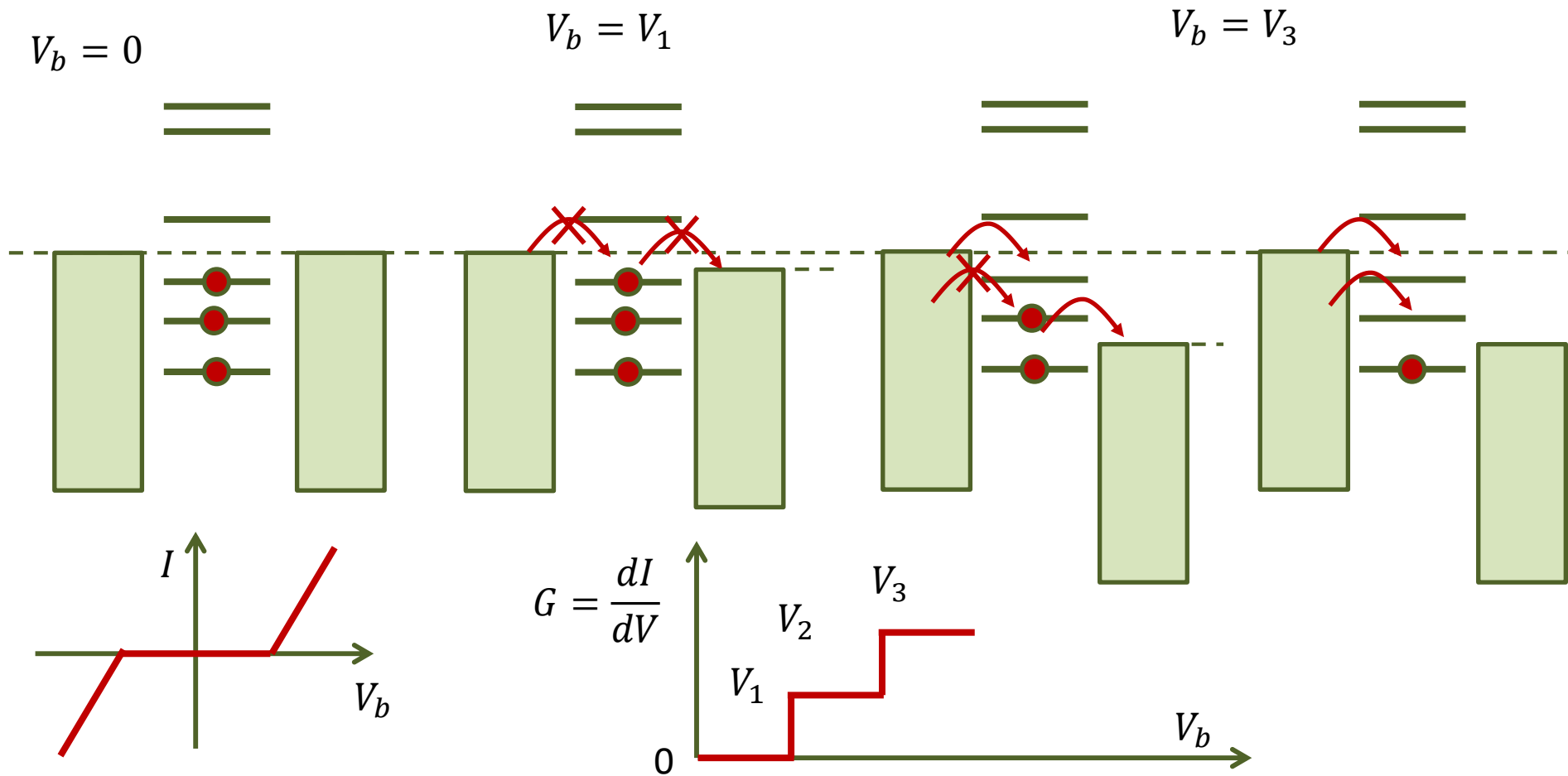
Coulomb blockade

Dot behaves like a small capacitor of energy $E_c \sim \frac{1}{2} \frac{e^2}{C}$



Coulomb blockade

Dot behaves like a small capacitor of energy $E_c \sim \frac{1}{2} \frac{e^2}{C}$



Coulomb blockade

Dot behaves like a small capacitor of energy $E_c \sim \frac{1}{2} \frac{e^2}{C}$

$$V_b = 0$$

$$V_g = 0$$

$$V_b = V_1$$

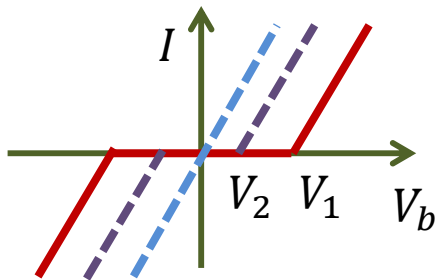
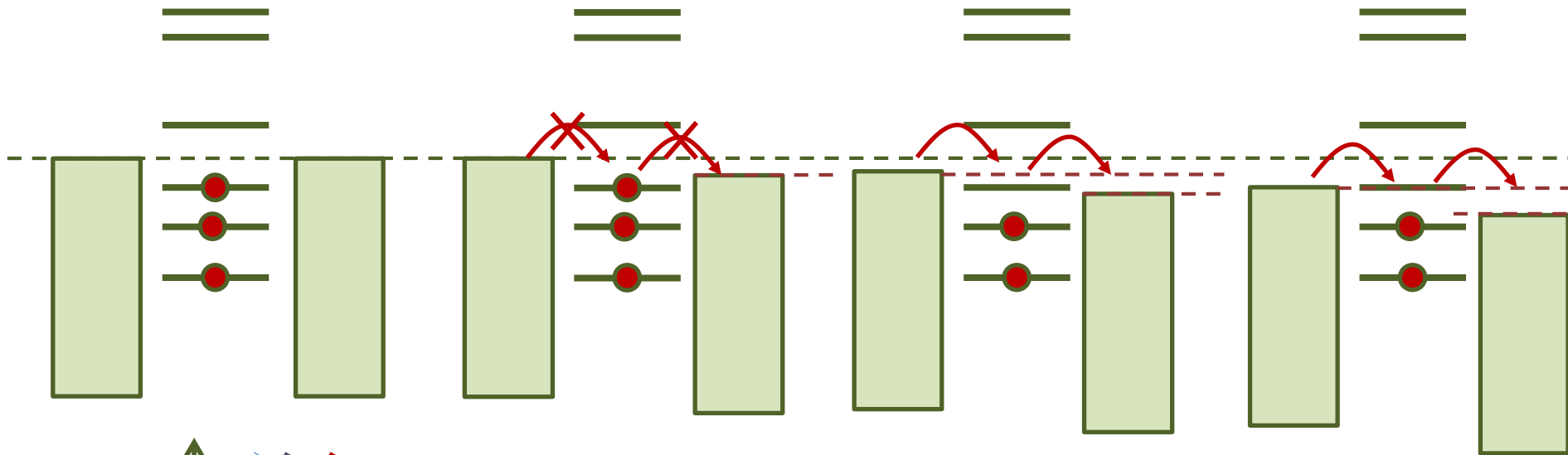
$$V_g = 0$$

$$V_b = V_2 < V_1$$

$$V_g \neq 0$$

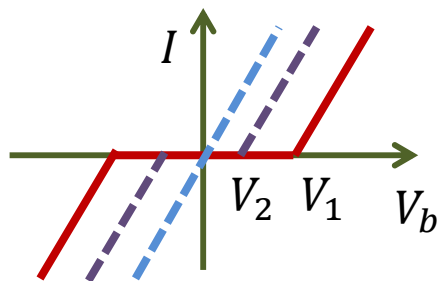
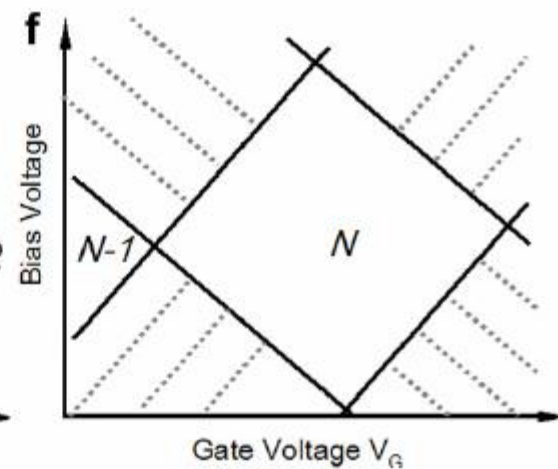
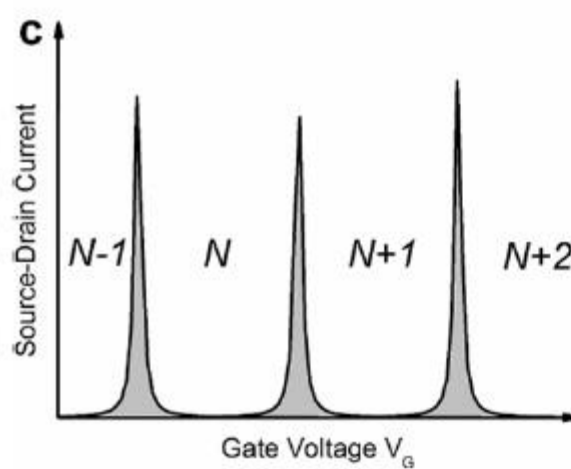
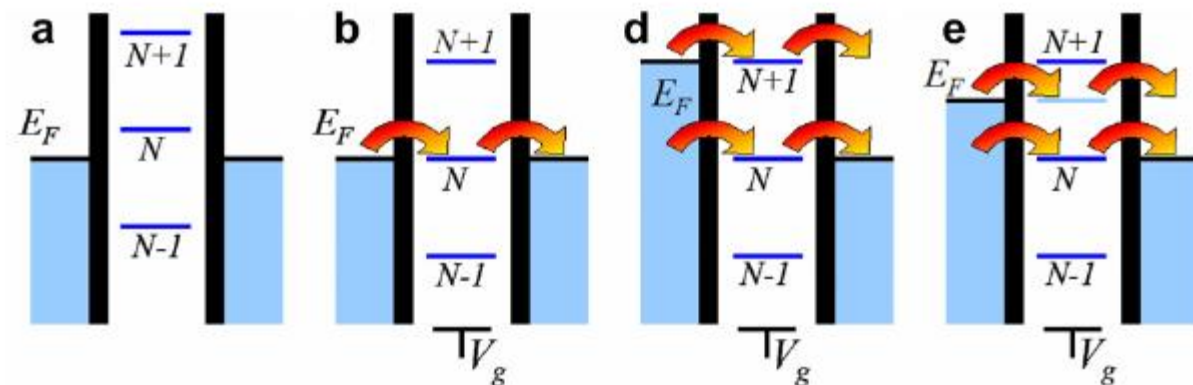
$$V_b = 0$$

$$V_g \neq 0$$



Coulomb blockade

Dot behaves like a small capacitor of energy $E_c \sim \frac{1}{2} \frac{e^2}{C}$



Inorganica Chimica Acta 361 (2008) 3807–3819

Coulomb blockade

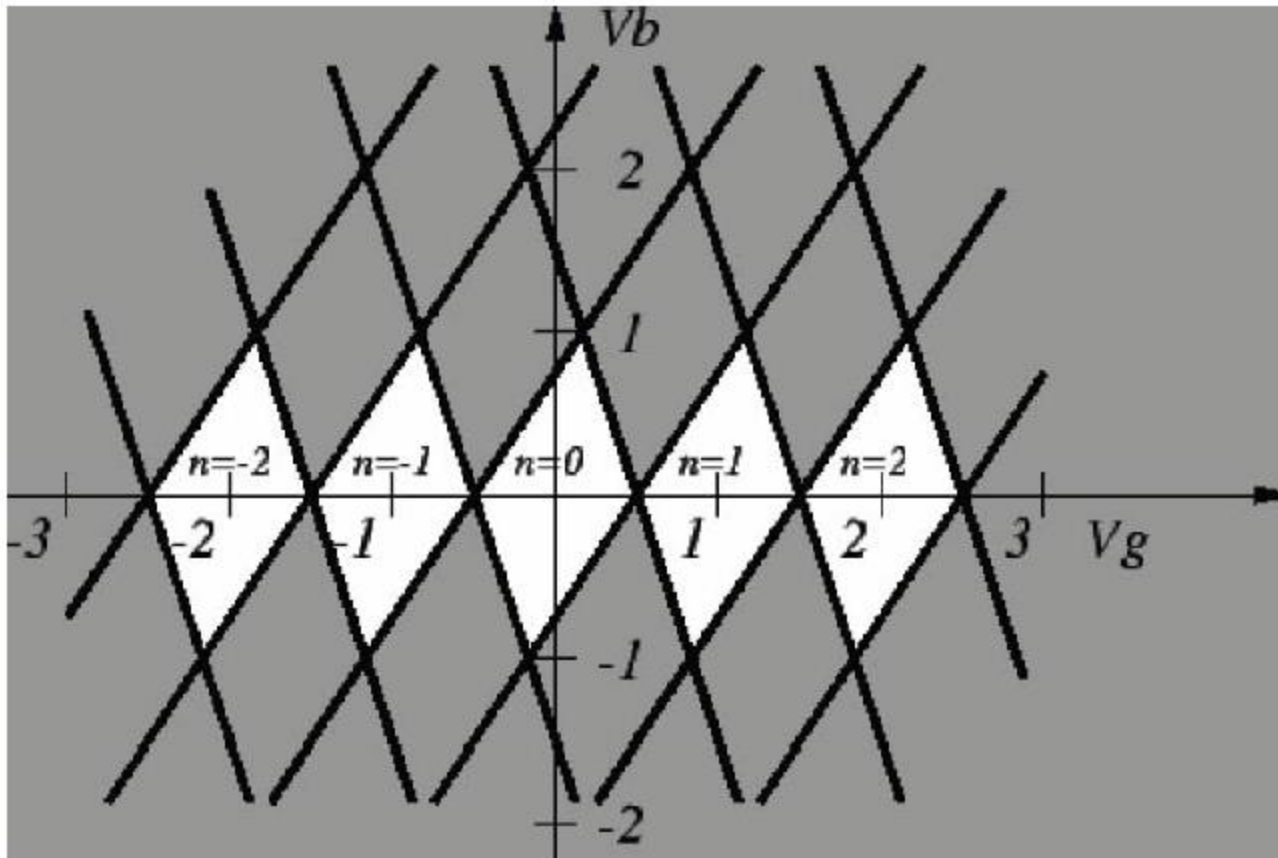


Figure 6: “Coulomb diamonds”

<http://www.dstuns.iitm.ac.in/teaching-and-presentations/teaching/undergraduate%20courses/vy305-molecular-architecture-and-evolution-of-functions/presentations/presentations-2007/seminar-2/P2.pdf>

Coulomb blockade

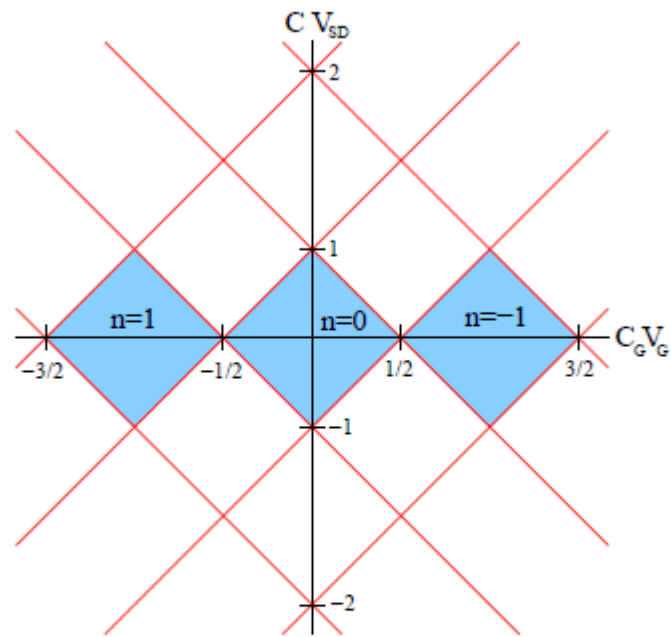
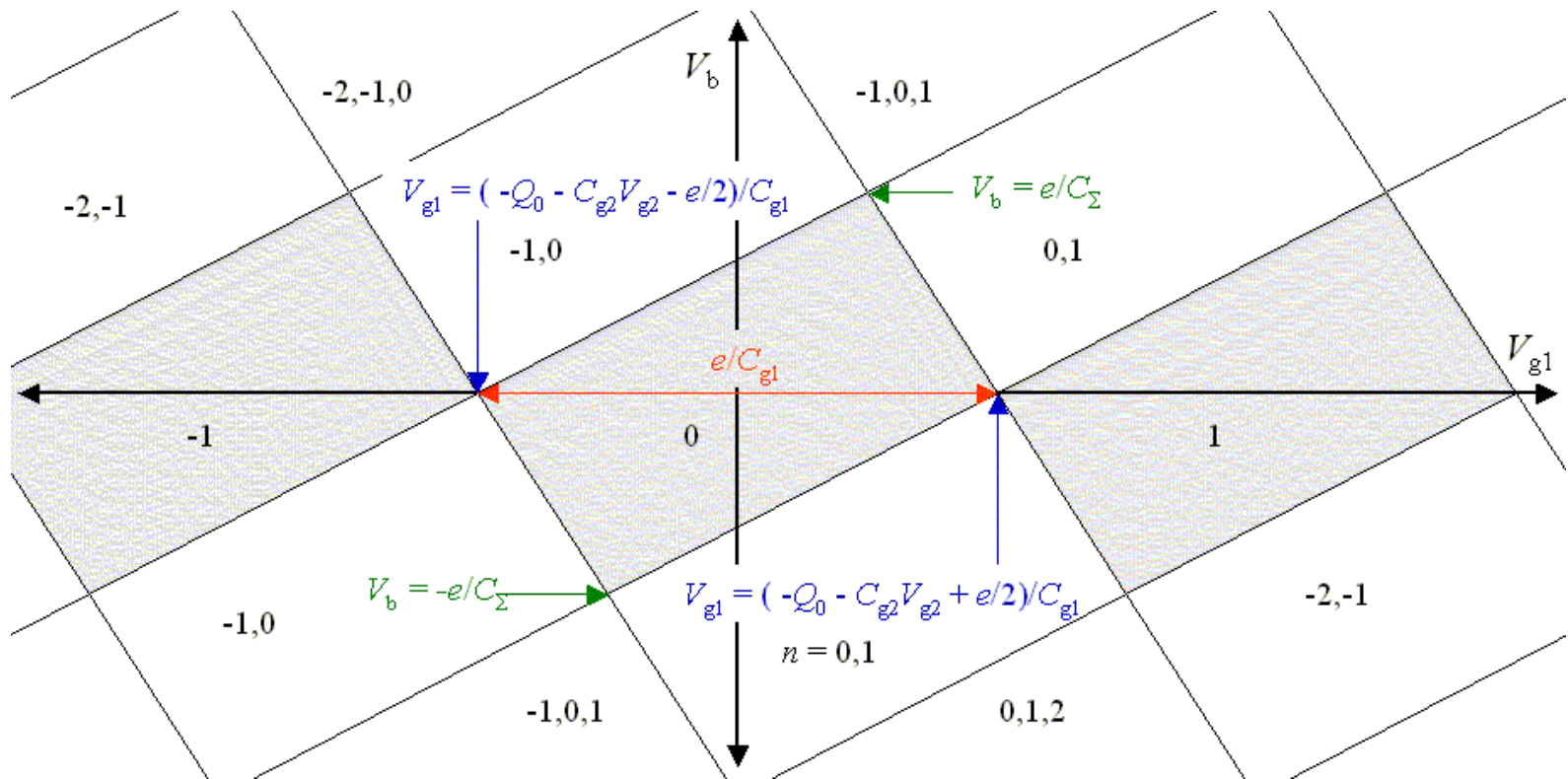


Figure 6.6: A stability diagram for a SET. The blue shaded regions are the Coulomb diamonds, where the number of electrons on the dot is fixed at n and transport through the dot is blocked. Red lines indicate voltages where the number of addition energies within the transport window changes by one. We have set $e = 1$ here for convenience.

Coulomb blockade



<http://lamp.tu-graz.ac.at/~hadley/ss2/set/transistor/coulombblockade.php>

Coulomb blockade

Excitation Spectra of Circular, Few-Electron Quantum Dots

L. P. Kouwenhoven, T. H. Oosterkamp, M. W. S. Danoesastro, M. Eto, D. G. Austing, T. Honda, S. Tarucha

SCIENCE • VOL. 278 • 5 DECEMBER 1997

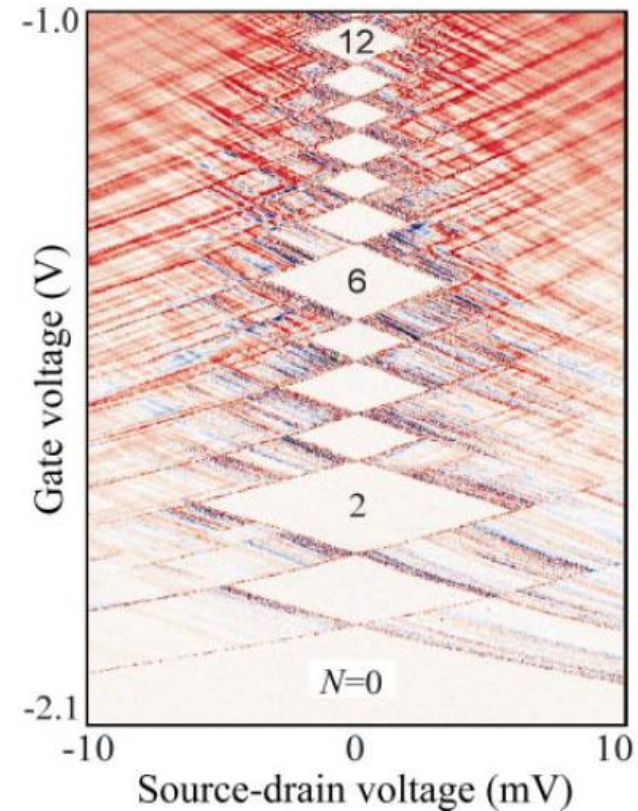
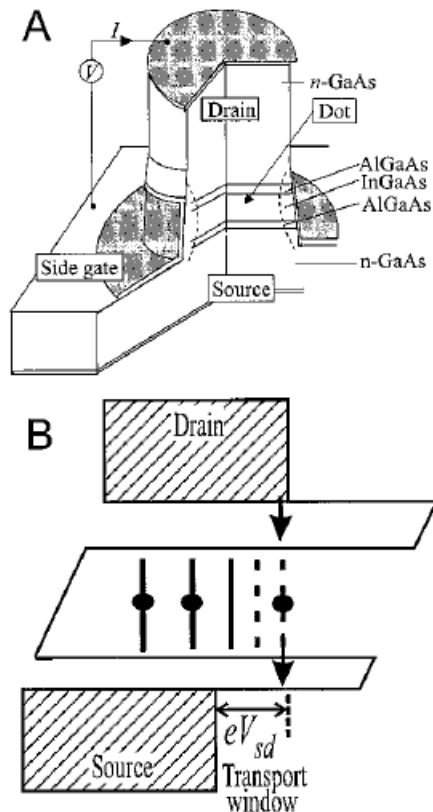
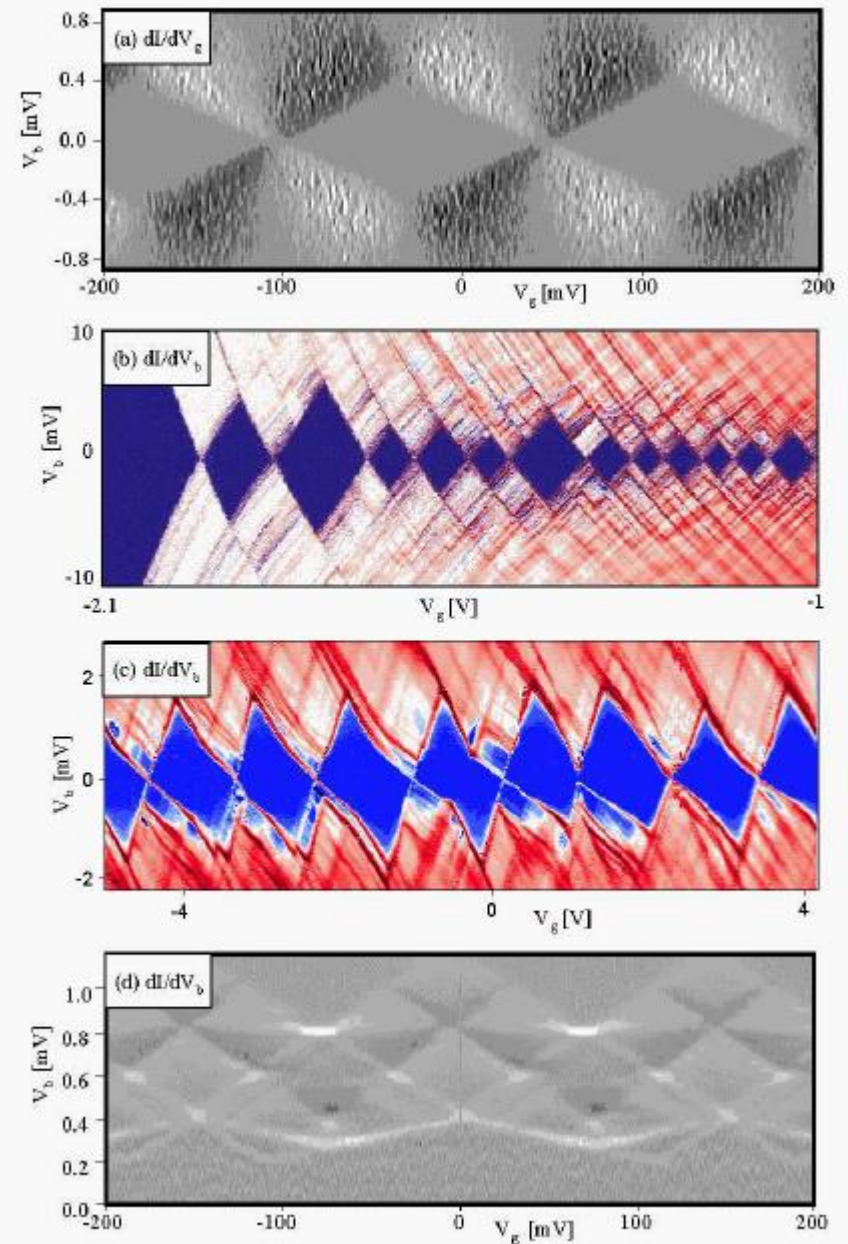


Fig. 2. Differential conductance $\partial I / \partial V_{sd}$ plotted in color scale in the $V_g - V_{sd}$ plane at $B = 0$. In the white diamond-shaped regions, $\partial I / \partial V_{sd} \approx 0$ as a result of Coulomb blockade. N is fixed in each of the diamond regions. The lines outside the diamonds, running parallel to the sides, identify excited states.

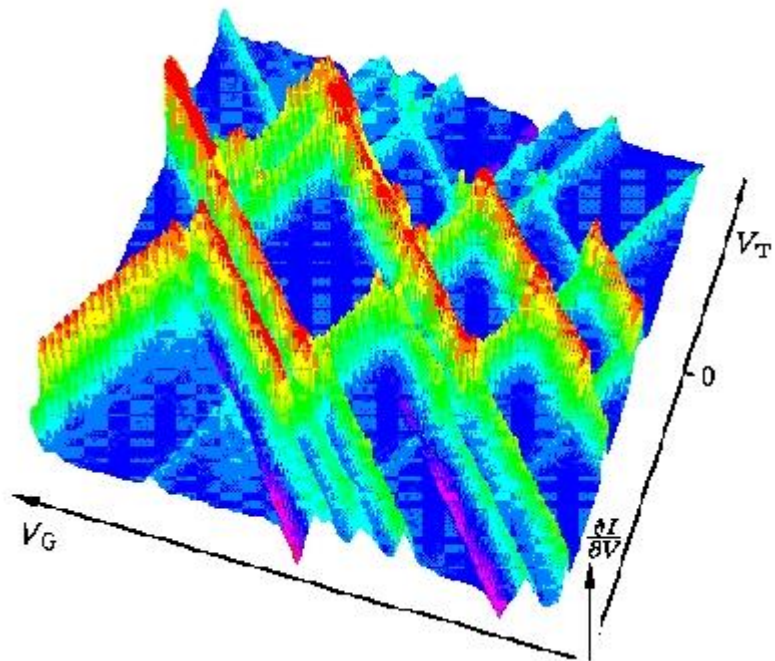
Coulomb blockade

Figure 6.7: The low temperature conductances of (a) a metal single-electron transistor (SET), (b) a semiconducting SET, (c) a carbon nanotube SET, and (d) a superconducting SET are plotted as a function of gate voltage and bias voltage. The diamond shaped regions along the zero bias voltage axis are regions of Coulomb blockade. The conductance is a periodic function of gate voltage for the metal SET and the superconducting SET where the confinement energy is negligible. The conductance is not a periodic function of gate voltage for the semiconductor SET and the carbon nanotube SET where the confinement energy is important. From: P. Hadley and J.E. Mooij, Delft University of Technology, <http://qt.tn.tudelft.nl/publi/2000/quantumdev/qdevices.html>



Clive Emary
Theory of Nanostructures nanoskript.pdf

Coulomb blockade



Dodatkowe „diamenty” – np. efekty spinowe , stany wzbudzone itp

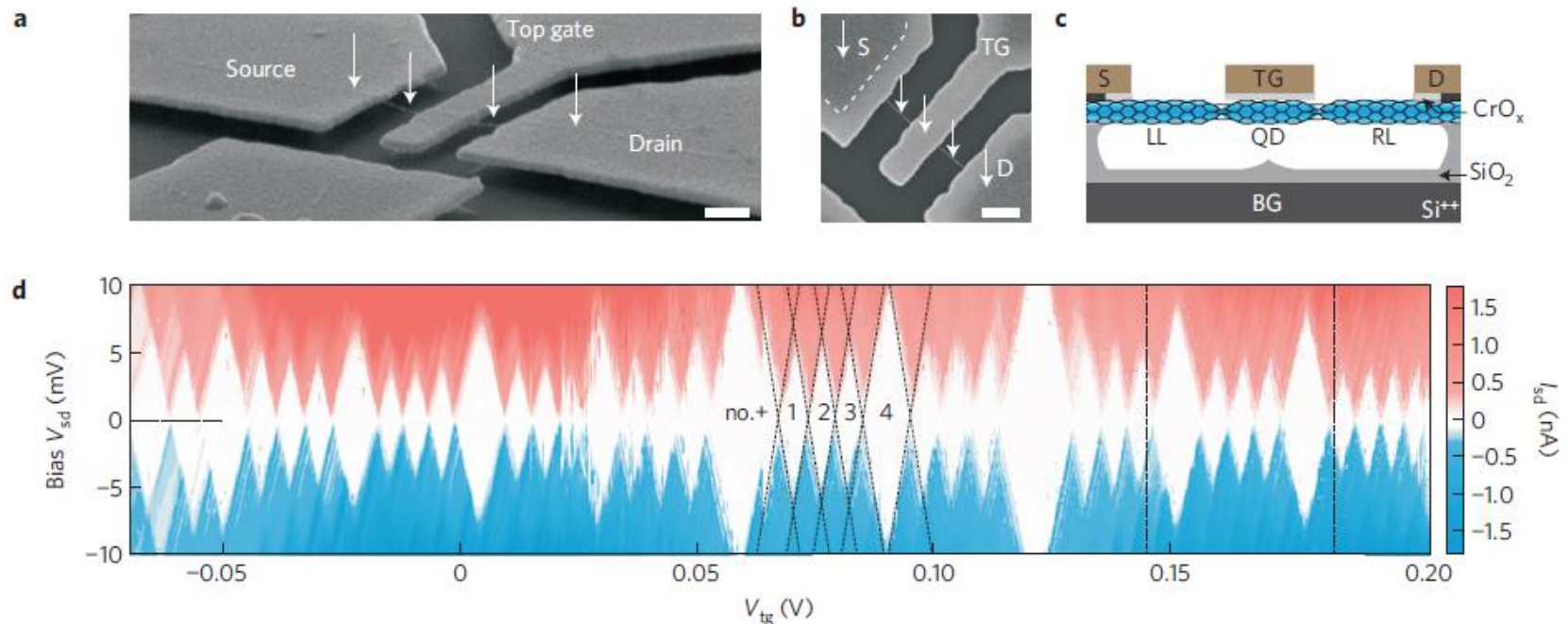
<http://www-ipcms.u-strasbg.fr/spip.php?article491&lang=en>

Figure 1 : The differential conductance, calculated in the regime of sequential tunneling through a one-dimensional quantum dot, as a function of the gate voltage (to the left) and the transport voltage. Green and red: Positive values. Blue: Close to zero. Pink: Negative differential conductance. The Coulomb blockade diamonds are aligned along the gate voltage axis. In parallel, one observes structures which are due to excited states of the dot. Electronic correlations combined with spin selection rules lead to the regions of negative differential conductance.

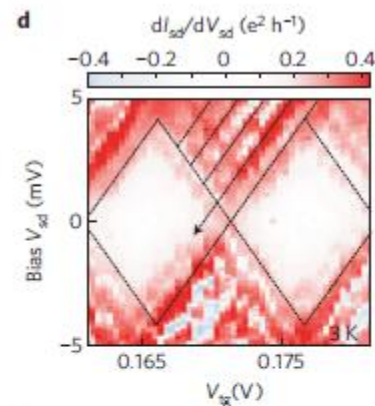
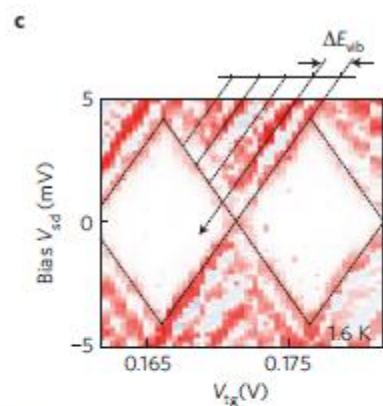
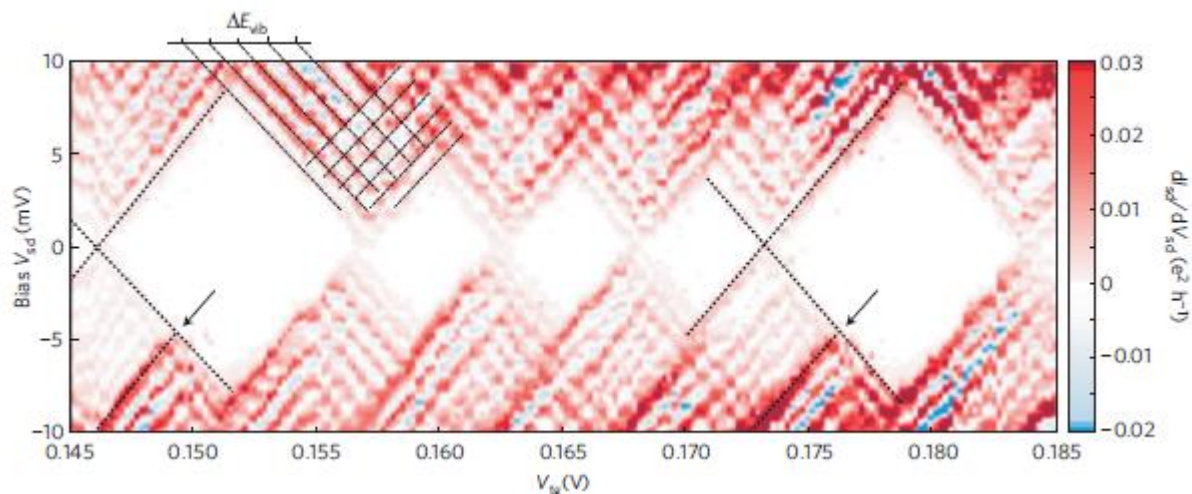
Coulomb blockade

Franck-Condon blockade in suspended carbon nanotube quantum dots

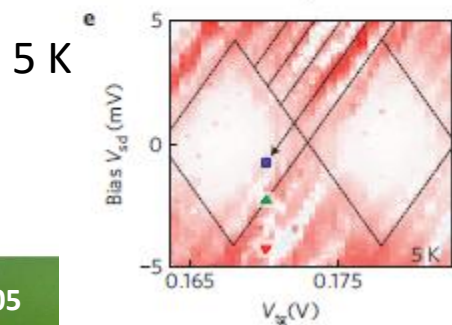
Renaud Leturcq^{1,2*}†, Christoph Stampfer^{1,3*}, Kevin Inderbitzin¹, Lukas Durrer³, Christofer Hierold³, Eros Mariani⁴, Maximilian G. Schultz⁴, Felix von Oppen⁴ and Klaus Ensslin¹



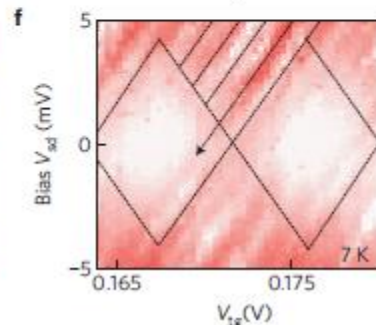
Coulomb blockade



3 K



5 K



7 K

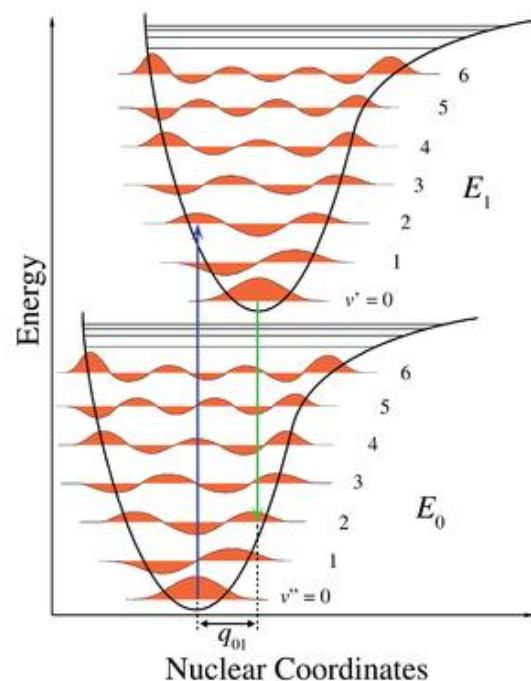
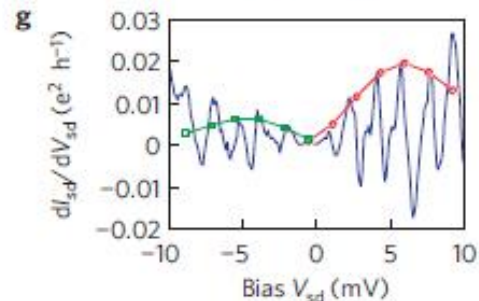
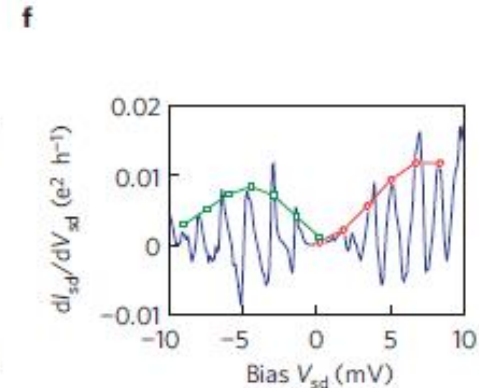
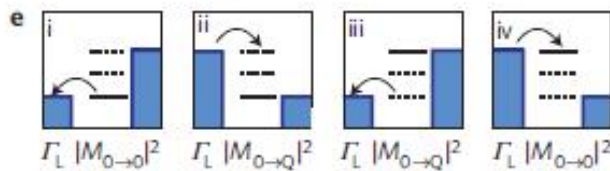
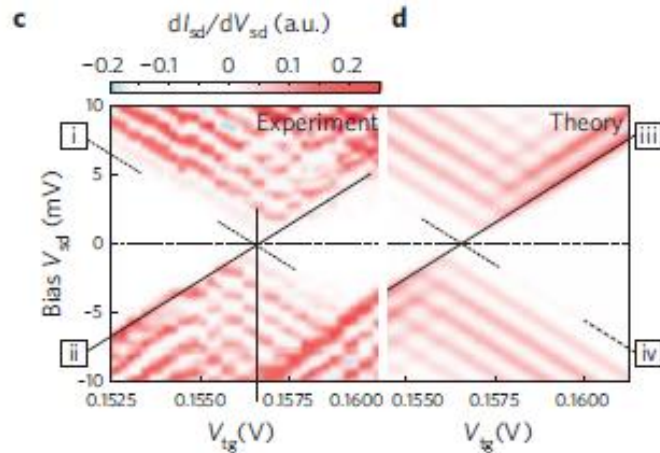
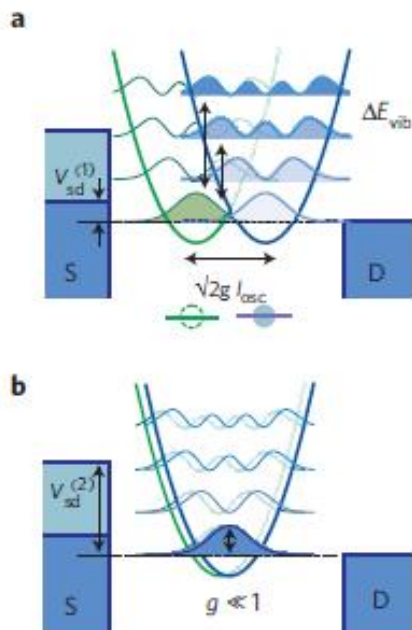
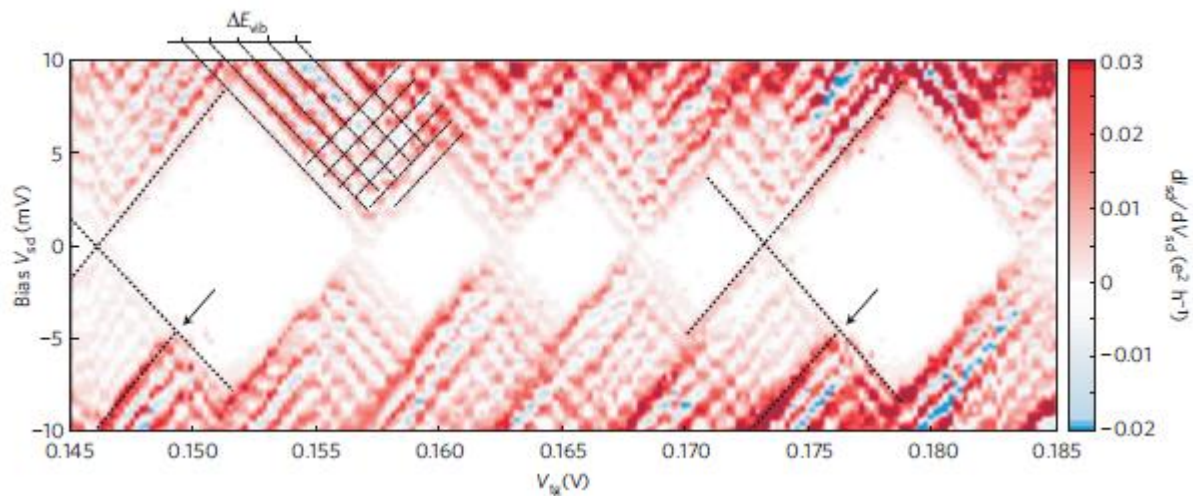
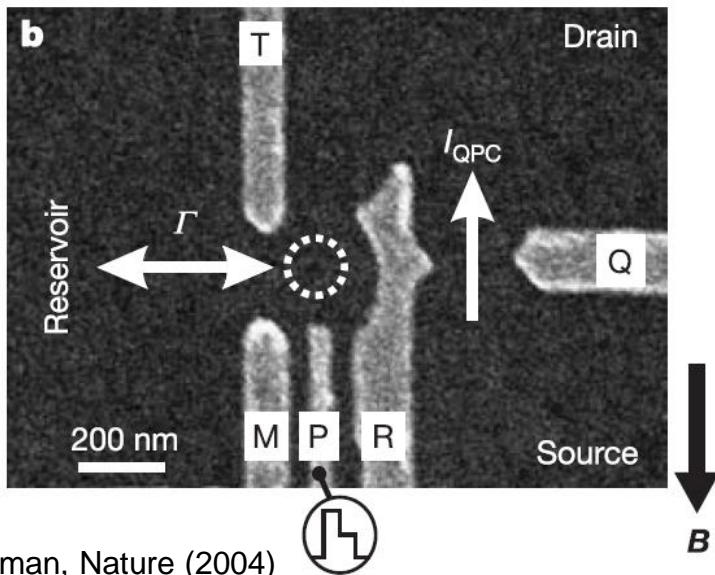
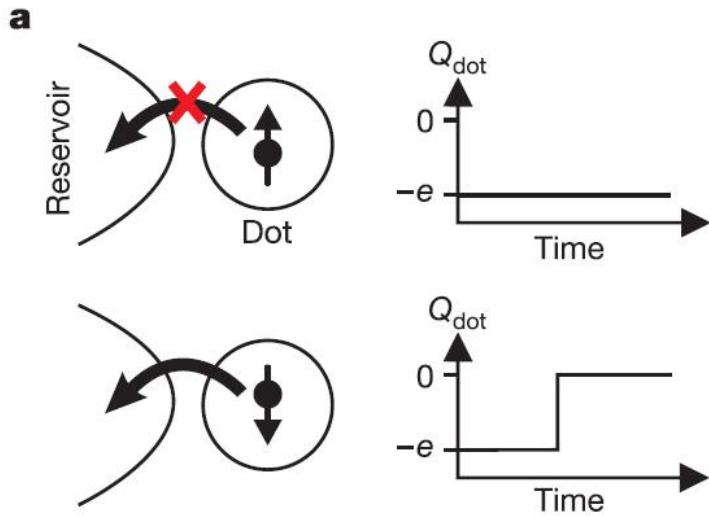


Figure 2 Evidence and temperature dependence of vibron-assisted transport. a, Differential conductance $dI_{sd}=dV_{sd}$ for a subset of the Coulomb diamonds shown in Fig. 1d, showing the quasi-periodic excited vibronic states (see dotted lines). The arrows point to electronic excited states, visible at higher energy.

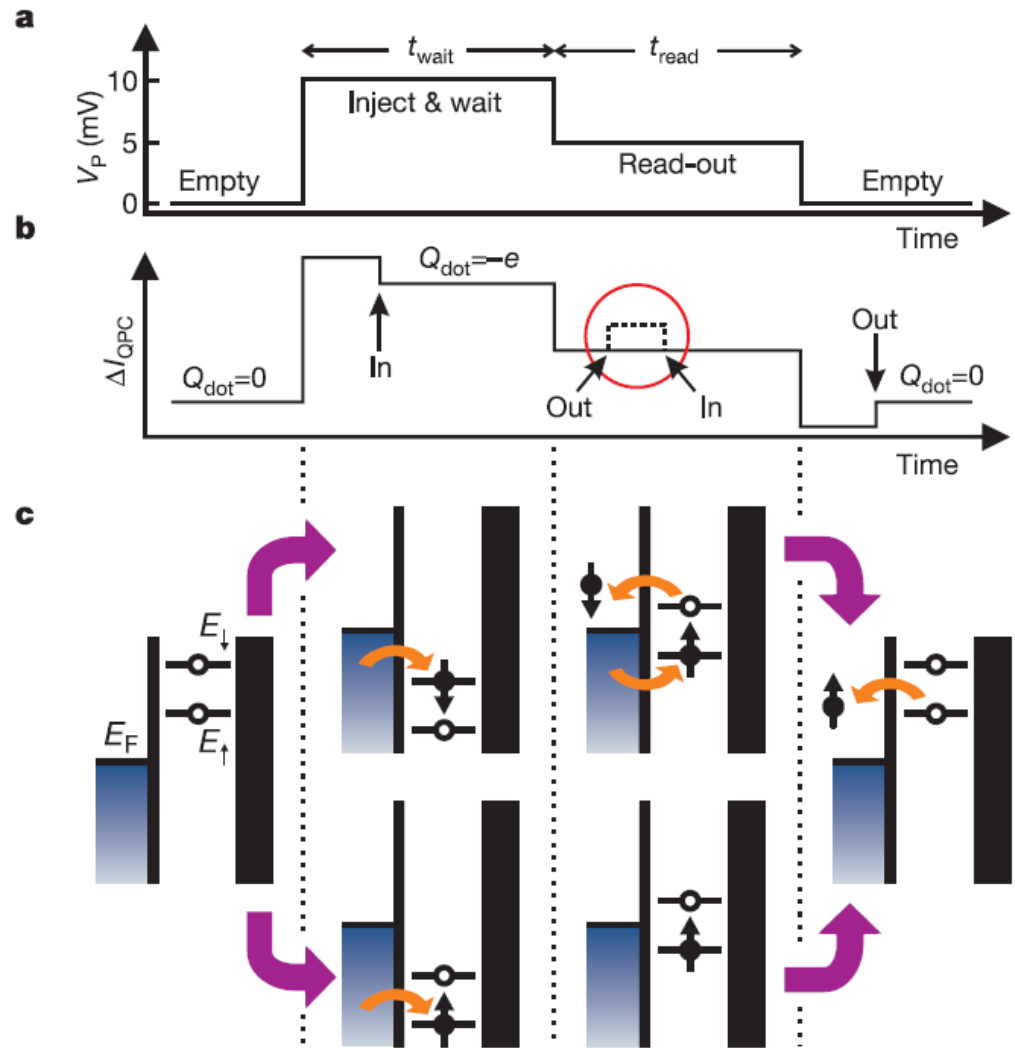
Coulomb blockade



Single spin read-out

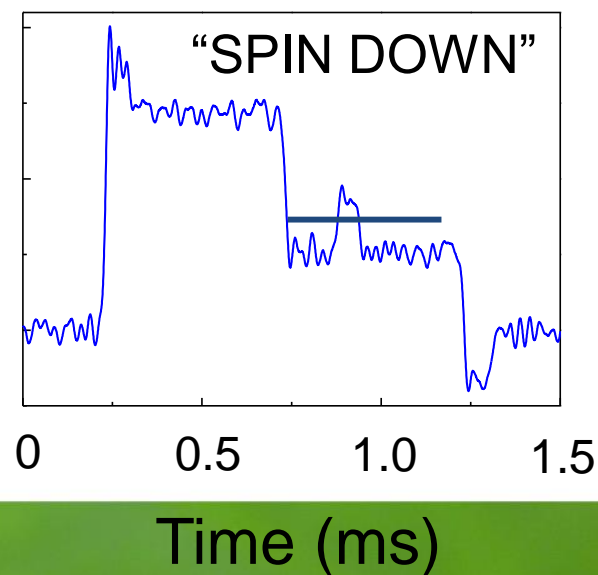
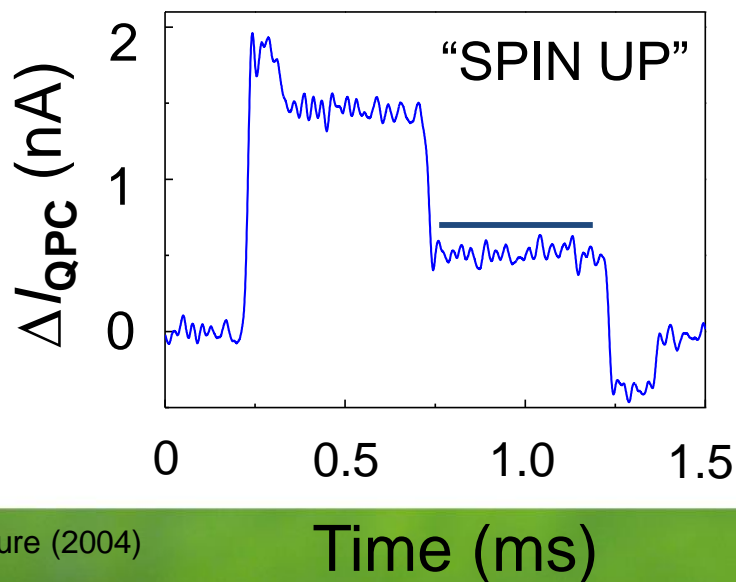
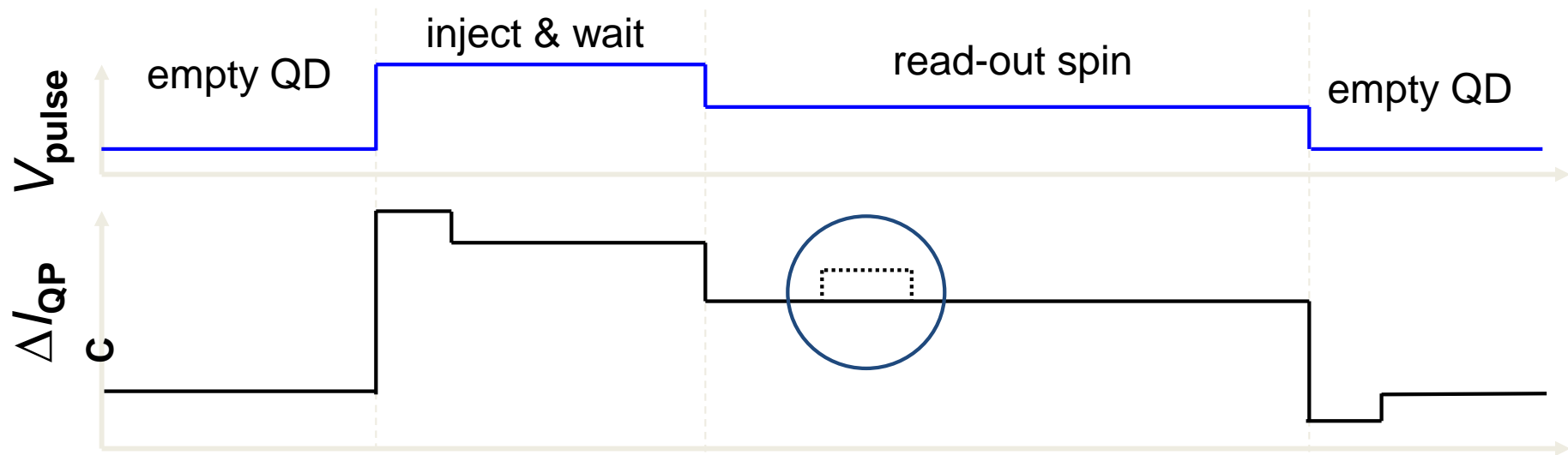


Elzerman, Nature (2004)

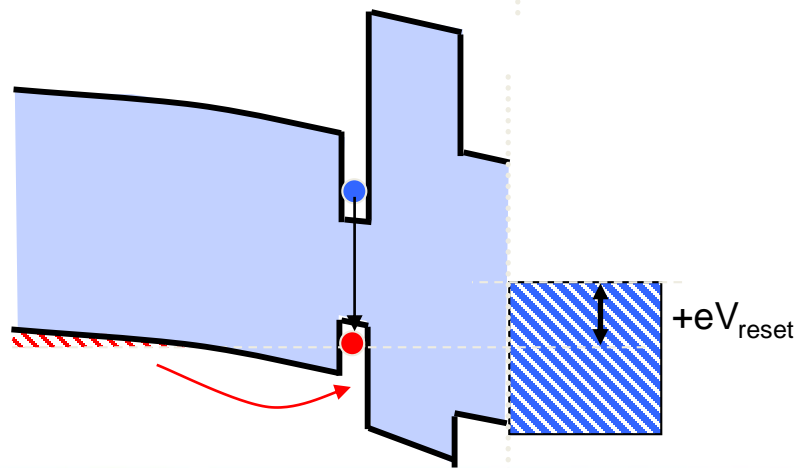
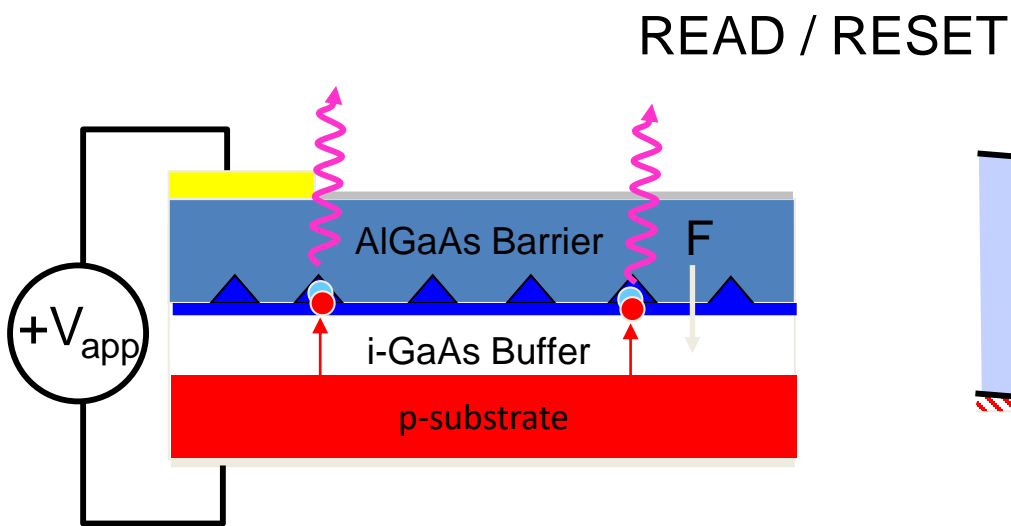
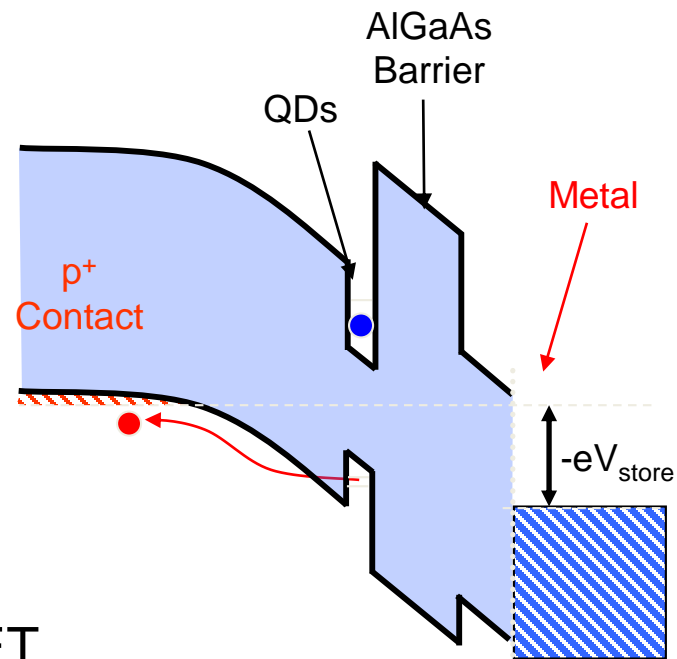
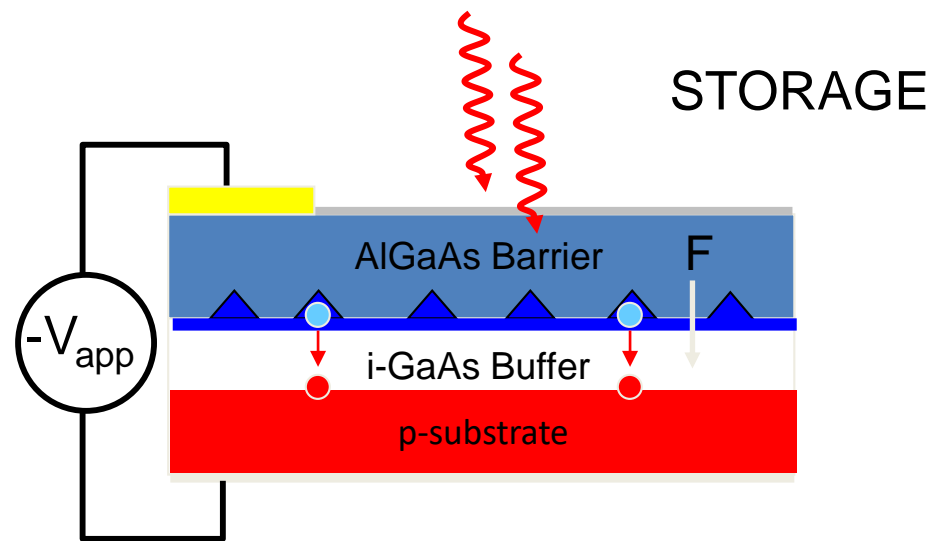


10T, mK

Single spin read-out

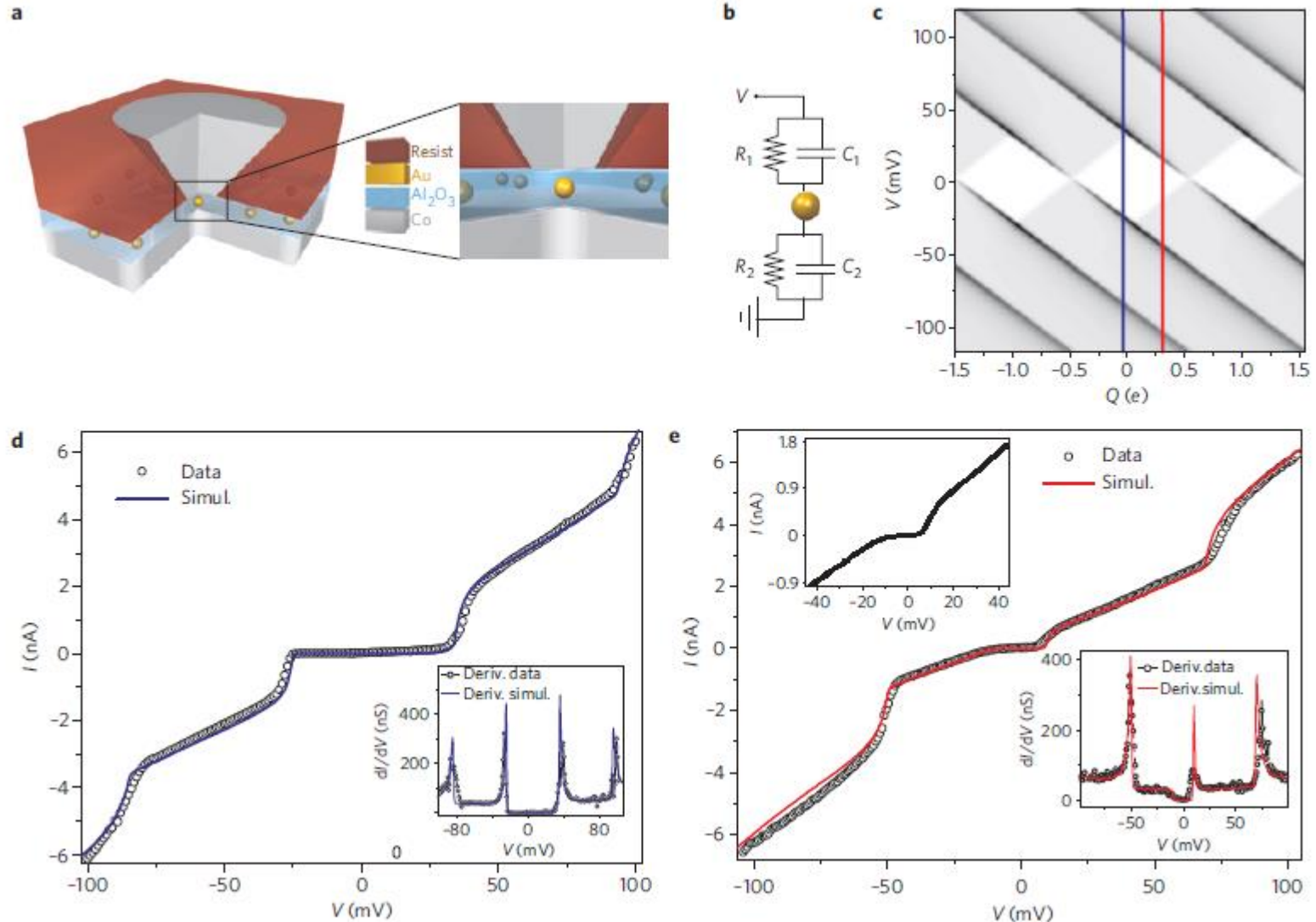


Spin storage



Anisotropic magneto-Coulomb effects and magnetic single-electron-transistor action in a single nanoparticle

Anne Bernard-Mantel, Pierre Seneor*, Karim Bouzehouane, Stéphane Fusil, Cyrille Deranlot, Frédéric Petroff and Albert Fert



Qubits

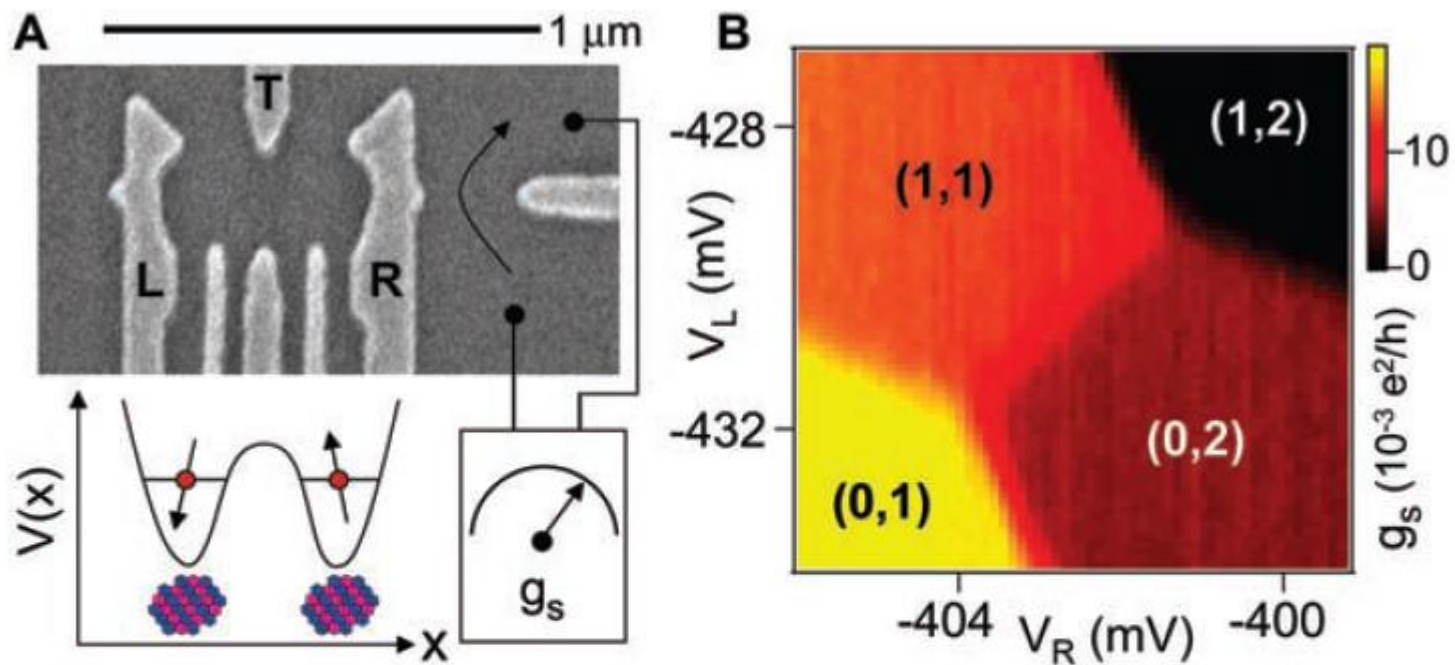
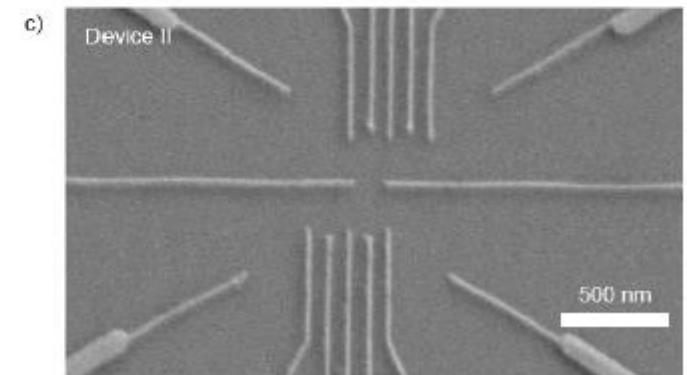
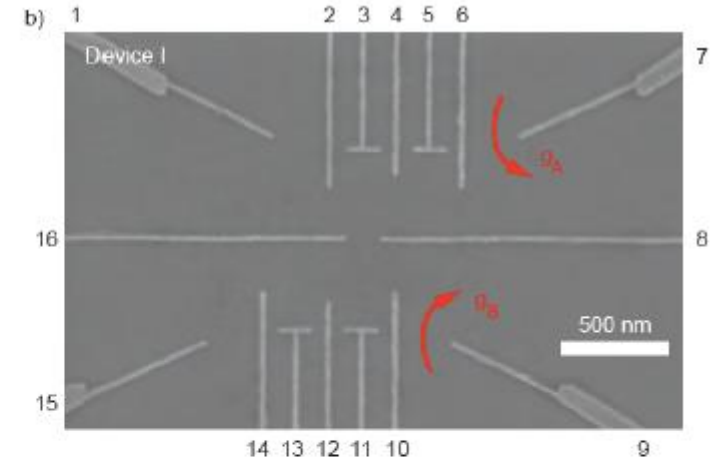
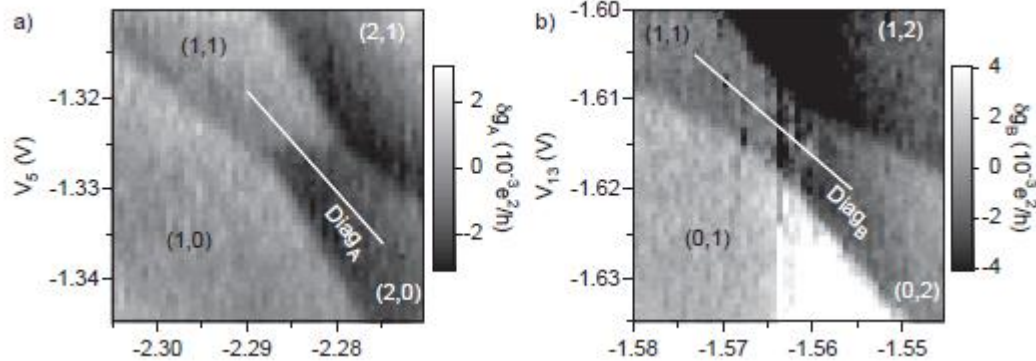
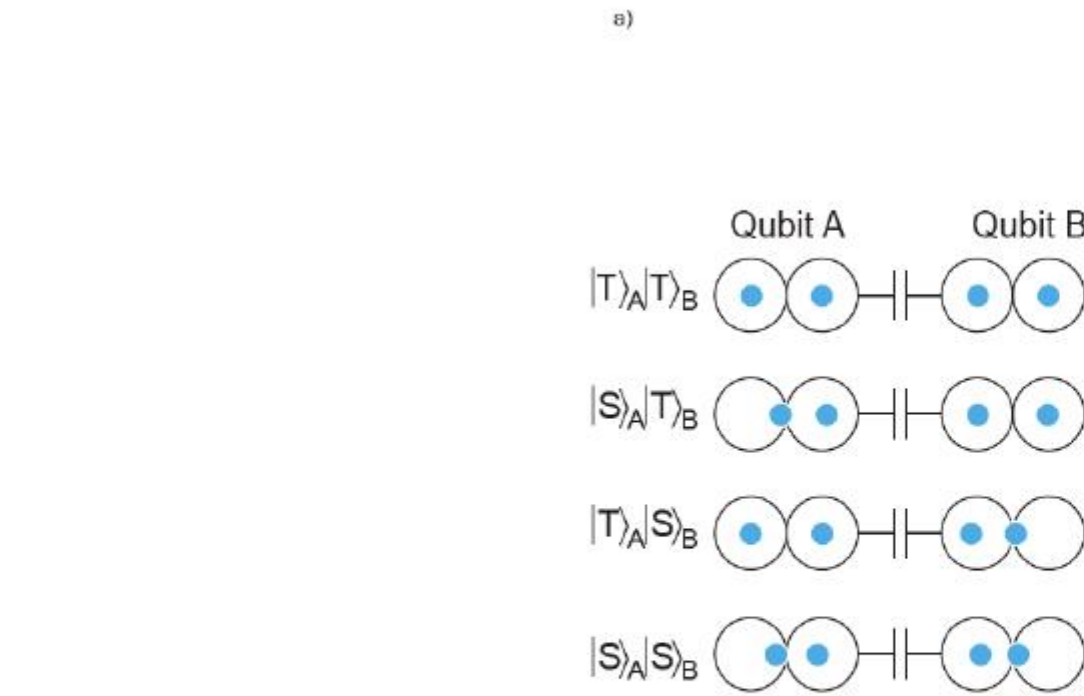


Fig. 1. (A) Scanning electron micrograph of a sample identical to the one measured, consisting of electrostatic gates on the surface of a two-dimensional electron gas. Voltages on gates L and R control the number of electrons in the left and right dots. Gate T is used to adjust the interdot tunnel coupling. The quantum point contact conductance g_s is sensitive primarily to the number of electrons in the right dot. (B) g_s measured as a function of V_L and V_R reflects the double-dot charge stability diagram (a background slope has been subtracted). Charge states are labeled (m,n) , where m is the number of electrons in the left dot and n is the number of electrons in the right dot. Each charge state gives a distinct reading of g_s .

Coherent Manipulation of Coupled Electron Spins in Semiconductor Quantum Dots
J. R. Petta, et al. *Science* 30 September 2005: 2180-2184.

Qubits



http://marcuslab.harvard.edu/theses/Laird_Thesis.pdf

Qubits

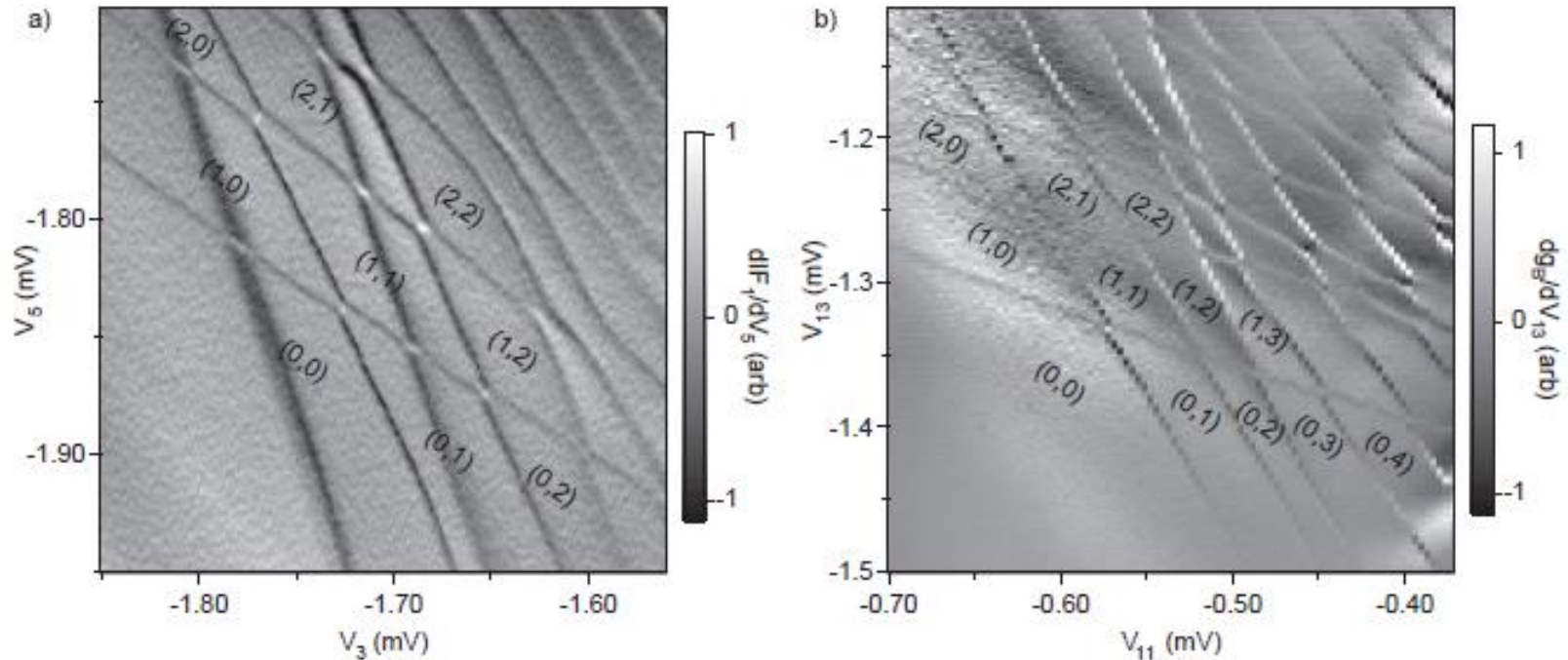
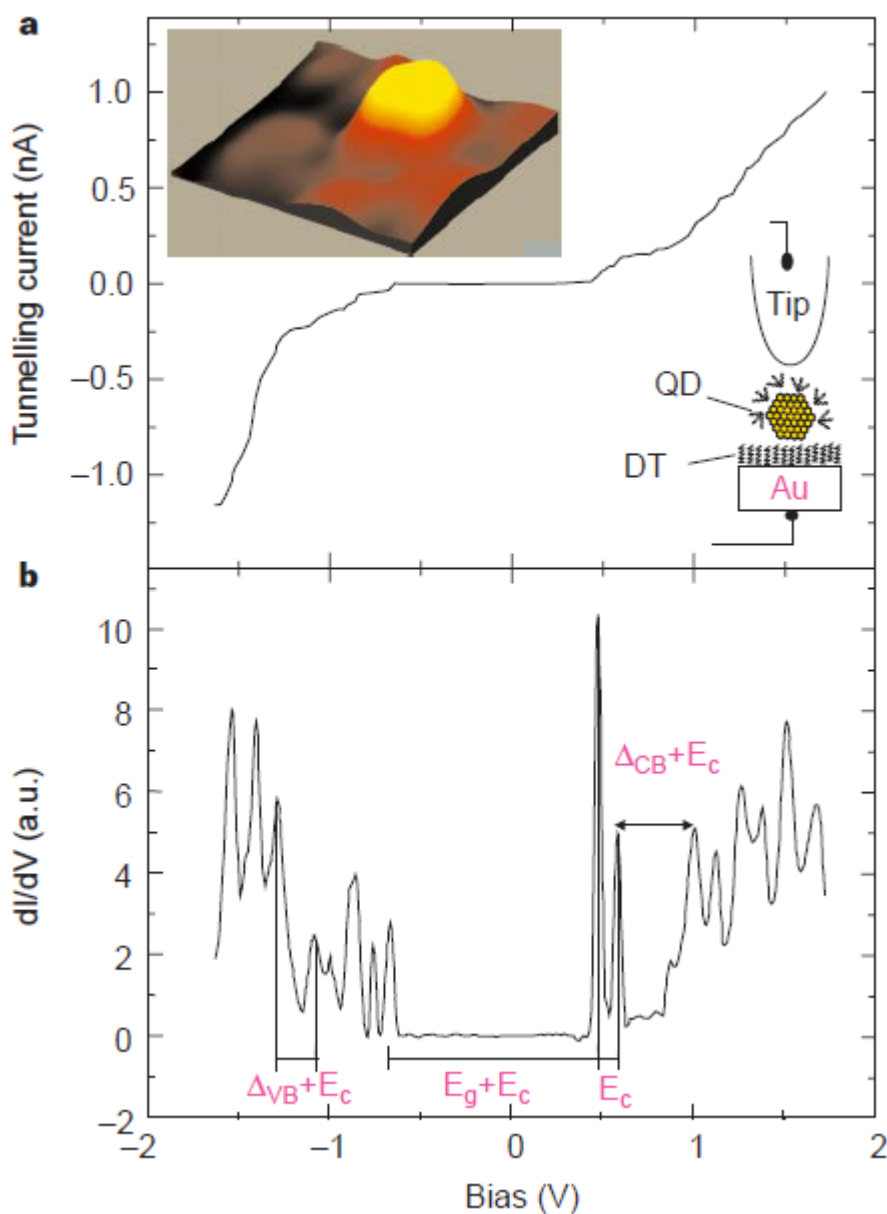


Figure 5.2: Charge stability diagrams of upper (a) and lower (b) double dots, measured using the charge sensors as a function of their respective plunger gate voltages. Both double dots can be tuned into the few-electron regime. The two broad near-vertical lines in (a) are resonances of the charge sensor.

Coulomb blockade

Tunnelling



letters to nature

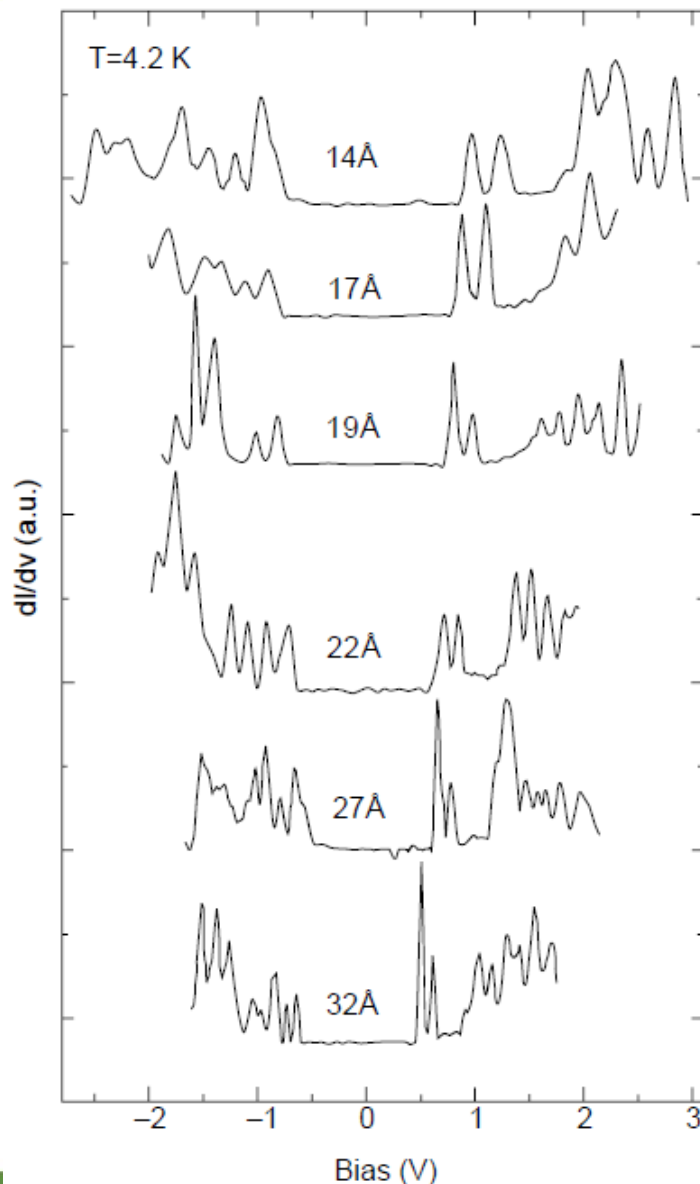
Identification of atomic-like electronic states in indium arsenide nanocrystal quantum dots

Uri Banin^{*}, YunWei Cao^{*}, David Katz[†] & Oded Millo[†]

^{*} Department of Physical Chemistry and the Farkas Center for Light Induced Processes, [†] Racah Institute of Physics, The Hebrew University, Jerusalem 91904, Israel

Figure 1 Scanning tunnelling microscopy and spectroscopy of a single InAs nanocrystal 32\AA in radius, acquired at 4.2 K. The nanocrystal quantum dots (QD) are linked to the gold substrate by hexane dithiol molecules (DT), as shown schematically in the right inset. Left inset, a $10 \times 10\text{ nm}$ STM topographic image, showing the nanocrystal. For measuring the I - V characteristics, the STM tip was positioned above the QD, thus realizing a double-barrier tunnel junction configuration. **a**, The tunnelling I - V characteristic, exhibiting single-electron tunnelling effects. **b**, The tunnelling conductance spectrum, dI/dV versus V , obtained by numerical differentiation of the I - V curve (a.u., arbitrary units). The arrows depict the main energy separations: E_c is the single-electron charging energy, E_g is the nanocrystal bandgap, and Δ_{VB} and Δ_{CB} are the spacing between levels in the valence and conduction bands, respectively.

Tunnelling



letters to nature

Identification of atomic-like electronic states in indium arsenide nanocrystal quantum dots

Uri Banin*, YunWei Cao*, David Katz† & Oded Millo†

* Department of Physical Chemistry and the Farkas Center for Light Induced Processes, † Racah Institute of Physics, The Hebrew University, Jerusalem 91904, Israel

Figure 2 Size evolution of representative tunnelling dI/dV versus V characteristics, displaced vertically. The position of the centre of the observed zero-current gap showed non-systematic variations with respect to zero bias, of the order of 0.2 eV, probably due to variations of local offset potentials. For clarity of presentation, we offset the spectra along the V direction to situate the centres of the observed zero-current gaps at zero bias. The nanocrystal radii are denoted in the figure. The range of displayed voltage for each curve reflects the experimental saturation limit of the detected current.

Tunnelling

„Kolokwium WAN IN”

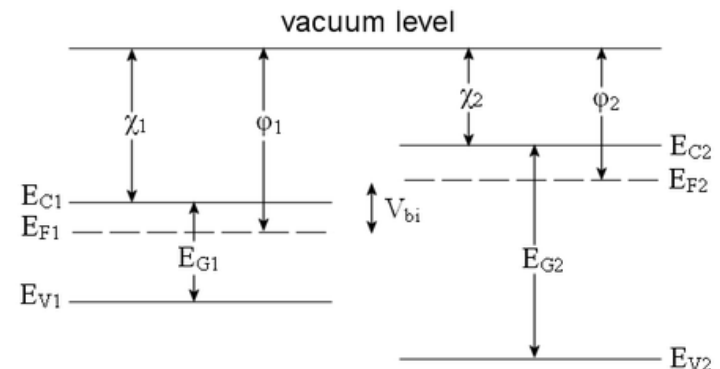
1. Znajdź w literaturze parametry pasmowe InAs (masy efektywne, powinowactwo elektr., ϵ_r) [0p]
2. Na podstawie danych z rys. 1 wyznacz pojemność kropki kwantowej o średnicy 32 Å. [5p]
3. Na podstawie danych z rys. 2 wyznacz pojemności wszystkich badanych kropek kwantowych. Ze wzoru na pojemność kuli wyznacz ϵ_r nanocząstek biorąc pod uwagę promienie wyznaczone eksperymentalnie. [10p]
4. Na podstawie rys. 2 oraz 3 wyznacz rozmiar nanocząstek InAs w przybliżeniu **nieskończonej** studni potencjału. Porównaj z wartościami mierzonymi oraz z rys. 3. [15p]
5. Na podstawie rys. 2 oraz 3 wyznacz rozmiar nanocząstek InAs w przybliżeniu **skończonej** studni potencjału przyjmując tablicowe parametry InAs z zad. 1. Porównaj z wartościami mierzonymi oraz z rys. 3. [25p] (zadanie numeryczne).
6. Jaka powinna być wartość wysokości bariery studni (powinowactwo objętościowego InAs), żeby uzyskać zgodność zad. 5. z wynikami STM? [20p] (zadanie numeryczne, oszacuj wartość najlepiej pasującą do wszystkich wyników).

letters to nature

Identification of atomic-like electronic states in indium arsenide nanocrystal quantum dots

Uri Banin*, YunWei Cao*, David Katz† & Oded Millo†

* Department of Physical Chemistry and the Farkas Center for Light Induced Processes, † Racah Institute of Physics, The Hebrew University, Jerusalem 91904, Israel



ϕ = work function
 χ = electron affinity
 E_G = band gap
 E_C = conduction band (powinowactwo)
 E_V = valence band

Tunnelling

„Kolokwium”

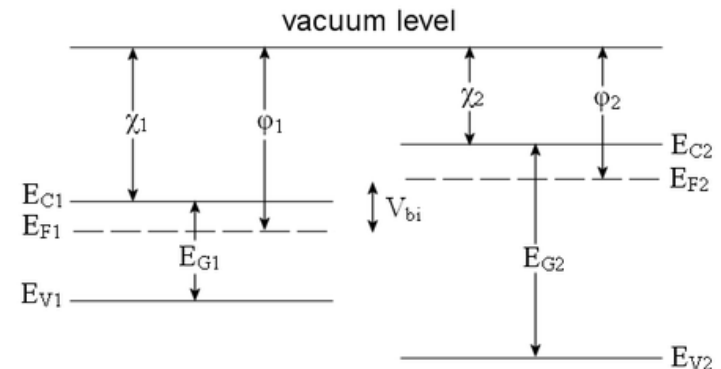
1. Find in the literature band parameters of InAs (effective masses, dielectric constant) [0p]
2. Based on the data shown in Fig. 1 determine capacitance of the 32 nm quantum dot. [10p]
3. On the basis of Fig. 2 and 3 find the size of the InAs nanoparticles in the infinite potential well approximation. Compare the values measured and shown in Fig. 3. [20p]
4. Assuming size of the nanoparticles shown in Figure 2, estimate the electron affinity (ionization energy from the bottom of the conduction band) (numerically) and the capacity of quantum dots in Fig. 2. [30p]

letters to nature

Identification of atomic-like electronic states in indium arsenide nanocrystal quantum dots

Uri Banin*, YunWei Cao*, David Katz† & Oded Millo†

* Department of Physical Chemistry and the Farkas Center for Light Induced Processes, † Racah Institute of Physics, The Hebrew University, Jerusalem 91904, Israel



ϕ = work function
 χ = electron affinity (powinowactwo)
 E_G = band gap
 E_C = conduction band
 E_V = valence band

Tunnelling

„Kolokwium WAN IN”

1. Znajdź w literaturze parametry pasmowe InAs (masy efektywne, powinowactwo elektr., ϵ_r) [0p]
2. Na podstawie danych z rys. 1 wyznacz pojemność kropki kwantowej o średnicy 32 Å. [5p]
3. Na podstawie danych z rys. 2 wyznacz pojemności wszystkich badanych kropek kwantowych. Ze wzoru na pojemność kuli wyznacz ϵ_r nanocząstek biorąc pod uwagę promienie wyznaczone eksperymentalnie. [10p]
4. Na podstawie rys. 2 oraz 3 wyznacz rozmiar nanocząstek InAs w przybliżeniu **nieskończonej** studni potencjału. Porównaj z wartościami mierzonymi oraz z rys. 3. [15p]
5. Na podstawie rys. 2 oraz 3 wyznacz rozmiar nanocząstek InAs w przybliżeniu **skończonej** studni potencjału przyjmując tablicowe parametry InAs z zad. 1. Porównaj z wartościami mierzonymi oraz z rys. 3. [25p] (zadanie numeryczne).
6. Jaka powinna być wartość wysokości bariery studni (powinowactwo objętościowego InAs), żeby uzyskać zgodność zad. 5. z wynikami STM? [20p] (zadanie numeryczne, oszacuj wartość najlepiej pasującą do wszystkich wyników).